CHARACTERISATION OF 'CLASS A' POLYMER COMPOSITES FOR THE AUTOMOTIVE INDUSTRY

BY

PETER JAMES SCHUBEL

BENG. (HONS.)

THESIS SUBMITTED TO THE UNIVERSITY OF NOTTINGHAM FOR THE DEGREE OF DOCTOR OF PHILOSOPHY

OCTOBER 2004

Abstract

Characterisation of 'Class A' Polymer Composites for the Automotive Industry

by

Peter Schubel

BEng

This thesis addresses problems associated with surface quality measurement and residual volatile organic compounds for composite laminates intended for use as cosmetic body parts based on unsaturated polyester resin containing shrinkage control additives. Surface quality measurement techniques were compared for composite laminates allowing for rapid characterisation and benchmarked to industrial standards. Thermal desorption and solvent elution techniques were used for the detection of residual volatiles with styrene and benzaldehyde being the main focus. The degree of conversion and residual volatiles were monitored for three peroxide initiators via a series of statistically developed experiments. This work highlighted the need for alternative shrinkage control methods. A novel approach was studied through the use of nano-scale silicates. An exfoliation process was developed with subsequent characterisation of thermal and mechanical properties for the nanocomposite. Finally, a series of hybrid matrices consisting of nanocomposite and low profile additive blends were monitored for effects on surface roughness, residual volatile levels and mechanical performance.

Acknowledgements

The author would like to thank his academic supervisors Professor Chris Rudd and Dr. Nick Warrior for their outstanding guidance and support during the course of this work, as well as Dr. Ken Kendall (Aston Martin Lagonda) for his commitment to the interests of the Polymer Composite Group at the University of Nottingham.

The financial support of the DTI/DfT and the collaborative support of the Ford Motor Company, Aston Martin Lagonda, Hexcel Composites, Scott Bader Company, Qinetiq, Tenax, Sotira and Atlas Co are gratefully acknowledged.

The project would not have been successful or as enjoyable without the much appreciated help from the technical support team of Roger Smith, Paul Johns, Dave Smith and Geoff Tomlinson.

Contents

1 Introduction

1.1 Polymer Reinforced Composites in the Automotive Industry

The high specific strength and specific stiffness of composite materials have made polymer-reinforced composites attractive not only in weight sensitive aerospace applications, but also in marine, armour, automobile, civil structures and sporting goods. Composite materials are a versatile product and can be engineered to provide many advantages compared to metals including: weight reduction, increased structural stiffness, chemical resistance, thermal resistance, diffusional barrier and dielectic properties and in some cases, reduced manufacturing costs. The automotive industry has realised the potential benefits that composites offer over conventional structural materials such as steel and has been a driving force in the development of material and processing conditions.

Polymer matrix composites can be generalised into thermoplastics (polymers that soften and can be re-shaped with the addition of heat) and thermoset (polymers that acquire a final form after an irreversible chemical process), with thermosets dominating approximately 70 % of the market. By 2003, the world market for polymer composites was 7.2 million tonnes, with the automotive industry consuming 25 % of the output [1]. This is a growth of 8 % from 2002 and has been driven by political, economical, social and technological issues such as environmental regulation towards lighter, more recyclable materials, improvements in manufacturing technology, form flexibility leading to popular new designs and increased steel prices due to tariffs [2].

Traditional micron level reinforcement such as glass, carbon, aramid and various other natural fibres have been and still are the focus of much research. However, the push for novel approaches in polymer composite design has led to the rapid development of materials that utilise reinforcement on a nanometre scale (nanocomposite). The total worldwide market for nanocomposites, nanoparticles, nanoclays and nanotubes reached 11 100 tonnes or £50 million, in 2003. This new

and innovative sector has a predicted annual growth of 18.4 % to reach £115 million by 2008 [3].

Lightweight body structures are being successfully produced from stamped and assembled aluminium alloys, which offer controlled dimensional stability, predictable surface quality, zero residual volatile organic compounds (VOCs) and excellent recyclability. At high volumes, aluminium alloy becomes cost competitive with composites due to rapid processability and current joining and welding techniques. Composite materials must offer benefits beyond the capabilities of aluminium alloy structures and overcome processing/recycling issues if they are to sustain strong growth within the lightweight automotive sector.

1.2 Moulding Developments in the Automotive Industry

The automotive industry utilises a variety of forming and consolidation processes in order to meet demands from niche markets up to high volume production. The process undertaken is influenced by production volume (Table 1.1), material type, component size, mechanical properties, dimensional stability and cost.

Table 1.1: Automotive volume definition [4].

Volume	Definition
Low Volume	< 10 000 parts per year
Medium volume	10 000 - 100 000 parts per year
High volume	>100 000 parts per year

Prototyping and low volume production are generally cost effectively produced using hand lay-up or vacuum infusion [5]. With traditional methods such as hand lay-up, the operator is exposed to uncured liquid resin systems and to any volatile compounds that may be emitted into the workplace atmosphere. This is a particular problem when using resin systems cured by addition crosslinking, such as polyester, which traditionally use styrene monomer. Styrene vapour has been

reported to cause detrimental effects in workers; notably depression and fatigue with slowing of reaction times [6]. The use of sealed moulding assemblies such as vacuum infusion, structural reaction injection moulding (SRIM), resin transfer moulding (RTM) and compression moulding utilising sheet and bulk moulding compounds (SMC and BMC) have been shown to reduce organic volatile emissions by up to 95 % [7].

Processes which utilise vacuum bagging techniques, such as vacuum infusion (VI), have been shown to be cost efficient for low volume production (Figure 1.1) due to the low cost of tooling. However, the necessary consumable costs make this system impractical for production over 10 000 parts. Further more, limitations to these processes include low inlet and compaction pressures (approx 100 kPa), which influence mechanical properties, surface quality and component thickness, leading to variation in batch tolerances.

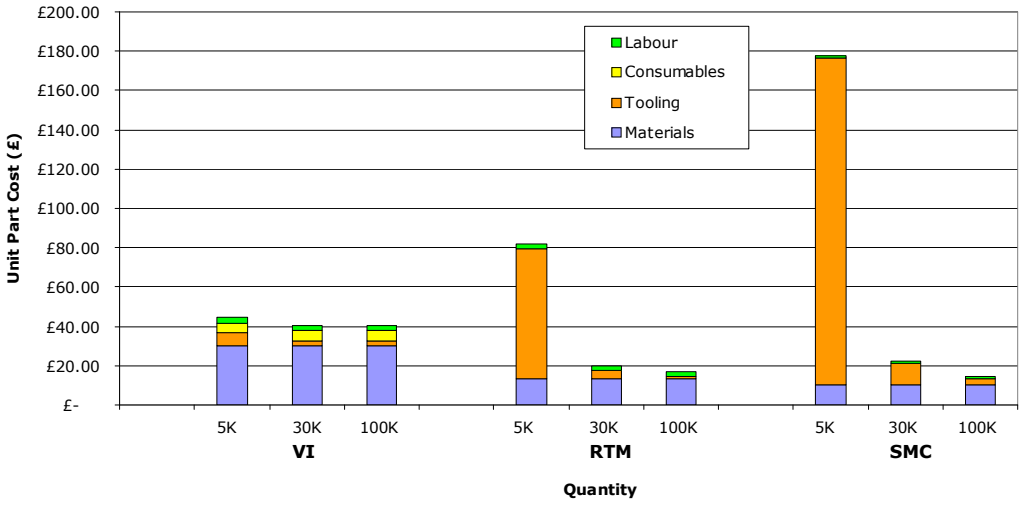

Figure 1.1: Component cost for a generic 1 m^2 part for carbon systems at low, medium and high production volumes [8].

To improve cost viability for medium to high production and overcome the limitations of vacuum bagging, a closed mould, matched tool assembly is generally employed. A matched tool assembly improves thickness control, facilitates higher injection and compaction pressures and reduces VOCs being

released into the work environment. Popular processes utilising a matched mould assembly include compression moulding and RTM.

Compression moulding with matched tooling using sheet moulding compound (SMC) is currently the most common method for producing high volume polymer composites due to the reduced cost of production for parts exceeding 100 000 per annum (Figure 1.1). Tooling capital is high for compression moulding due to the high moulding temperature and pressures (approx 150 ºC and 5.5 MPa respectively). However this is justified by low cycle times of one to four minutes depending on the complexity of the part [9, 10].

Resin transfer moulding (RTM), is economic for low to medium volume manufacture (Figure 1.1) of structural and non-structural composite components. It has especially created interest in the niche automotive market where production runs less than 100 000 are typical. The major attraction to the automotive industry is the ability to mould fully integrated components (Figure 1.2), including inserts, mounting points and foam cores to produce complex structural shapes with close control of component dimensions and reduced emissions of volatiles over open moulds [11, 12].

Figure 1.2: Upper cargo deck for the Aston Martin Vanquish (2001), produced using RTM. This figure shows the complexity of shapes that can be manufactured as a single component using RTM. (Courtesy of Ford Motor Company)

RTM utilises matched mould tooling in which a pre-catalysed liquid thermosetting resin is injected into a heated closed mould containing a dry fibre preform (Figure 1.3). The preform can be engineered using both random and directional reinforcements to meet a range of service loadings. A comprehensive review of filling and cure phenomena in RTM can be found in [13]. Although the underlying principals of RTM appear at first to be simple, this is often not the case. The challenge for RTM is to bring together disciplines of preforming, mould design and process development with existing fibres and resins.

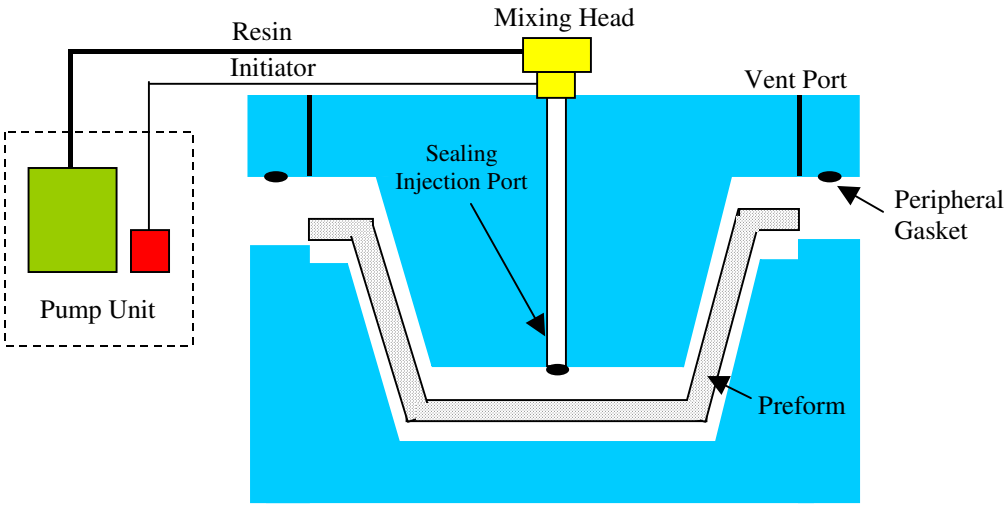

Figure 1.3: Process schematic of RTM.

1.3 Issues Associated with Polyester RTM

RTM has been the subject of extensive study over the past decades in the hope to understand critical issues such as resin flow during mould filling [14-17] and resin chemistry [18, 19]. Developments in these areas have made RTM an efficient and attractive technique to produce high quality fibre reinforced composite parts. One such benefit is the manufacture of high surface quality (Class A) panelling. The term ‘Class A’ is widely used in the automotive industry to characterise the surface quality of a cosmetic composite. However, no absolute standards exist. Subjectively, it is believed that a laminate made of composite material represents a ‘Class A’ surface if its optical appearance is identical to an adjacent steel panel. This criterion is susceptible to individual interpretation.

RTM is adaptable to a range of material types, allowing for flexibility in design, material properties and component cost. Automotive RTM generally relies upon low cost resin systems such as unsaturated polyesters. Unsaturated polyesters account for 11.5 % of the world thermoset resin market, with 2.495 million tonnes being consumed in 2003 [20, 21]. The strong market share and 3.9 % predicted annual growth is due to its good mechanical properties, environmental resistance and most importantly, low cost. They also provide advantages over other thermosetting resins such as ease of handling, excellent wetting capabilities of fibre reinforcement and good compatibility to glass fibres, which are one of the cheapest forms of fibre reinforcement on the market.

Many styles of unsaturated polyester resin are available; including orthophthalic, isophthalic, terephthalic and bisphenol-fumarate resins [22]. Orthophthalic resins are the most common and are formed from the condensation reaction between phthalic anhydride, maleic anhydride, and propylene glycol. The resin is then diluted with a vinyl monomer, usually styrene, to achieve the desired viscosity and reactive ratio. The maleic anhydride provides the reactive double bond, which then reacts with the double bond of the vinyl monomer to form a rigid three-dimensional network.

Organic peroxides are introduced to initiate the free radical polymerisation reaction which involves the conversion of double bonds into single covalent bonds. Chemical decomposition provides exothermic heat for a partial cure. The initiator can be derived from peroxide compounds that are broken down into free radicals when subjected to heat or ultraviolet radiation. Most organic peroxides decompose slowly when added to unsaturated polyester resins and are generally promoted by using an accelerating system such as a metal oxide (cobalt) or naphthenate. Several authors have suggested that the type [23-25], amount [25, 26] and cure temperature [27] are critical to the final properties of rigid thermosets. These curing factors become critical in structural and cosmetic composites where a balance of properties is required for long-term performance.

1.3.1 *Cure Induced Resin Shrinkage*

The cure process of a thermosetting resin is commonly described as three distinct regions (Figure 1.4). In Region I, the resin is uncured and behaves as a viscous fluid (negligible stiffness). Each monomer molecule can be considered as a discrete chemical entity occupying a unit volume (Figure 1.5) dictated by its van der Waals volume (V_w) and thermal energy [28].

Region II denotes the curing stage of the resin, where a significant increase in stiffness (chemical hardening) and a reduction in specific volume (chemical shrinkage) begin to occur. In this region the monomer units become joined by covalent bonds to form repeat units in a polymer chain (Figure 1.5). The additional bonding means that each polymer unit is more constrained than the corresponding monomer and has fewer degrees of freedom to store thermal energy. The reduction of thermal energy means that each polymer unit occupies less space than it did in the monomeric state. As a result, the density of the polymer increases in comparison to the monomer. The resin chemical shrinkage is assumed to occur at the point of resin gelation and is assumed to be completed once the resin is fully cured or diffusion limitations limit further development (α^{shr}).

Region III marks the end of the curing process and no further polymerisation shrinkage occurs. In this region, the resin exhibits viscoelastic behaviour at elevated temperatures and approaches elastic behaviour at lower temperatures. Thermal expansion is the only mechanism contributing to changes in specific volume in Region III.

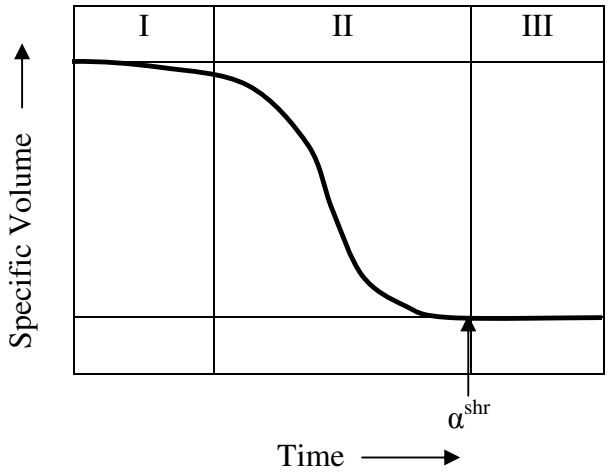

Figure 1.4: Three distinct regions in which the physical properties of resin change throughout the polymerisation process [29].

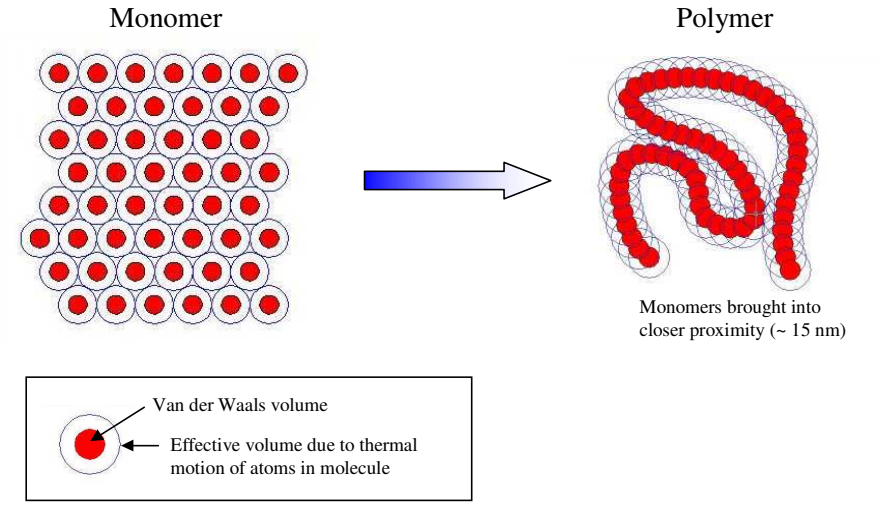

Figure 1.5: Schematic of unit cell contraction occurring during the cure process [28].

Cure Simulation

The thermal expansion and polymerisation shrinkage contribute to changes in material specific volume and represent important sources of internal loading. Being able to predict such phenomena is an important step when designing laminates for specific load and dimensional tolerances. Processing concerns associated with thermosetting composites become increasingly important for components of appreciable thickness. The most common problem is an increase in

temperature resulting from the resin exothermic chemical reaction. Significant effects are also seen with resin systems that exhibit high chemical shrinkage formed by the process described in Figure 1.5. Processing induced residual stresses can have a significant effect on the performance of a laminate and can be high enough to cause cracking within the matrix even before mechanical loading [30]. This micro-cracking of the matrix can expose the fibres to degradation by chemical attack [31], with strength being adversely affected since a pre-loading has been introduced.

Extensive investigations have been centred on understanding the cure kinetics and associated residual stresses induced in a laminate by thermal and chemical shrinkage [29-37]. This work has lead to the development of a range of numerical models which predict cure characteristic of various resin systems and can be used to accurately predict internal residual stress due to the inherent contraction created by chemical shrinkage and thermal effects. Analysis of residual stresses in thermosetting composite laminates are based on thermal expansion mismatch between adjacent plies, a uniform temperature difference between the cure temperature and ambient conditions and no stress development prior to completion of the curing process [33]. This approach is successful in predicting residual stresses in thin section laminates, where a uniform through-thickness temperature distribution assumption is justified. However, such an approach is not appropriate for thick section laminates where complex temperature and degree of cure gradients develop during the cure process [29].

Various cure simulations have been developed for two-dimensional analysis [32, 34, 35] with the governing equation based on the Fourier and Laplace heat conduction equation for transient anisotropic heat transfer with constant material properties and an internal heat generation source term:

$$q + k_{xx}\frac{\partial^2 T}{\partial x^2} + 2k_{xz}\frac{\partial^2 T}{\partial x \partial z} + k_{zz}\frac{\partial^2 T}{\partial z^2} = \rho\, c_p \frac{\partial T}{\partial t} \qquad [1.1]$$

for *T(x,z) in D*

where D is the domain of interest defined in an orthogonal (x,z) coordinate system. The term q represents internal heat generation and k_{xx}, k_{zz}, k_{xz} are the effective anisotropic thermal conductivities, ρ is the density and c_p is the specific heat of the composite. T and t are absolute temperature and time, respectively.

Fibre reinforced composites exhibit anisotropic thermal conductivities defined in a principal coordinate system with coordinate axes parallel and perpendicular to the fibre direction. Fibre orientation will generally vary with respect to the global coordinate system in an arbitrary shaped geometry. The effective anisotropic thermal conductivities in Equation 1.1 are based on the second order tensor transformation of the principal thermal conductivities given by:

$$\begin{bmatrix} k_{xx} \\ k_{zz} \\ k_{xz} \end{bmatrix} = \begin{bmatrix} m^2 & n^2 & mn \\ n^2 & m^2 & -mn \\ -mn & mn & -n^2 \end{bmatrix} \begin{bmatrix} k_{11} \\ k_{33} \\ k_{13} \end{bmatrix} \qquad [1.2]$$

In Equation 1.2, $m = cos\ (\theta)$, $n = sin\ (\theta)$ and k_{11}, k_{33} and k_{13} are the longitudinal, transverse and cross-term thermal conductivities of the composite in its principal (1,3) material coordinate system, respectively. Fibre orientation within the domain is assumed coincident with the curvilinear coordinate system, (η, ξ), shown in Figure 1.6.

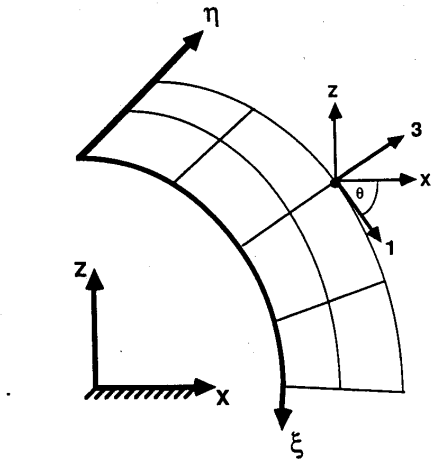

Figure 1.6: Thermal conductivity transformation between coordinate system [32].

A simplified version of the two-dimensional cure simulation analysis has been proposed [29, 38], which omits heat conduction from the *x* coordinate plane and isolates through-thickness processing effects on a fundamental level. The one-dimensional model is effective for thin and thick laminates without the extra computational effort required in a two-dimensional model. The reduction in the degrees of freedom for the one-dimensional model limit heat conduction to through-thickness effects and do not consider thermal changes as a result of neighbouring regions. However, this style of analysis has shown good correlation with experimental data [29, 31, 34]. For the one-dimensional cure simulation, Fourier's heat conduction equation reduces to:

$$q + k_z \frac{\partial^2 T}{\partial z^2} = \rho\, c_p \frac{\partial T}{\partial t} \qquad \text{for } T(z, t) \text{ in } (0 < z < L) \qquad [1.3]$$

The internal heat generation term in Equation 1.3, q, represents the instantaneous heat liberated per unit volume of material from the cross-link polymerisation reaction:

$$q = \rho H_r \frac{d\alpha}{dt} \qquad [1.4]$$

The heat of reaction, H_r, is the total heat liberated for complete cure and $d\alpha/dt$ is the instantaneous cure rate. The degree of cure at any time is defined in terms of the instantaneous cure rate through an integral representation:

$$\alpha(t) = \int_0^t \frac{d\alpha}{dt} dt \qquad [1.5]$$

The complete description of the cure kinetics for the composite includes the total heat of reaction and a description of the rate of reaction as a function of temperature and degree of cure. The instantaneous reaction rate is required to calculate the heat generation (Equation 1.4) and degree of cure (Equation 1.5) during the cure process. Both the total heat of reaction and the reaction rate expression are typically characterised empirically with isothermal Differential

Scanning Calorimetry (DSC). Reaction rate expressions for unsaturated polyester, vinyl ester and epoxy are different in form due to the inherent differences in the overall order of the reaction kinetics. Typical reaction rates for various resin types have been derived and can be found in the following references [29, 33-35, 39].

Cure Dependent Resin Chemical Shrinkage

Chemical resin shrinkage only occurs during the cure process and ceases once diffusion limitations inhibit further reaction, Region II (Figure 1.4). The volumetric change of a cubic volume element of dimension l_1 by l_2 by l_3 can be expressed in terms of its overall dimensions and the finite dimensional changes in three principal directions, Δl_1, Δl_2, Δl_3, as:

$$\Delta V = l_1 \Delta l_2 l_3 + \Delta l_1 l_2 l_3 + \Delta l_1 \Delta l_2 l_3 + l_1 l_2 \Delta l_3 + l_1 \Delta l_2 \Delta l_3 + \Delta l_1 l_2 \Delta l_3 + \Delta l_1 \Delta l_2 \Delta l_3 \qquad [1.6]$$

An associated change in specific volume, Δv, can be defined in terms of the principal strain components:

$$\Delta v = \frac{\Delta V}{V} = \varepsilon_1 + \varepsilon_2 + \varepsilon_3 + \varepsilon_1 \varepsilon_2 + \varepsilon_1 \varepsilon_3 + \varepsilon_2 \varepsilon_3 + \varepsilon_1 \varepsilon_2 \varepsilon_3 \qquad [1.7]$$

Assuming a uniform strain contraction for all principal strain components, the incremental isotropic shrinkage strain, $\Delta\varepsilon_r$, of a unit volume element of resin resulting from an incremental specific volume resin shrinkage, Δv_r becomes:

$$\Delta\varepsilon_r = \sqrt[3]{1 + \Delta v_r} - 1 \qquad [1.8]$$

The incremental volume resin shrinkage is based on an incremental change in degree of cure, $\Delta\alpha$, and the total specific volume shrinkage of the completely cured resin, v_T, through the following expression:

$$\Delta v_r = \Delta\alpha \, . \, v_T \qquad [1.9]$$

Thermal Expansion Strain

Incremental thermal expansion strains are also computed over each time increment during the cure simulation. They are based on the lamina temperature increment, ΔT, and the instantaneous effective transverse thermal expansion coefficient, α_1. The incremental transverse strain increment is calculated by:

$$\Delta\varepsilon^{th} = \alpha_1 \, . \, \Delta T \qquad [1.10]$$

This work has led to developments in numerical modelling of the cure kinetics and associated chemical and thermal expansion strain. The foreseeable next step in this development is to model the cure kinetics and residual strain to simulate variations in matrix and reinforcement interactions. Applying this analysis to simulated fabric weave patterns has the potential for development of surface roughness prediction. Such a predictive tool would allow detailed studies of the influence fabric weave style and matrix contraction have on resulting surface quality.

1.3.2 *The use of Low Profile Additives for a Reduction in Resin Shrinkage*

To assist in achieving good surface quality and dimensional stability, it is paramount that the polymerising component does not shrink away from the mould surface during cure. Standard unsaturated polyester resins shrink between 6 and 9 % [40, 41], which can be reduced, but not eliminated, by the addition of inert fillers or fibrous reinforcements. The use of low profile additives (LPAs) as thermoplastic modifiers in unsaturated polyester resin, can substantially reduce the shrinkage caused by the copolymerisation between unsaturated polyester and styrene [42, 43]. Other techniques used to address surface quality and shrinkage related problems include:

- In mould coating (gel coat)
- Secondary finishing operations
- Modification of the moulding process, such as variations to mould temperature, pressure, initiator type etc.

These methods are equipment and or labour intensive and LPA remains a cost effective alternative for the formation of low shrinkage or zero shrinkage components.

The function of LPA is to compensate for the thermal and polymerisation shrinkage of the unsaturated polyester resin. However, the LPA does not participate in the free radical polymerisation. Several interpretations regarding the mechanism of volume shrinkage compensation caused by low profile additives have been proposed [44-50]. However, it is generally agreed that a two phase structure must be formed between the LPA and crosslinked unsaturated polyester. Styrene conversion in the initial stage of the reaction causes the LPA to become insoluble and is precipitated [48, 49]. As the polymerisation process continues, the temperature and degree of polymerisation increases causing shrinkage of the unsaturated polyester phase (microgelling). This causes strain relief through microscopic stress cracking between the two phases. As the polymerisation process proceeds, the concentration of microgel increases, leading to a macrogel formation. The increased size of the particles caused by agglomeration causes a competition for space, which creates microvoids. The elevated temperature causes volume expansion of the unreacted monomer trapped inside the thermoplastic shell thereby compensating for polymerisation shrinkage. The coefficients of thermal expansion of the LPA and unsaturated polyester phases are similar above the glass transition temperature (T_g). However, once the temperature is below the T_g, the LPA phase contracts more than the unsaturated polyester, thereby creating more voids. The subsequent microvoid formation at the interface between the LPA and the crosslinked unsaturated polyester phase, as well as microstress cracking formed by contraction of the LPA phase lead to the volumetric shrinkage compensation [46] (Figure 1.7).

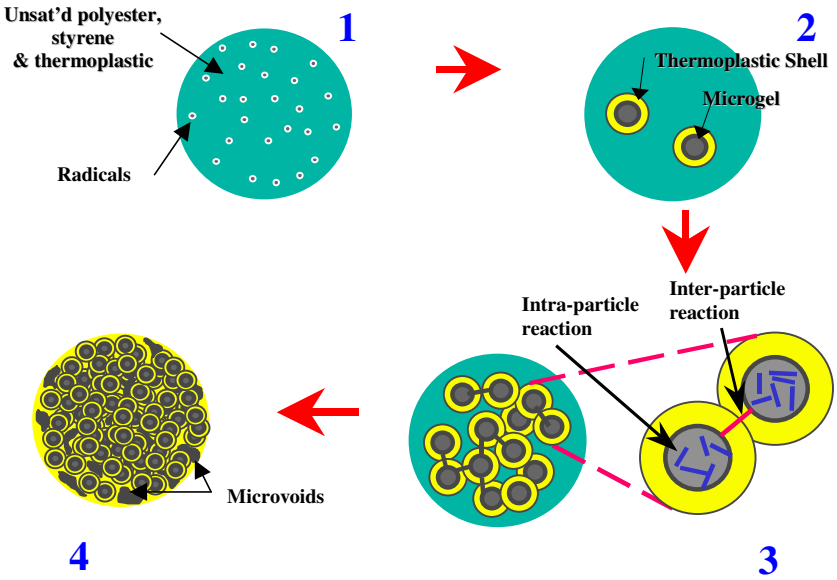

Figure 1.7: Low profile mechanism (1) initiation reaction, (2) microgelling, (3) polarity effect, intra and inter-particle reactions experienced during the polymerisation process (4) the role of the microvoid formation [51].

1) Peroxide decomposition: The unsaturated polyester and styrene react to form a carbon double bond (C=C). Once introduced into the matrix, the peroxide begins to decompose and free radicals attack the carbon double bonds. This results in one free group and one free radical. The radical can then react with the unsaturated polyester and styrene groups to form a chain (3 dimensional polymerisation).

2) High polarity thermoplastics readily form a stable shell structure: In the initial stages of polymerisation, the polyester resin particles form a micro gel surrounded by a thermoplastic shell.

3) Competing reactions – Intra-particle reaction versus inter-particle reaction: Intra and inter particle reactions occur (phase separation) where the stable microgel structures agglomerate to form larger particles (macrogel).

4) Phase inversion and microvoid formation: The agglomerating particles compete for space with the thermoplastic additive. Polarity forces push the LPA towards the outer edges of the structure and form a physical bond with the

polymerising particles. Microvoids are formed by two processes; the agglomeration of particles and polarity of the LPA to the outer surfaces. Microvoids are not usually seen on the outer edges of the structure due to the high thermoplastic content.

LPAs are traditionally used in moulding compounds and more recently in RTM resins. The latter involves generally lower temperatures, which affects the performance of the LPA as heat drives the thermal expansion mechanism. Several thermoplastic additives are commercially available; including polystyrene (PS), polyethylene, poly(vinyl acetate) (PVAc), thermoplastic polyurethane, and poly(methyl methacrylate) (PMMA). Of these, PVAc, PMMA and PS are reported to best control volumetric shrinkage [42]. PVAc is miscible with unsaturated polyester resin and has better compatibility than PMMA.

PVAc has a high viscosity (2.51 Pas), which requires the addition of solvent, such as styrene, to assist in uniform dispersion within the polyester matrix and to create a suitable viscosity for injection and fibre wetting purposes. This increases residual styrene content in the part [52], which has been related to diminished paint quality and increased volatile organic emissions [52-56]. Residual styrene also has potential to oxidise and form benzaldehyde [52, 57]. This further adds to the volatile organic compounds (VOCs) released from a moulded laminate, which aside from being unpleasant to the human respiratory system, also poses a potential health risk [6, 58].

Material characterisation, coupled with numerical modelling [46, 59], has demonstrated the influence LPA has on the cure kinetics of an unsaturated polyester resin. However, a complete understanding of the influence of LPA on residual organic volatiles seems to be lacking. The latter is important to efficient and safe production of low profile laminates. There is also scope for development of alternative means of shrinkage control in unsaturated polyester resins due to potential health risks associated with exposure to increased levels of styrene vapour. Alternative measures such as inert fillers have been employed in the hope

of controlling resin shrinkage whilst minimising VOCs [60, 61]. This has met with limited success as this method only acts as a reactive mass diluent and serves to reduce the mechanical properties of the moulded laminate. Other avenues have been explored here, in particular the use of high aspect ratio silicates which form a nanocomposite structure. The reports of resin immobilisation around the interface of the silicate platelets [62] warrants further investigation into its potential for shrinkage control.

1.4 Theme of this work

The work presented has formed part of a DTI and DfT funded research project entitled 'Affordable Lightweight Body Structures' (ALBOS). Several publications have been produced from this project (listed in Appendix 1). The project was concerned with developing a low cost process for the manufacture of body skins for the automotive industry with high specific structural properties, acceptable cosmetic surface finish and low component cost. The process utilised a proprietary preforming process and impregnation using RTM.

The aim of this thesis was to address problems associated with surface quality measurement and residual volatiles for cosmetic automotive laminates based on low profile unsaturated polyester resin. An initial study into the levelling effects of paint on a laminate surface was conducted to determine the masking capabilities of a coating process. Three surface analysis techniques were then validated for measuring surface quality of bare and painted laminates and compared to industrial standards.

A variety of process conditions and formulation variables were assessed for cure efficiency and volatile organic compound emission of unsaturated polyester impregnated laminates produced using RTM. Thermal desorption and solvent elution techniques were used for the detection of residual volatiles with styrene and benzaldehyde being the main focus. Key areas were identified for optimisation of low profile resin processing which highlight the need for

alternative shrinkage control methods. A novel approach using nanoscale silicate clay was investigated to reduce resin shrinkage within styrene based unsaturated polyester resin. A suitable exfoliation process was established with investigations into volumetric shrinkage, glass transition temperature and mechanical properties of the resulting nanocomposite. This work lead to the study of a series of hybrid matrices consisting of nanocomposite and low profile additive blends. The evaluation techniques developed for surface characterisation, residual volatile detection and mechanical performance were used to demonstrate the effectiveness of the hybrid matrix in producing a cosmetic laminate.

References are included at the end of each chapter.

1.5 References

1. Trewin, E., *The advanced composites industry - Global markets, technology trends and applications 2002-2007*. 2003: Materials Technology Publications. p. 290.
2. Benjamin, B. and Red, C., *Advanced composites global outlook for 2003*, in *Composites fabrication*. 2003. p. 26.
3. Mc Williams, A., *Nanotechnology: A realistic market evaluation*. 2004, Business Communications Company, Inc.: Connecticut. p. 146.
4. Rudd, C.D., Long, A., Kendall, K., and Mangin, C., *Liquid moulding technologies*. 1997, Cambridge: Woodhead publishing limited.
5. Ragondet, A., *Experimental characterisation and modelling of the vacuum infusion process*, in *Mech. Eng., PhD Thesis*. 2004, University of Nottingham: Nottingham. p. 180.
6. Groth-Marnat, G., *Neuropsychological effects of styrene exposure: a review of current literature.* Journal of Perceptual and Motor Skills, 1993. **77**: p. 1139-1149.
7. Cao, X. and Lee, J., *Control of shrinkage and residual styrene of unsaturated polyester resins cured at low temperatures: I Effects of curing agents.* Polymer, 2003. **44**: p. 1893-1902.
8. Warrior, N., Harper, L., Turner, T., Schubel, P., Rudd, C., and Kendall, K. *Affordable Lightweight Body Structures (ALBOS) Dti/DfT Foresight Vehicle Programme*. in *JSAE Japan Society of Automotive Engineers Annual Congress*. 2004. Yokohama: Paper No. 20045470.
9. Castro, J.M. and Griffith, R., *Handbook of engineering polymeric materials / edited by Cheremisinoff, N.P.* 1997: New York. p. 84.
10. *Technology update: compression moulding*, in *Reinforced Plastics*. 2003, Elsevier Science. p. 20-21.
11. Pantelelis, N.G., *Optimised cure cycles for resin transfer moulding.* Composites Science and Technology, 2003. **63**: p. 249-264.

12. Thagard, J.R., Okoli, O.I., Liang, Z., Wang, H.P., and Zhang, C., *Resin infusion between double flexible tooling: prototype development.* Composites: Part A, 2003. **34**: p. 803-811.
13. Kendall, K.N. and Rudd, C.D., *Flow and cure phenomena in liquid composite moulding.* Polymer Composites, 1994. **15**(5): p. 334-348.
14. Shojaei, A., Ghaffarian, S.R., and Katrimian, S.M.H., *Simulation of the three-dimensional non-isothermal mold filling process in resin transfer molding.* Composite Science and Technology, 2003. **63**: p. 1931-1948.
15. Bechet, E., Ruiz, E., Trochu, F., and Cuilliere, J., *Adaptive mesh generation for mould filling problems in resin transfer moulding.* Composites: Part A, 2003. **34**: p. 813-834.
16. Mathur, R., Fink, B.K., and Advani, S.G., *Use of genetic algorithms to optimize gate and vent locations for resin transfer molding process.* Polymer Composite, 1999. **20**(4): p. 224-236.
17. Spoerre, J., Zhang, C., Wang, H.P., and Parnas, R., *Integrated product and process design for resin transfer molded parts.* Journal of Composite Materials, 1998. **32**(13): p. 35-45.
18. Cheung, A. and Pochiraju, K., *Three-dimensional finite element simulation of curing of polymer composites.* Finite Element Analysis and Design, 2004. **40**: p. 895-912.
19. Rouison, D., Sain, M., and Couturier, M., *Resin transfer moulding of natural fiber reinforced composites: cure simulation.* Composites Science and Technology, 2004. **64**: p. 629-644.
20. Starr, T.F., *Composites: A profile of the worldwide reinforced plastics industry, markets and suppliers to 2005*. 2003, Elsevier Science. p. 120.
21. Forsdyke, K.L. and Starr, T.F., *Thermoset resins market report*. 2002, RAPRA. p. 124. http://www.netcomposites.com/netcommerce_features.asp?715.
22. Peters, S.T., *Handbook of composites*. Vol. 2. 1998, London: Chapman & Hall.
23. Tawfik, S.Y., Asaad, J.N., and Sabaa, M.W., *Effects of polyester backbone structure on the cured products properties.* Polymer Testing, 2003. **22**: p. 747-759.
24. Rot, K., Huskic, M., Makarovic, M., Ljubic Mlakar, T., and Zigon, M., *Interfacial effects in glass fibre composites as a function of unsaturated polyester resin composition.* Composites: Part A, 2001. **32**: p. 511-516.
25. Huang, Y.-J. and Leu, J.-S., *Curing of unsaturated polyester resin. Effects of temperature and initiator: 1. Low temperature reactions.* Polymer, 1993. **34**(2): p. 295-304.
26. Caba, K., Guerrero, P., Eceiza, A., and Mondragon, I., *Kinetic and rheological studies of an unsaturated polyester cured with different catalyst amounts.* Polymer, 1996. **37**(2): p. 275-280.
27. Segovia, F., Ferrer, C., Salvador, M.D., and Amigo, V., *Influence of processing variables on mechanical characteristics of sunlight aged polyester-glass fibre composites.* Polymer Degradation and Stability, 2001. **71**: p. 179-184.
28. Tilbrook, D.A., Pearson, G.J., Braden, M., and Coveney, P.V., *Prediction of polymerization shrinkage using molecular modeling.* Journal of Polymer Science: Part B: Polymer Physics, 2003. **41**: p. 528-548.

29. Bogetti, T.A. and Gillespie, J.W., *Process-induced stress and deformation in thick-section thermoset composite laminates.* Journal of Composite Materials, 1992. **26**(5): p. 626-659.
30. Stone, M.A., Schwartz, I.F., and Chandler, H.D., *Residual stresses associated with post-cure shrinkage in GRP tubes.* Composites Science and Technology, 1997. **57**: p. 47-54.
31. White, S.R. and Hahn, H.T., *Process modeling of composite materials: Residual stress development during cure. Part II. Experimental validation.* Journal of Composite Materials, 1992. **26**(16): p. 2423-2453.
32. Bogetti, T.A. and Gillespie, J.W., *Two-dimensional cure simulation of thick thermosetting composites.* Journal of Composite Materials, 1991. **25**: p. 239-273.
33. White, S.R. and Hahn, H.T., *Process modeling of composite materials: Residual stress development during cure. Part . Model formulation.* Journal of Composite Materials, 1992. **26**(16): p. 2403-2421.
34. Lee, S.-Y. and Springer, G.S., *Filament winding cylinders: Process Model I.* Journal of Composite Materials, 1990. **24**: p. 1270-1298.
35. Springer, G.S. *A model of the curing process of epoxy matrix composites*. in *ICCM-4*. 1982. Tokyo.
36. Schapery, R.A., *Thermal expansion coefficients of composite materials based on energy principles.* Journal of Composite Materials, 1968. **2**(3): p. 380-404.
37. Fahmy, A.A. and Ragai-Ellozy, A.N., *Thermal expansion of laminated fiber composites in the thickness direction.* Journal of Composite Materials, 1974. **8**: p. 90-92.
38. Loos, A.C. and Springer, G.S., *Curing of epoxy matrix composites.* Journal of Composite Materials, 1983. **17**: p. 135-169.
39. Yun, Y.-M., Lee, S.-J., Lee, K.-j., Lee, Y.-K., and Nam, J.-D., *Composite cure kinetic analysis of unsaturated polyester free radical polymerisation.* Journal of Polymer Science, 1997. **35**: p. 2447-2456.
40. Murphy, J., *The reinforced plastics handbook (2nd edition).* Elsevier Science, 1998: p. 34.
41. Reddy, J., *Mechanics of composite materials and structures*. 1998, Boston: Kluwer Academic Publishers. 312.
42. Huang, Y.-J. and Liang, C.-M., *Volume shrinkage characteristics in the cure of low-shrink unsaturated polyester resins.* Polymer, 1996. **37**(3): p. 401-412.
43. Kinkelaar, M., Muzumdar, S., and Lee, L.J., *Dilatometric study of low profile unsaturated polyester resins.* Polymer Engineering Science, 1995. **35**(10): p. 823-836.
44. Kinkelaar, M. and Lee, L.J., *Development of a dilatometer and its application to low-shrink unsaturated polyester resins.* Journal of Applied Polymer Science, 1992. **45**: p. 37-50.
45. Atkins, K.E. and Rex, G.C. *The low profile effect, morphology and internal pigmentation, Part II*. in *48th Annual Conference, Composites Institute, The Society of the Plastics Industry*. 1993. Session 6-D.
46. Huang, Y.-J. and Su, C.C., *Effects of poly(vinyl acetate) and poly(methyl methacrylate) low-profile additives on the curing of unsaturated polyester resins. I. Curing Kintetics by DSC and FTIR.* Journal of Applied Polymer Science, 1995. **55**: p. 305-322.

47. Kinkelaar, M., Wang, B., and Lee, L.J., *Shrinkage behaviour of low-profile unsaturated polyester resins.* Polymer, 1994. **35**(14): p. 3011-3022.
48. Hsu, C.P. and Lee, L.J., *Structure formation during the copolymerization of styrene and unsaturated polyester resin.* Polymer, 1991. **32**(12): p. 2263-2271.
49. Bucknall, C.B., Partridge, I.V., and Phillips, M.J., *Mechanism of shrinkage control in polyester resins containing low-profile additives.* Polymer, 1991. **32**(4): p. 636-640.
50. Bartkus, E.J. and Kroekel, C.H., *Low shrink reinforced polyester systems.* Applied Polymer Symposium, 1970. **15**: p. 113-135.
51. Montagne, M., *The low profile effect, morphology and internal pigmentation.* Dow Chemicals, 2001(www.dow.com/info/poly/lp/e34).
52. Reijnders, H., *The influence of cure systems on the formation of volatile components in RTM processed UP articles.* 2001(www.akzonobel.de/).
53. Rodriguez, E.L., *Residual styrene monomer in cured unsaturated polyester resins.* Polymer Materials Science Engineering, 1988. **58**: p. 575-580.
54. Cao, X. and Lee, L.J., *Control of volume shrinkage and residual styrene of unsaturated polyester resins cured at low temperatures. II Effects of comonomer.* Polymer, 2003. **44**: p. 1507-1516.
55. Forrest, M.J., Jolly, A.M., Holding, S.R., and Richards, S.J., *Emissions from processing thermoplastics.* Annals of Occupational Hygiene, 1995. **39**(1): p. 35-53.
56. Yang, X., *Measurement of residual styrene content in unsaturated polyester resin by gas chromatography.* Huaxue Shijie, 1993. **34**(5): p. 220-223.
57. Weir, N.A. and Ceccarelli, A., *Photodecomposition of polystyrene hydroperoxide: Part I - reactions in dilute solution.* Polymer Degradation and Stability, 1993. **41**(1): p. 37-44.
58. Russo, J., Chung, S., Contreras, K., Lian, B., Lorenz, J., Stevens, D., and Trousdell, W., *Identification of 4-(N,N-Dipropylamino) benzaldehyde as a potential reversible inhibitor of mouse and human class I aldehyde dehyrdogenase.* Biochemical Pharmacology, 1995. **50**(3): p. 399-406.
59. Boyard, N., Vayer, M., Sinturel, C., Erre, R., and Delaunay, D., *Analysis and modeling of PVTX diagram of an unsaturated polyester resin, thermoplastic additive, and mineral fillers blend.* Journal of Applied Polymer Science, 2003. **88**: p. 1258-1267.
60. Lucas, J.C., Borrajo, J., and Williams, R.J., *Cure of unsaturated polyester resins: 2. Influence of low-profile additives and fillers on the polymerization reaction, mechanical properties and surface rugosities.* Polymer, 1993. **34**(9): p. 1886-1890.
61. Pietrzak, M. and Szalinska, H., *Reducing the resin shrinkage and setting dose in polyester resins by addition of metal oxides.* Radiation Physics and Chemistry, 1984. **23**(4): p. 409-411.
62. Tsagaropoulos, G. and Eisenberg, A., *Dynamic mechanical study of the factors affecting the two glass transition behavior of filled polymers. Similarities and differences with random ionomers.* Macromolecules, 1995. **28**: p. 6067-6077.

2 Surface Characterisation of Cosmetic Polymer Composites

2.1 Introduction

The term ‘Class A’ has been widely used as a colloquial classification of cosmetic surface quality for automotive exterior body panels. However, type segment, market and brand all influence the definition for a ‘Class A’ standard [1]. A cosmetic polymer composite must compete with existing materials, such as processed sheet steel and aluminium alloys, which have been refined over the past century to form cost efficient, cosmetic structures. Traditional materials and polymer composites exhibit surface characteristics which are induced by material type and or moulding process. These characteristics are either masked or emphasised by a painting process, depending upon the severity and nature of the feature and the gloss of the paint finish.

This chapter seeks to determine the relationship between pre and post-coated surface characteristics for polymer composites. A review of methods for surface characterisation was conducted to determine suitable measurement techniques. The influence of tool surface roughness, tow size and resin shrinkage was also investigated.

2.2 Issues Associated with Coated Polymer Composite Surfaces

Like all processed materials, polymer composites potentially exhibit a range of surface characteristics, which can be attributed to manufacturing, the application of coatings or to a combination of these factors (Figure 2.1). Repetitive features that occur due to the structure of a material or arising from a manufacturing process are amongst the most common defects seen. Fibre composites are susceptible to mould surface effects and the fabric architecture visibility (fibre strike-through). Reproduction of the tooling surface is normal for polymer mouldings due to the low viscosity of the resin. Tool surface conditioning through milling or grinding processes contribute to the repetitive surface defects on the moulded article. Significant improvements in surface characteristics have been

observed when processing with polished tool surfaces (*Ra* = 0.25 µm) as opposed to ground flat tools (*Ra* = 0.63 µm) [2]. Consolidation pressure has also been found to influence the reproduction of the tool surface roughness [2, 3].

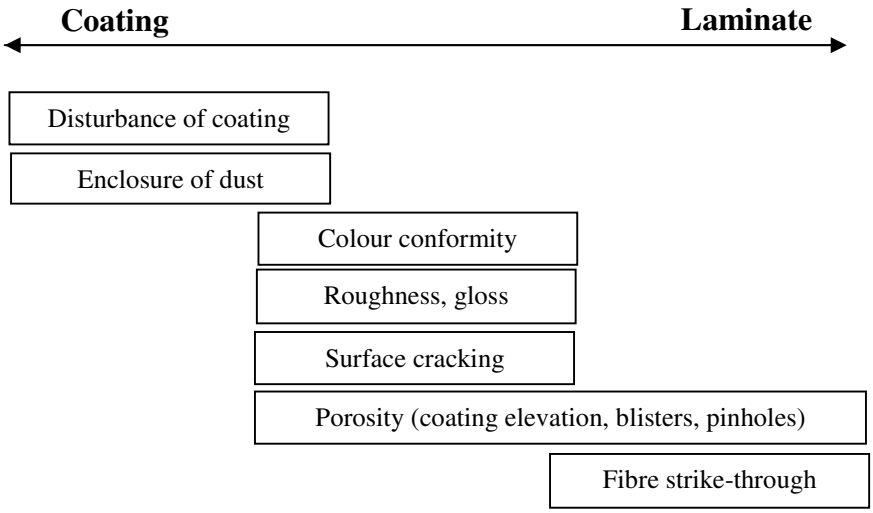

Figure 2.1: Allocation of surface defects on coated laminates [1].

Fibre strike-through (Figure 2.2) is a well documented problem and is influenced by volumetric changes in the matrix due to polymerisation shrinkage and thermal expansion of the matrix (Section 1.3.1). Contraction of localised resin rich regions around overlaying tows cause regular surface patterns relating to the fabric architecture (Figure 2.3).

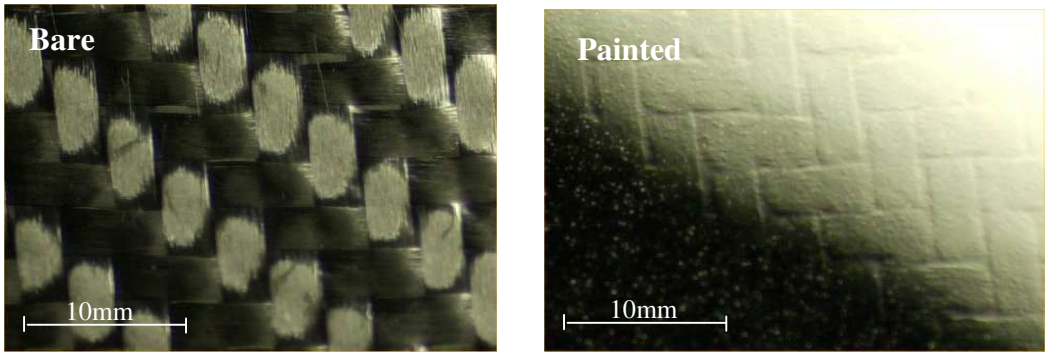

Figure 2.2: Fibre strike-through evident in a 2x2 twill weave carbon fabric (HTS 5631) moulded with a vinyl ester matrix resulting in a fibre volume fraction of 43 %, and coated in an automotive paint process using high gloss clear polyurethane top coat.

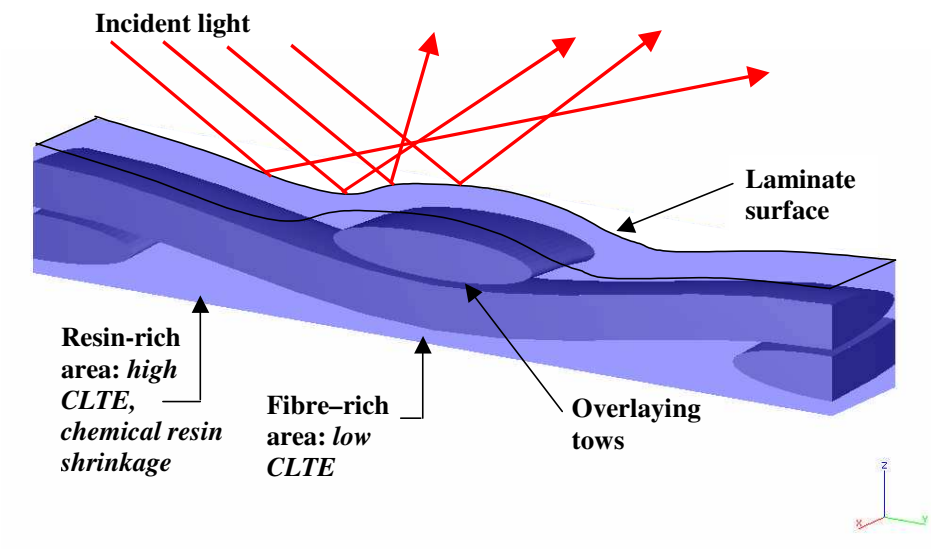

Figure 2.3: Schematic drawing of a woven laminate illustrating the fibre strike-through phenomenon for a thermosetting matrix.

Porosity is a common manufacturing induced defect in composites. Voids are formed primarily due to air entrapment in resin rich regions, moisture absorption and volatile release [4, 5]. Surface voids cause pinholes after painting (Figure 2.4). A pinhole is formed due to a discontinuity in wet or dry film, resulting from the failure of liquid film former to wet a pinpoint area [6]. Stoving during paint curing may also promote pinhole formation [1]. Surface air entrapment can also cause an elevation of the coating or destroy the coating layer due to the expansion of the entrapped air- blistering.

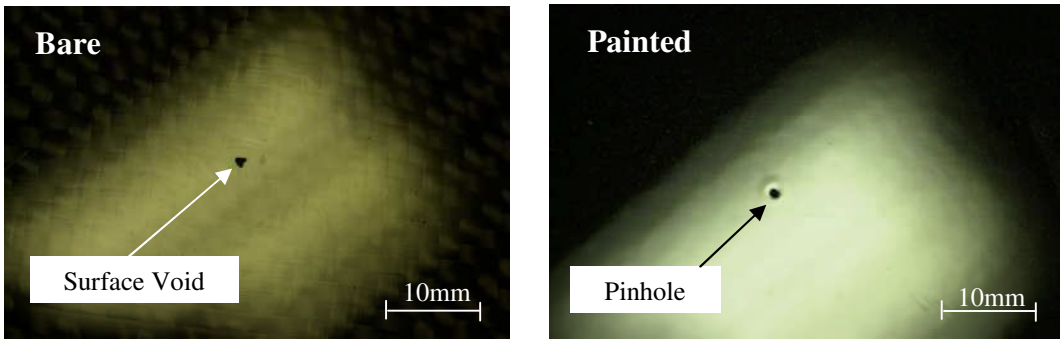

Figure 2.4: The formation of a pinhole on a painted laminate due to a surface void created during moulding. This picture is of the same area of a laminate, pre and post-painting, moulded using 2x2 twill weave carbon fabric and epoxy resin in an RTM process.

Dimensional distortion may be observed due to matrix shrinkage and this is amplified by asymmetry in the part geometry or the ply lay-up. [7-12]. This characteristic not only influences surface quality but also affects dimensional control. Longwave ($\lambda > 10$ mm) characteristics are immediately obvious to the naked eye and generally require major rework to form a satisfactory body skin [13].

2.3 Methods for Measuring Surface Quality

Surface quality measurements and specifications impact many automotive products but particularly bearing surfaces and cosmetic components. Each surface has a specific characteristic and functionality with some proving difficult to estimate and quantitatively measure. Hence, a wide range of measurement techniques and statistical methods for topographic analysis has evolved. Surface irregularities can usually be classified into three categories, as illustrated in Figure 2.5:

- **Roughness:** irregularities less than 0.8 mm in amplitude.
- **Short term waviness:** surface characteristics less than 1mm in amplitude and 3 mm in wavelength.
- **Long term waviness:** shape deviations or undulations affecting large-scale flatness, generally having a wavelength greater than 10 mm.

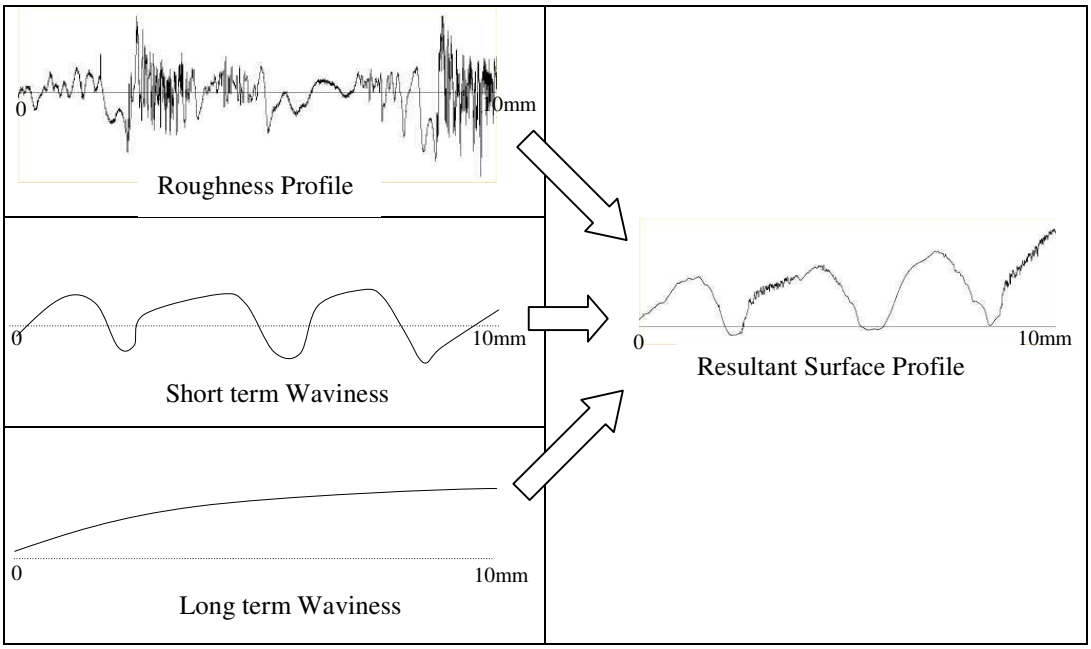

Figure 2.5: Resultant surface profile broken into the 3 main elements: roughness, short-term waviness and long-term waviness.

2.3.1 *Surface Roughness*

Roughness is a primary measure for surface quality and is extensively used to characterise engineering components. Measurements are made by passing a stylus tip or laser over a surface. The resulting roughness profile is derived from a primary profile by suppressing the longwave component using a profile filter [14]. A filter normalises the primary profile within set boundary conditions to eliminate the waviness component. Statistical manipulation of the amplitude and spacing for each point generates numerous surface characterisations [14]. Surface roughness can be characterised by three general parameters:

- **Amplitude:** measure of the vertical characteristics of the surface deviations with respect to the mean line.
- **Spacing:** measures of the horizontal characteristics of the surface deviation with respect to the mean line.
- **Hybrid:** combination of amplitude and spacing parameters.

Roughness can be characterised by *'R'*, which is the average depth of the characteristic features [15]. A range of roughness parameters [16] are used.

However, not all are applicable to cosmetic composite surfaces due to their localised representation or hybrid spacing analysis. The literature suggests that, potentially, seven parameters are suited to characterisation of polymer composite laminates [1-3, 15, 17]:

- ***Ra*:** the arithmetic mean of the departures from the roughness profile line.
- ***Rz*:** the average height difference between the five highest peaks and five lowest valleys.
- ***Rt*:** the sum of the height between the highest peak and lowest valley from the mean line.
- **Peak count (*Pc*):** the number of peak and valley pair cycles per centimetre along the profile length.
- **Peak height (*Rp*):** the maximum value of the profile deviations from the mean line.
- **Skewness (*Rsk*):** the degree of bias either in the positive or negative direction from the mean line.
- **Kurtosis (*Rku*)**: the degree of concentration around the mean line of a roughness profile.

One of the most common and universally recognised parameters for roughness measurement is *Ra* - the arithmetic mean of the departures of the roughness profile from the mean line within the evaluation length *L* [16] (Figure 2.6) (Equation 2.1). The evaluation length (*L*) is dependant on surface characteristics in question, but in practise is also restricted by processor memory. Generally the evaluation length is maximised to encompass a representative section.

$$Ra = \frac{1}{n}\sum_{i=1}^{n}\left|Y(i)\right| \qquad [2.1]$$

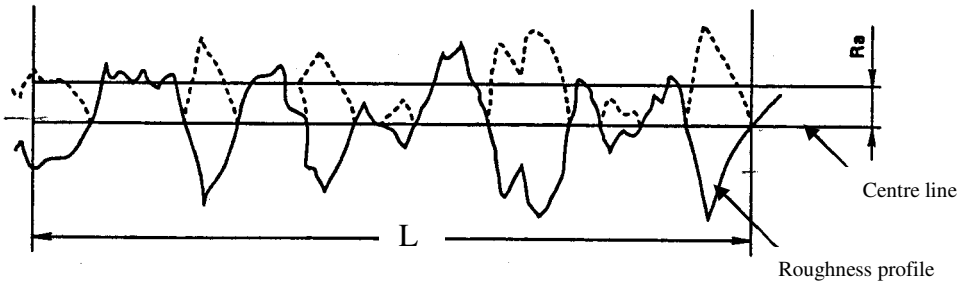

Figure 2.6: A roughness profile showing superimposed peaks for calculation of *Ra.*

Ra is the most widely used parameter for measuring polymer composite surface quality. It is simple, widely understood and allows cross-referencing of results with existing metallic and non-metallic materials. However, there is no reported use of *Ra* for measuring paint surface quality. Literature has suggested that the effects of paint are best measured by surface mapping or utilising wavelength parameters [1, 13, 18].

Surface mapping is obtained by stitching like surface roughness traces together to represent the surface topography (Figure 2.7). This process allows detailed representation of the surface characteristics and calculates the numerical parameters based on a greater area. The improved graphical representation comes at a cost, as in 2004 a laboratory grade 3D topographer cost £90k compared to £4k for an equivalent 2D profilometer.

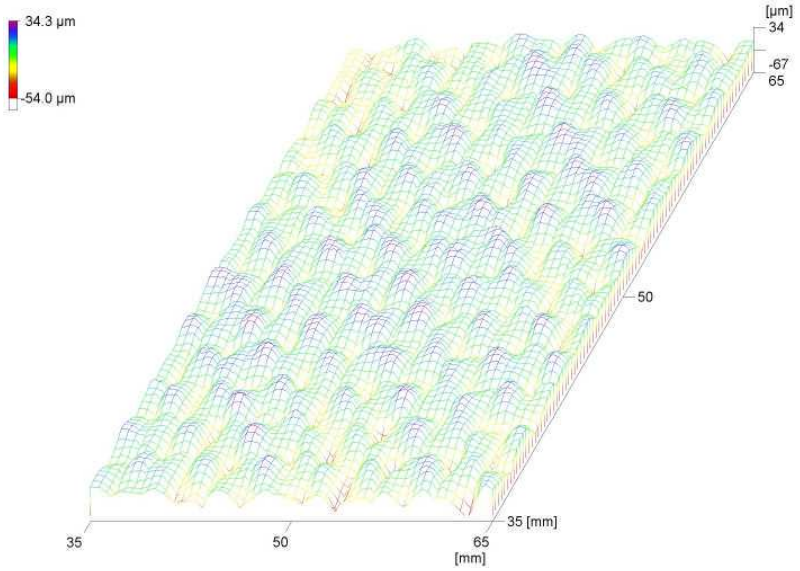

Figure 2.7: 3D stylus topography created by stitching 2D fields which shows extensive detail of the surface characteristics. The image is of a 3k, 2x2 twill carbon fabric with a vinyl ester matrix produced using RTM. ***(Courtesy of Ford Motor Company)*****.**

2.3.2 *Short and Long-Term Waviness*

Waviness is a surface characteristic that is primarily associated with highly polished or high gloss surfaces and arises from scattering light or dark patterns reflected from a surface when viewed under a light source (Figure 2.8) and is extensively used in the paint industry to characterise surface quality. The distortion resulting from the scattering of the reflected light is generalised under two categories: short-term and long-term waviness. Short-term waviness is created by surface irregularities with wavelengths (λ) between 1 and 3 mm and is generally below 1 mm in amplitude. This style of surface characteristic is most obvious to the human eye at distances less than 40 cm from the source. This is close to the maximum ocular resolution and appears as a distortion of the outline (fuzziness). Long-term waviness is associated with wavelengths greater than 10 mm and can be seen by the human eye at approximately 3 m from the source [19] (Figure 2.9).

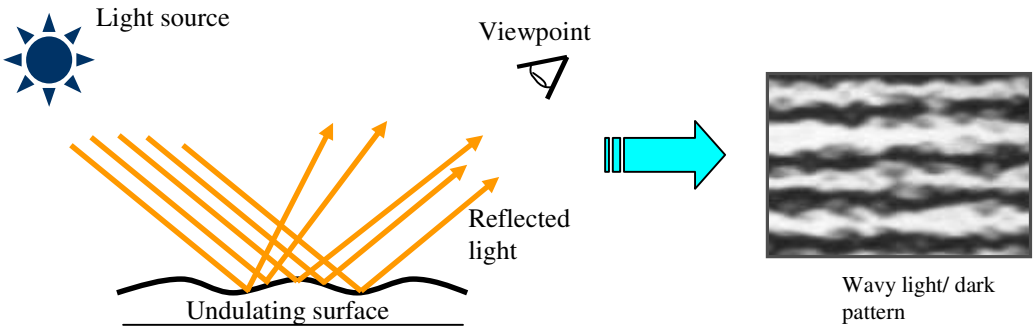

Figure 2.8: Schematic representation of the reflected light patterns seen from and undulating surface.

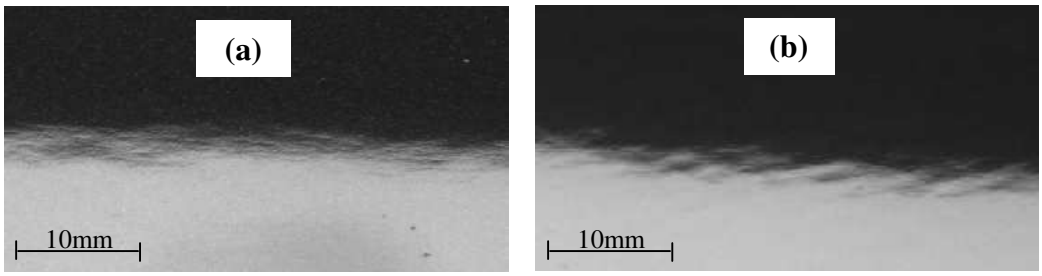

Figure 2.9: The two types of waviness seen by the human eye: (a) short term waviness (λ ≤ 1mm), (b) long term waviness (λ ≥ 10mm). The two laminates were painted with a high gloss dark base and photographed under a florescent light.

Short and long-term waviness are further divided into five wavelength categories labelled $W_{a\text{-}e}$, which span the visible spectrum (Figure 2.10). This is used to define the spectrum in which both short and long-term waviness lie. Figure 2.10 illustrates that each is associated with wavelengths approximately between 0.3 to 1.2 mm and 3 to 30 mm respectively. In addition to the visible spectrum ($W_{a\text{-}e}$), a non-visible wavelength (dullness) is used to assess the sharpness of the image. Image sharpness is produced by a reduction in contrast due to light scattering by surface structures below 0.1 mm wavelength. Surface analysis techniques utilise a combination of the six spectra (Dullness, $W_{a\text{-}e}$) to create hybrid wavelength parameters used for characterising the surface structure. Two commonly used systems include *Distinctness of Image* (DOI) [13] and *Combined Ford* (CF) [20].

The *Combined Ford* reading was derived for the purpose of replacing the *Quality Measurement System* (QMS) analysis, which was used from 1982 till 2001 by the majority of automotive companies for paint quality measurement. The *Combined Ford* parameter relates to the level of reflectivity of the painted surface and is a weighted value that relates dullness and $W_{a\text{-}e}$. This inverts the short and longwave readings; hence a higher value indicates an improved surface quality.

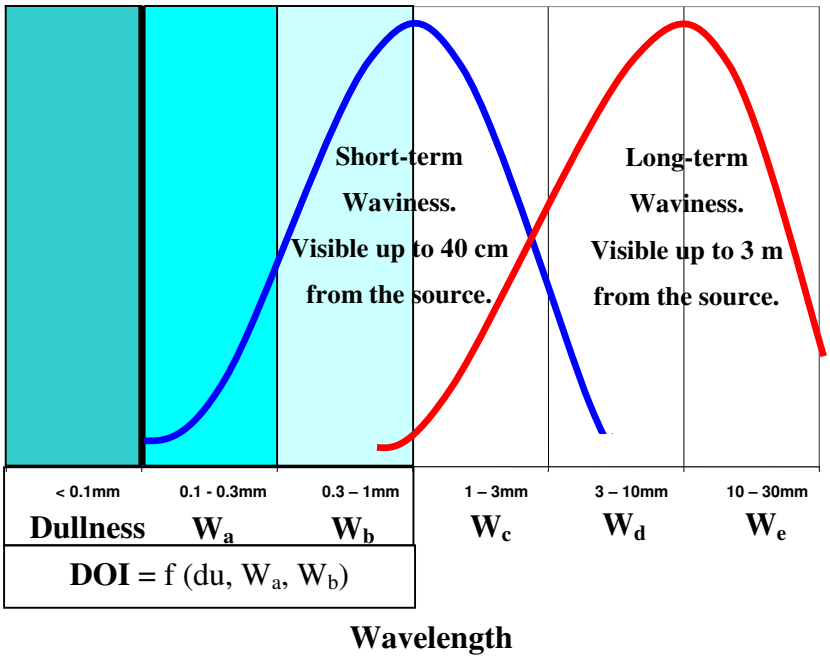

Figure 2.10: The spectra of wavelengths associated with short and long-term waviness. The use of dullness, W_a and W_b to form the DOI is illustrated.

2.4 In House Industrial Standards

Acceptable limits of surface waviness depend on manufacturer, proposed market and segment type; and this, to some degree, influences the showroom price of a vehicle. The *Combined Ford* measurement is a widely recognised standard and allows a direct comparison of acceptable paint quality between market types. It is shown in Table 2.1 that not only vehicle type, but also paint type and position of the panel (Figure 2.11) influence the expected paint quality. Subjective in-house industrial trials conducted by Ford Motor Company suggest that lighter metallic shades hide surface imperfection better than darker solid based systems [20]. The choice of paint style or colour allows for a 10 % variation in *Combined Ford* readings. Similarly, vertical surfaces are less likely to reflect light at a low angle

to the observer and are allowed approximately 10 % increase in *Combined Ford* value as opposed to the highly reflective and visible horizontal surfaces. It has been shown that acceptable paint quality threshold (via *Combined Ford*) can vary by 20 % depending on the vehicle, paint type and scan position.

Polymer composites studied here are derived from those intended for low volume, prestige vehicles. Therefore, the coated surfaces were compared to the most stringent scenario, which is a *Combined Ford* reading greater than 65 pts. The prestige vehicle sector also utilises short and long-term waviness measurements for analysis of the painted surfaces. Acceptable short and long-term values are below 20 and 8 pts respectively [20].

Table 2.1: Acceptable *Combined Ford* (CF) readings for different vehicles, paint types and positions. *(Courtesy of Ford Motor Company).*

Vehicle Type	Paint Type	Combined Ford Reading Horizontal (pts)	Combined Ford Reading Vertical (pts)
Commercial	Light metallic	> 53	> 44
	Dark metallic	> 58	> 49
	Light solid	> 58	> 49
	Dark solid	> 60	> 50
Passenger	Light metallic	> 58	> 49
	Dark metallic	> 63	> 53
	Light solid	> 63	> 53
	Dark solid	> 65	> 55
Prestige	General	> 65	> 65

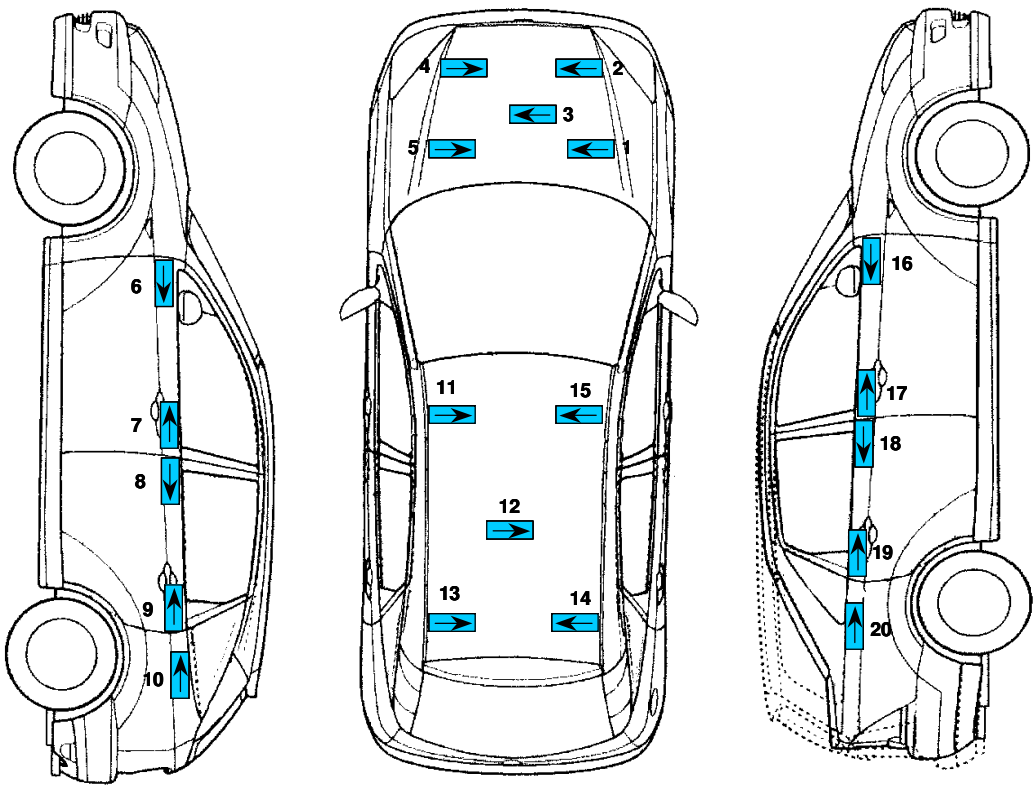

Figure 2.11: Measurement positions for a standard automotive paint analysis. Arrows indicate the scan direction. ***(Courtesy of Ford Motor Company).***

This section has drawn attention to the prevailing surface quality issues associated with polymer composites when used in cosmetic applications. The review reveals a variety of surface characteristics, techniques and some application data relating product quality against various standards. However, most of the available data relate to finished painted surfaces. One of the objectives here is to characterise materials and moulding processes and therefore it was determined to try to isolate the influence of the paint in determining the final surface profile.

Clearly, mould tool surface quality will influence laminate surface quality, but studies have not demonstrated the knock-on effects on resulting paint quality. It is necessary to investigate tool induced defects and the effectiveness of paint levelling. Hence, it was determined to study a range of tooling surfaces with a

varying degree of surface finishes and measure the associated effects on the moulded and painted article.

Literature has linked fibre strike-through and other prevailing defects to variations in matrix and fibre expansion. The damaging effect this has on surface quality has been shown but the degree in which matrix shrinkage (thermal and chemical) influences surface quality and resulting paint quality is unclear. Similarly, fabric architecture is believed to influence fibre strike-through and subsequent surface quality through changes in relative matrix and fibre rich regions. A measure of the prevailing surface quality and influence of paint on the variations in matrix volume and fibre structure is necessary to assist understanding of the relative influences to assist in suitable material selection.

2.5 Experimental Methods

2.5.1 *Materials*

An extensive range of materials were investigated throughout the surface quality study. However, a representative selection are presented here. The following materials were studied due to their existing association with automotive manufacture either within body panelling systems or structural components. A summary of materials in Table 2.2 shows a selection of thermoset matrix composites. Conversion processes included compression moulding, vacuum bagging and RTM. Strip steel was used as the reference material.

C1

Low alloy automotive strip steel was supplied by Corus at 0.7 mm thickness with an untreated surface. The elemental analysis was [21]: C 0.06, Mn 0.2, S 0.01, P 0.010, Si 0.009, Al 0.058, N 0.005. The maximum yield stress was 280 MPa and a ultimate tensile strength (UTS) was between 270 and 410 MPa. This material is commonly stamped to form body panelling for high volume production. (i.e. for mainstream passenger vehicles)

C2

The system denoted by *C2* is a low profile unsaturated polyester matrix with random E-glass preform processed by RTM (Section 2.5.2). The resin (Crystic® RT2557) was supplied by Scott Bader Company Ltd with a number average molecular weight between 800 and 900 g/mol and the equivalent molecular weight /mol C=C between 200 and 250 g/mol. Styrene to unsaturated polyester molar ratio was in the range of 1.8 to 2.0. A low profile additive, PVAc (43,043-9), was supplied by Dow Chemicals and included at 30 wt% to the base system. This was dispersed by shear mixing at 2000 rpm for 5 minutes. Akzo Nobel supplied tertiary-Butyl peroxybenzoate (TBPB) initiator in 80 % solution with acetylacetone (Trigonox® 93). 0.5 % cobalt accelerator G was required for the two stage peroxide initiator and was supplied by Scott Bader Company Ltd. Calcium carbonate ($CaCO_3$) filler with a 5.7µm nominal particle size was supplied by Omya UK Ltd and used at 30wt% of resin. Flat plaque preforms were produced using a proprietary chop and spray system developed by Ford Motor Company. The preforms were produced from E-glass fibres (OC R25H 1200 tex) to an areal density of 2875 g/m^2 with 1.6 wt% epoxy powder binder (Pretex 110). Chop-strand E-glass surface veil (OC 950A-AB 3307 tex) at an areal density of 150 g/m^2 per layer was used on both sides of the preform. The structural glass and surface veil were processed to provide a nominal fibre volume fraction of 25 % and thickness of 5 mm.

C3

The semi-preg (supplied by SP Systems) was a 6k carbon ST85 epoxy based on 300 gsm high strength carbon (230 GPa modulus, 3.5 GPa UTS). The weave style was 2x2 twill with 3.7 ends/cm and equal fibre weights in the 0˚ and 90˚ directions of 149.1 g/m^2. The epoxy matrix was SE84 with 42 % resin content at manufacture. The B-stage cured epoxy resin film was laminated between dry carbon fabric reinforcement (SPRINT® ST85), which sandwiched a 1 mm syntactic core (Figure 2.12). A sandable E-glass (CBS) surfacing film (700 gsm) sandwiched with epoxy film and was used on the ‘A’ surface. The semi-preg was consolidated using the vacuum bag process described in Section 2.5.2.

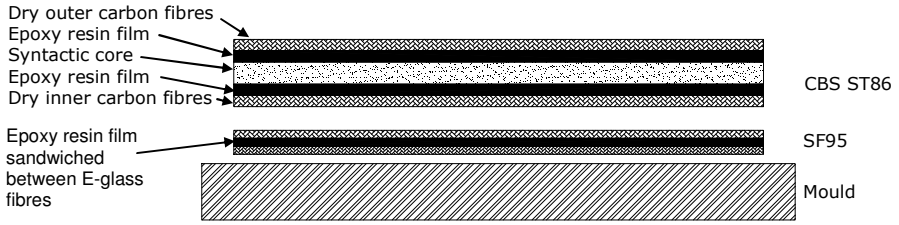

Figure 2.12: Schematic of semi-preg lay-up.

C4

The system denoted by *C4* was a pre-preg (supplied by SP Systems) based on a 6k, 300 gsm, high strength carbon (RC300) (230 GPa modulus, 3.5 GPa UTS). The weave style was 2x2 twill with 3.7 ends/cm and equal fibre weights in the 0˚ and 90˚ directions of 149.1 g/m^2. The epoxy matrix was denoted SE84 with 42 % resin content at manufacture and consolidated using a vacuum bag process (Section 2.5.2).

C5

A sheet-moulding compound manufactured by Hexcel Composites was compression moulded (Section 2.5.2), to produce a 2 mm thick laminate. The epoxy sheet-moulding compound was made from plane random 50 mm × 8 mm strips of chopped carbon fibre prepreg Fortafil® 503 fibres and formulated with an internal release agent. The areal weight off the roll was 2000 g/m^2, and the nominal fibre volume fraction was 57 %.

C6

The vacuum infusion (VI) laminate used the same fabric as the pre-preg system (*C4*) but the epoxy matrix was a low cost system formulated by Hexcel Composites under the product name DLS 1648. This comprised 10-30 wt% butanedioldiglycidyl ether, 1-10 wt% triglycidyl-P-aminophenol and 60-100 wt% epoxy resin. Part B comprised 60-100 wt% 1,2-diaminocyclohexane, 10-30 wt% 2-piperazin-1-ylethylamine, 1-15 wt% polyoxyalkyleneamine and 10-30 wt% 2,4,6-tris(dimethylaminomethyl)phenol. The VI laminate was produced using the

vacuum bag process described in Section 2.5.2 with a cure schedule of 2 hours at 90 ºC.

The 3k, 6k and 12k carbon fabrics were used with unsaturated polyester and epoxy resin and processed by RTM. The carbon reinforcement was supplied by Tenax Fibers® with a 2x2 twill weave. The unsaturated polyester resin (HS) was the same system as the base orthophthalic resin (without PVAc) used in *C2*. The epoxy system (LS) was the DLS 1648 used in *C6*.

Table 2.2: Constituents used in surface quality trials.

Sample ID	Material	Manufacturer	Tow Size (K)	Weave Style	Areal Fibre Mass (gsm)	Resin Type	Moulding Process
C1	Uncoated $FeP0_4$	Corus	-	-	-	-	-
C2	E-glass preform + E-glass surface veil	Scott Bader (resin) Sotira (fibre)	-	Random mat	3025	Ortho UP, 30wt% PVAc, 30wt% $CaCO_3$	RTM
C3	Sprint® ST85 CBS SF95	SP Systems SP Systems	6 E-glass	2x2 twill Continuous	600	ST 86 S2	RFI
C4	RC300 carbon	SP Systems	6	2x2 twill	600	ST85	Vacuum bag
C5	Carbon SMC	Hexcel	50x8mm strips	Random mat	-		Compression moulding
C6	RC300 carbon	SP Systems/Hexcel	6	2x2 twill	600	DLS 1648 (epoxy)	Vacuum Infusion
3k HS	Style 452 carbon	Tenax Fibers	3	2x2 twill	200	RT2557 (polyester)	RTM
6k HS	Style 428 carbon	Tenax Fibers	6	2x2 twill	285	RT2557 (polyester)	RTM
12k HS	Style 424 carbon	Tenax Fibers	12	2x2 twill	660	RT2557 (polyester)	RTM
3k LS	Style 452 carbon	Tenax Fibers	3	2x2 twill	200	DLS 1648 (epoxy)	RTM
6k LS	Style 428 carbon	Tenax Fibers	6	2x2 twill	285	DLS 1648 (epoxy)	RTM
12k LS	Style 424 carbon	Tenax Fibers	12	2x2 twill	660	DLS 1648 (epoxy)	RTM

2.5.2 *Moulding Process*

Resin Film Infusion

The pre-preg and semi-preg systems were processed by vacuum bagging to consolidate the fabric preform on a 600 x 600 x 5 mm tempered glass plate, heated by a silicon rubber mat (CAL9500) rated at 750 W. The surface temperature was controlled by a CAL9500P programmable process controller. A thermocouple was centrally positioned in the vacuum bag to verify the laminate temperature. Thermal images of the glass tool taken at 80 ºC and 120 ºC (Figure 2.13) show a working area of 450 x 450 mm without a significant temperature gradient.

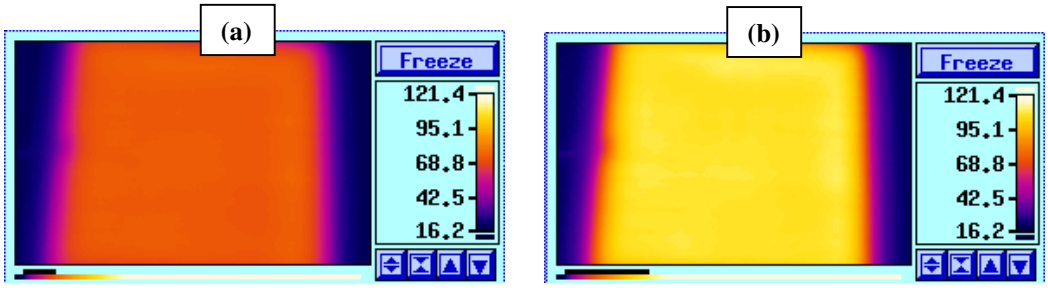

Figure 2.13: Thermal image of glass moulding plate at (a) 80 ºC (b) 120 ºC.

The charge was positioned centrally on the glass plate (Figure 2.14) then covered by a dry polyamide peel ply membrane (Stitch ply A). This was then covered by a perforated release film (WL3600 P90), single breather layer (Ultraweave® 606) and a bagging film (WN1500). The bagging film was sealed using a mastic tape (AT140). A vacuum of 950 mbar was maintained until the surface temperature had fallen below 40 ˚C, whereupon the part was demoulded. The average overall cycle time was 3 hours 15 minutes as shown by Figure 2.15. Both samples were postcured for 2 hours at 90 ºC using the process described in Figure 2.16.

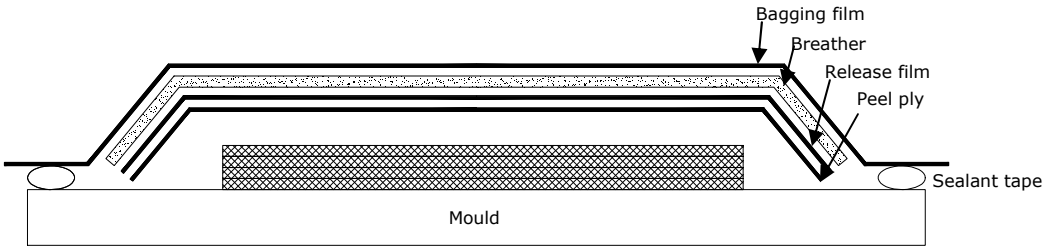

Figure 2.14: Schematic of prepreg moulding technique.

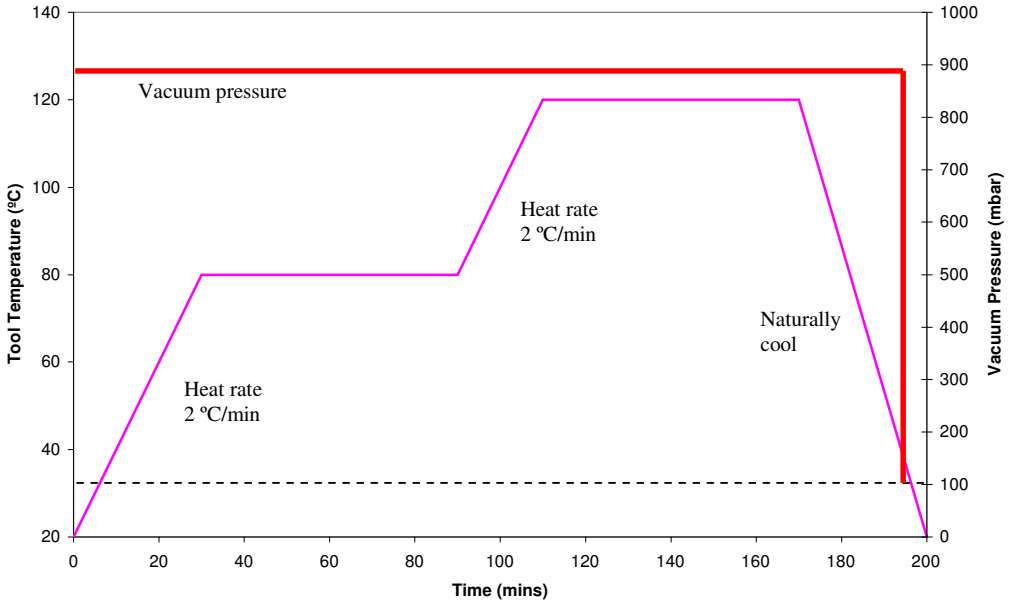

Figure 2.15: Representative moulding cycle–pressure, temperature schedule.

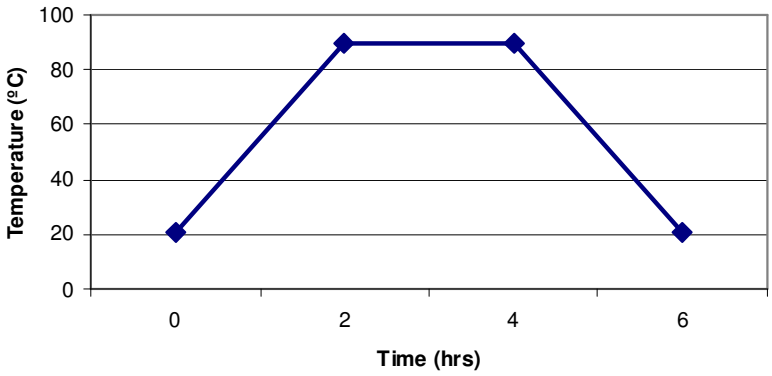

Figure 2.16: Postcure process.

Resin Transfer Moulding

The RTM laminates were produced in a 737 x 500 mm picture frame mould tool (Figure 2.17), produced from monolithic steel and mounted in a hydraulic manipulator [22]. The lower platen was ground, polished and chromium plated to produce a final surface roughness of *Ra* 0.07 µm. An array of thermocouples and pressure transducers were incorporated into the tool design to generate process data. Test laminates were impregnated in a preheated mould at 95 ºC. The resin was introduced along an edge gate using a pressure pot held at 500 kPa then sealed prior to polymerisation. All samples were postcured using the process described in Figure 2.16.

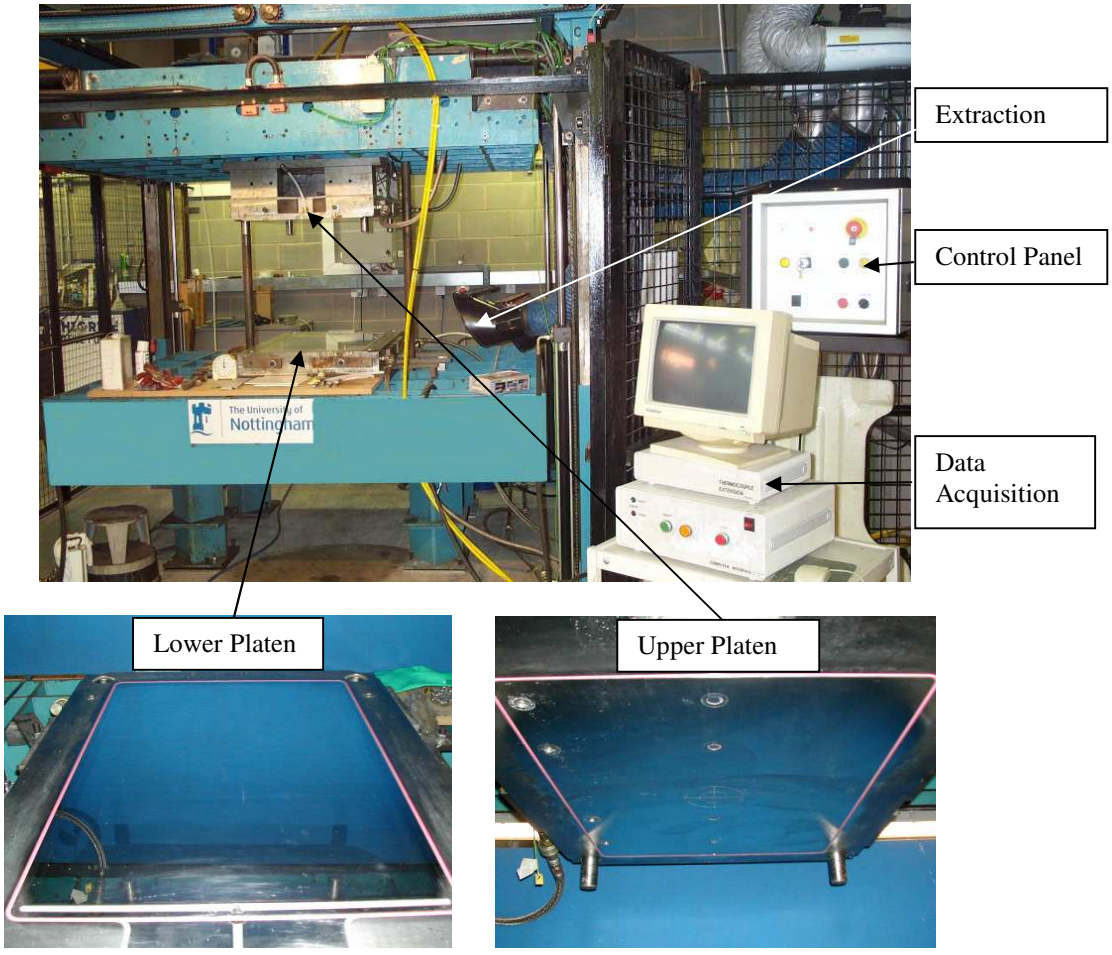

Figure 2.17: RTM manipulator, Lower and upper moulding platens.

Compression Moulding

The SMC was processed by compression moulding in a Bradley & Turton 150 tonne hydraulic transfer moulding press. The steel tool (265mm×125mm) was ground to 0.53 µm *Ra* and heating was provided by two 250 W cartridge heaters per platen [23]. A charge sufficient enough to cover 80 % of the mould surface was used to account for flow. The compression moulding compound was placed in the pre-heated press at 120 ºC and consolidated at 5 MPa clamping pressure based on the tool surface area. It was heated for 5 minutes and then demoulded to produce a 2 mm laminate.

2.5.3 *Paint Process*

The laminates were cut to 300 x 210 mm using a water-cooled diamond coated circular saw. Conventional 3M® masking tape was used to blank half of each laminate before being put through a representative automotive painting cycle (Figure 2.18) at Aston Martin Lagonda. A summary of the paint layers and products are shown in Table 2.3. All products used in the painting cycle were supplied by PPG Industries. The panel was degreased with solvent (PPG D846), keyed using a 3M® sanding sponge (P400) then degreased again. Two coats of high build acrylic primer (PPJ D839) were sprayed to obtain a film build of 80 µm. This was then baked at 80 ºC for 20 mins. Once cooled, the surface was lightly sanded with P400 paper and an acrylic sealing primer (A3877P6653/SK) was applied and baked, followed by a light sanding with P400 paper. Two base coats of dark waterborne paint (PPJ Envirobase colour) and two coats of clear polyurethane (PPJ ECC 38010/XK) were applied with each clear coat being baked at 80 ºC for 20 mins. The total average film build was 160 µm with the individual coating thickness for each panel being detailed in Appendix 2. The panels were not flattened or polished after the paint process.

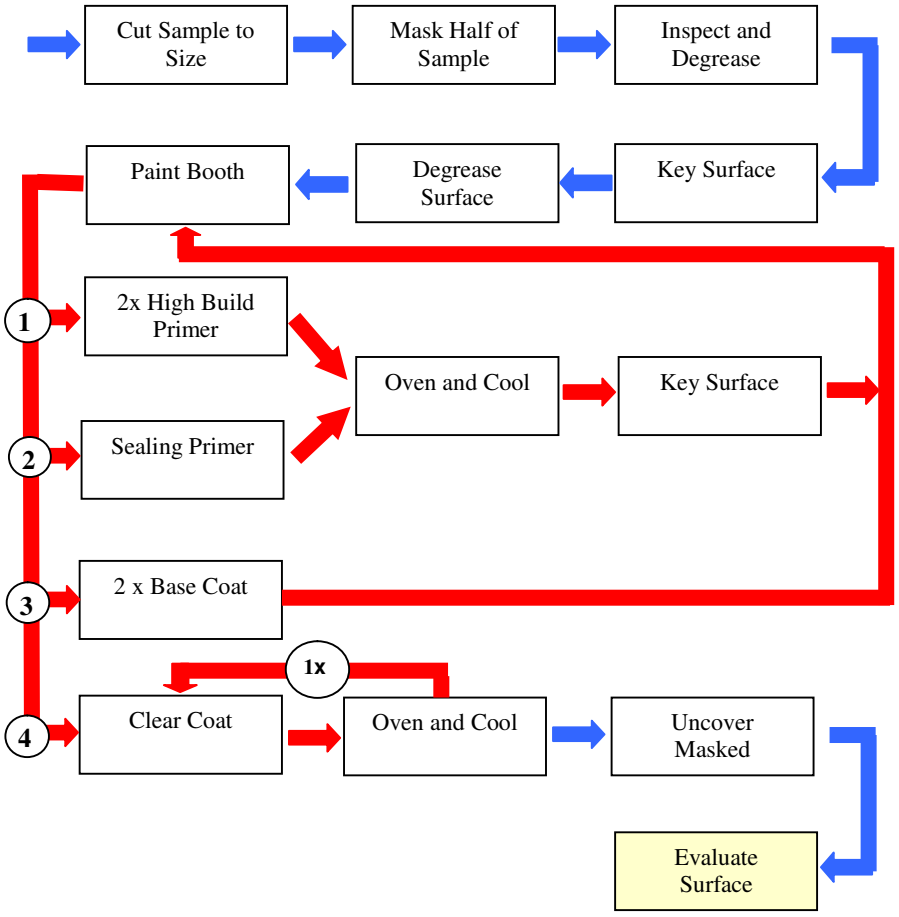

Figure 2.18: Flow chart of the paint cycle used at Aston Martin Lagonda.

Table 2.3: Coating processes and associated product type.

Coating Process	Paint Type	Supplier	Product Code	Average film thickness (µm)
High build primer	Acrylic	PPG Industries	PPJ D839	80
Sealer primer	Acrylic	PPG Industries	A3877P6653/SK	28
Dark Base	Waterborne	PPG Industries	PPJ Envirobase colour	10
Clear coat	Polyurethane	PPG Industries	PPJ ECC 38010/XK	53

2.5.4 *Surface Evaluation*

Once the paint process was complete, the laminates were analysed to determine the surface characteristics of the bare and coated sections. In each experiment, an

average of 5 repeats were systematically taken from various locations on the sample to obtain an average reading.

Optical Microscopy

Optical microscopy using a Zeiss Axiolab microscope was used to assess the potential levelling effects of paint layers. A 10 x 20 mm sample was cut from the painted section and mounted using an unfilled polyester resin (supplied by Reichhold) and was initiated by 2 wt % of Butanox M50 (supplied by Akzo Nobel). Upon demould, the samples were polished using a Struers® DAP-7 laboratory polisher equipped with an automatic holder (Struers® Pedemin-S). The cast samples were consecutively ground and washed using abrasive waterproof papers from 240, 600, 1200 and 2400 grade.

Stylus Profilometry

Stylus profiling was used to measure the surface roughness of the bare and painted laminates. A Mitutoyo Surftest SV622 profiler with 5 µm stylus (996133-996153) and auto drive unit was used to measure an evaluation length of 12.5 mm at a speed of 0.5 mm/s and pitch of 0.8 µm. A cut-off length of 0.8mm was used to exclude surface waviness and a Gaussian filter was applied.

Light Reflectometry

The surface waviness of the painted laminates was measured using a BYK Gardner Wavescan DOI with a built–in laser diode light source and an optical sensor. Scans in the x and y directions were taken over a scan length of 100 mm to obtain an average value. The Wavescan DOI returned longwave, shortwave, *Combined Ford* and the full wave spectrum from Wa-e. The data were manipulated using Autochart® 2.20 software which normalises all readings to a scale ranging from 0 (smooth) to 100 (highly structured).

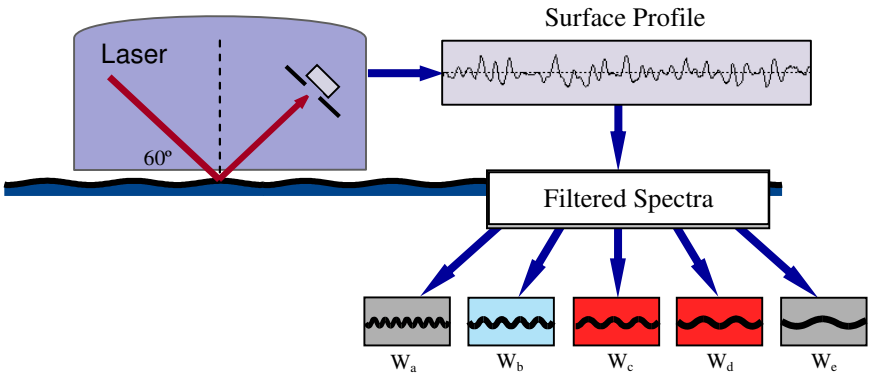

Figure 2.19: Laser measurement principle of the BYK Gardner Wavescan DOI®.

Subjective Assessment

Visual assessment of the laminates was conducted to characterise paint surface quality in order to relate human visual perception to machine sensitivity. The laminates were assessed under fluorescent light to determine the visibility of the defects on the painted surface as a direct result of imperfections seen on the bare laminate. The laminates were rated into 2 categories: acceptable and unacceptable paint quality, by four people (details in Appendix 3) who each had a minimum of five years experience in the field of automotive coating processes. The appraisers assessed the painted laminates under the same conditions and each appraiser rated the surface twice with a three-hour interval between tests. Statistical analysis was conducted on the observations using MiniTab® software to determine the repeatability of each appraiser and the reproducibility between appraisers.

2.6 Results and Discussion

2.6.1 *Levelling Effects of Paint on Polymer Composite Surface Structure*

The levelling effect of paint on the surface characteristics of a polymer composite was investigated using three-dimensional topography. A carbon 2x2 twill weave fabric with a vinyl ester matrix, processed by RTM was used as a representative laminate. Readings were taken from a representative section of laminate before and after the paint process. A comparison of the plots before and after painting

(Figure 2.20, Figure 2.21) show a significant reduction in trough depth through the application of the paint layers. The representative traces taken before and after painting (Figure 2.22) show a significant reduction in short-term waviness for the painted surface. A wavelength of approximately 4 mm is seen for the bare surface, which corresponds with the weave parameters of the fabric (insert Figure 2.22). The coating process reduced valley depth to 2.2 µm, which is a 10-fold reduction when compared to the bare surface. However, regular patterns of fibre architecture are still visible on the painted surface (Figure 2.21), indicating that complete attenuation of the surface characteristics was not achieved. Characteristics associated with long-term waviness ($\lambda \geq 10$ mm) do not appear to be reduced by the paint process (Figure 2.22), as wavelengths spanning between 25 and 50 mm are visible on both traces. This supports Halden's [17] suggestions of paint being unable to mask structures spanning wavelengths greater than 10 mm.

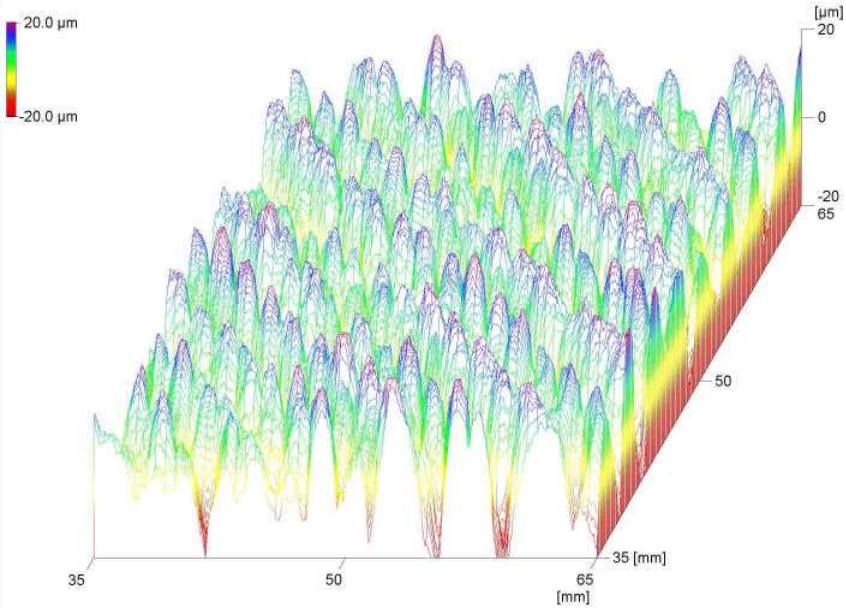

Figure 2.20: Surface topography of a 3k, 2x2 twill weave carbon fabric, processed by RTM with a vinyl ester matrix. A regular trough depth of 15 to 20 µm relating to the weave of the fabric is observed.

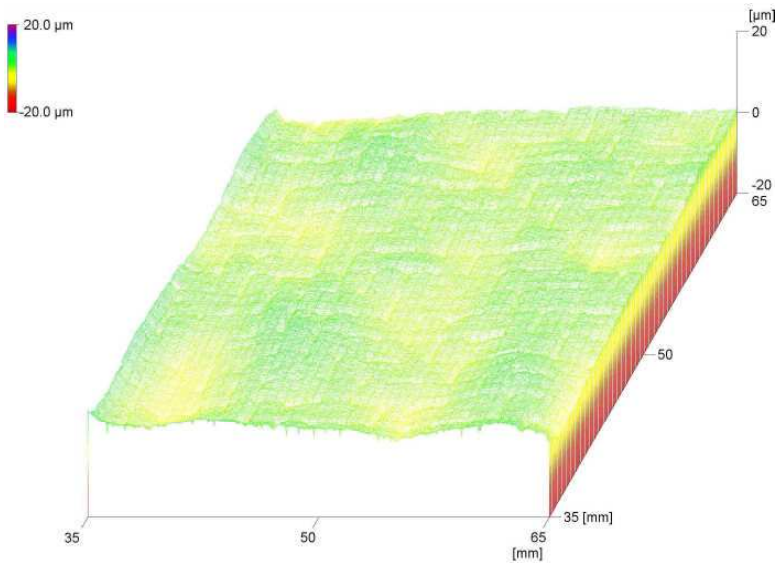

Figure 2.21: Surface topography of the painted surface from a 3k, 2x2 twill weave carbon fabric, processed by RTM with vinyl ester matrix. The plot shows significant reduction in periodicity on the basis of evidence presented.

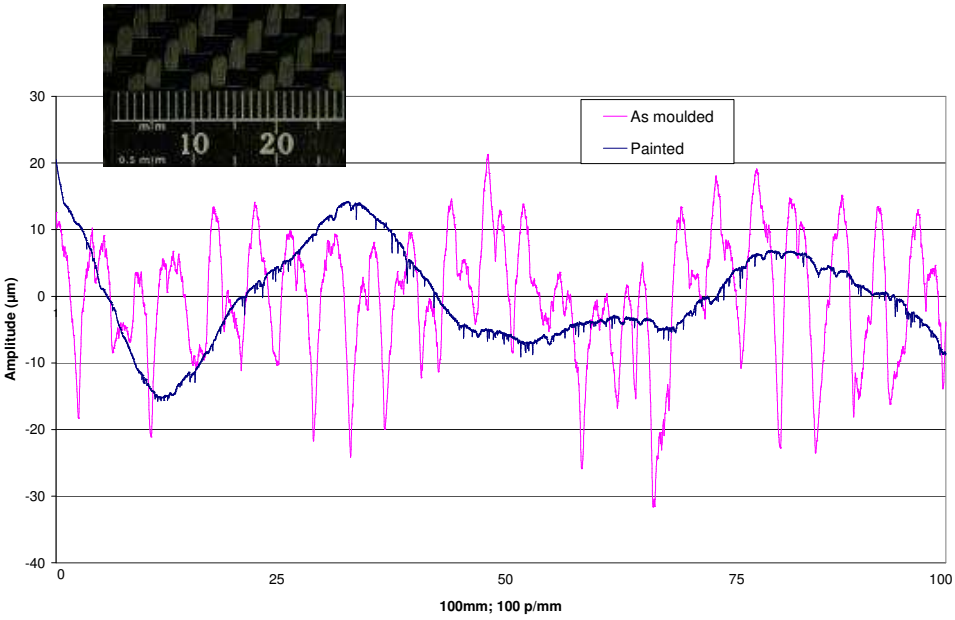

Figure 2.22: Representative profiles of the bare and painted laminate obtained from surface topography. A significant reduction in short-term waviness is seen for the painted surface when compared to the bare surface plot. However, long-term waviness was unaffected.

Optical microscopy was conducted on the cross-section of the painted surface to better understand the attenuation of surface roughness and shortwave characteristics. The images in Figure 2.23 show a representative section where the warp and weft tows overlay on the surface layer of fabric with successive paint

coatings characterised by variation in pigmentation. The progressive increase in magnification shows the levelling effects of paint layers on the trough formed by shrinkage in the resin rich region between the warp and weft tows. At x50k magnification, it can be clearly seen that a variation in thickness of the high build primer and successive sealer primer exists where the surface trough was formed. This phenomenon is shown to fill the majority of the trough with the successive base coat and clear coat showing no visible evidence of the underlying characteristic.

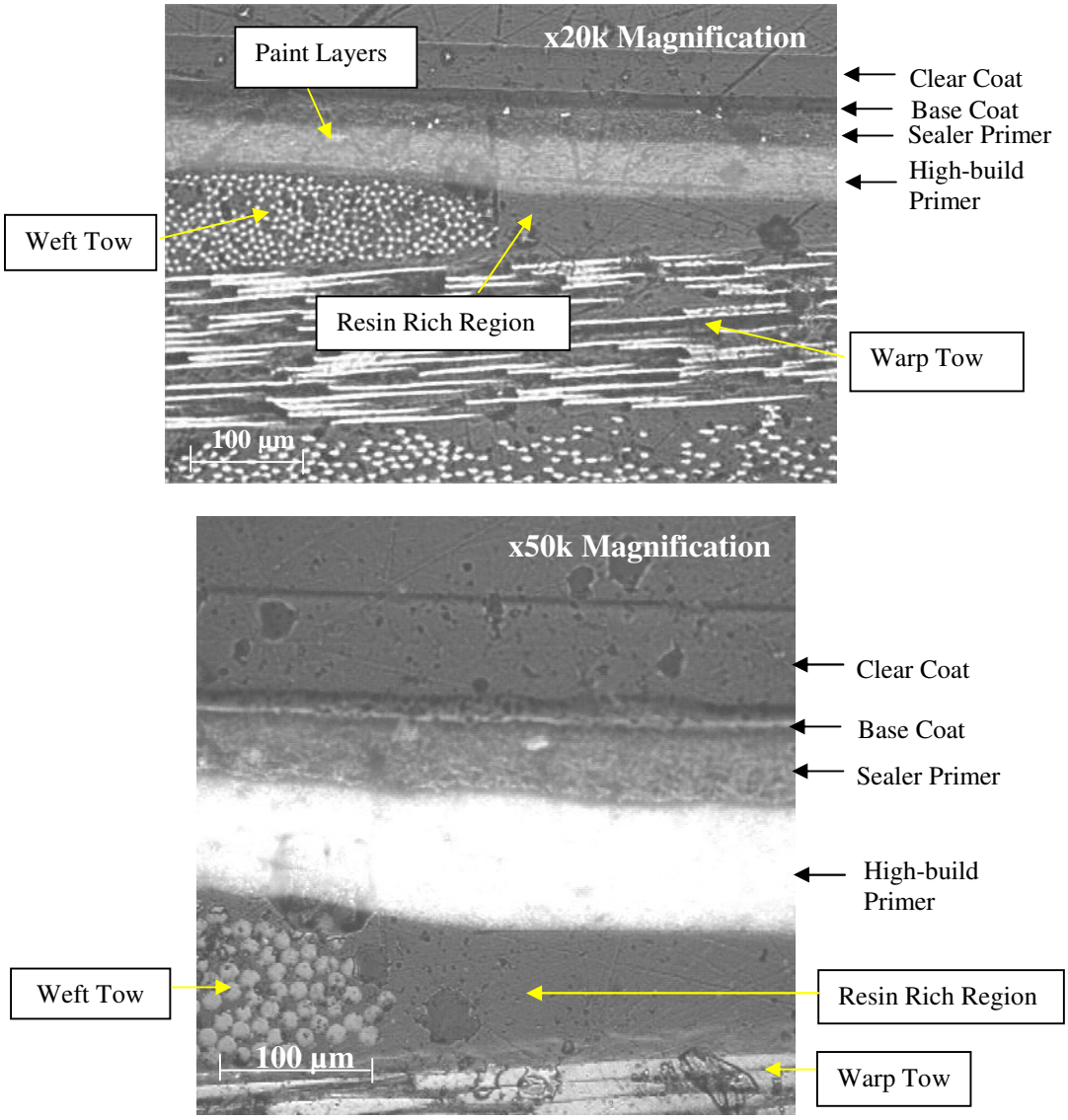

Figure 2.23: Optical micrographs (20k and 50k magnification) on the cross-section of the painted surface of a 2x2 twill weave carbon fabric, moulded in an RTM process with vinyl ester resin. The successive micrographs show the effectiveness of the high-build primer and sealer primer in levelling out the fibre strike-through effect created by the resin rich region at the overlap of a warp and weft tow.

Figure 2.24 shows the surface characteristics of the individual coating layers and the effect each layer has on the proceeding layer. It is shown that each layer has its own level of surface roughness, which is generally masked by the successive layer. This supports Neitzel's [1] suggestions that the paint process produces its own characteristic surface roughness. However, there is no visible evidence that each layer directly influences the successive layer, as surface characteristics were not seen to transfer from one layer to the next.

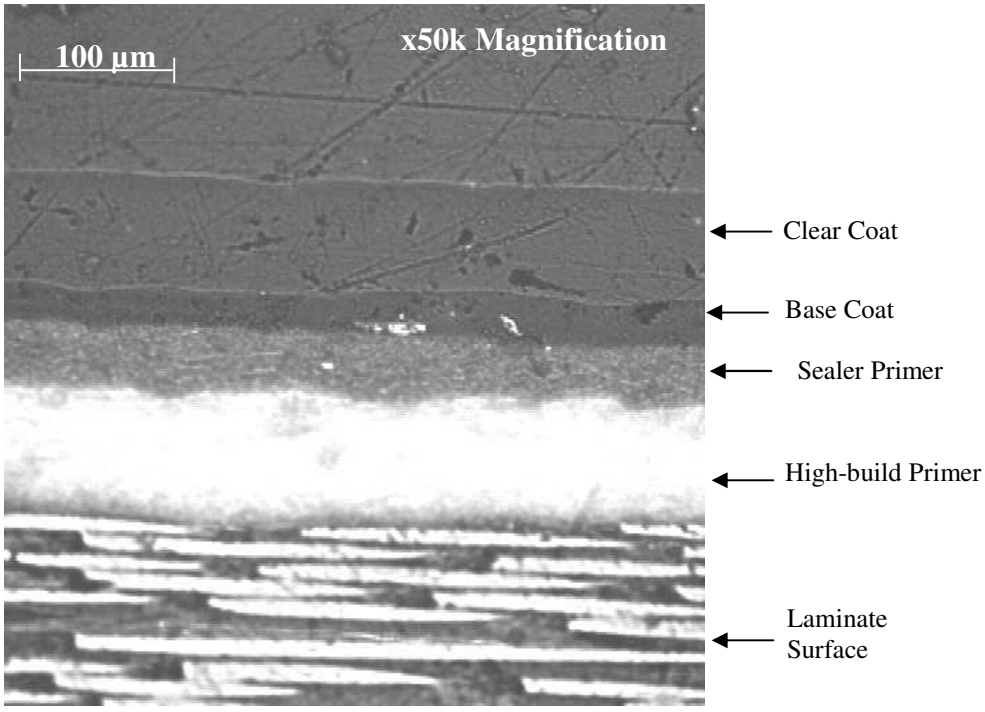

Figure 2.24: Optical microscopy of successive paint layers. Each layer has its characteristic level of surface roughness. However, the roughness of each layer is not seen to affect the successive coating surface.

2.6.2 *Validation of Surface Measurement Techniques*

Visual Subjective Assessment

Subjective assessment was used to provide a reference point against the quantitative methods. Two scenarios were investigated to study the effect of appraiser training. The first study (Group 1) utilised 15 appraisers with no paint quality experience whilst the second study (Group 2) utilised four appraisers with automotive coating background.

The observations made by the appraisers in the visual assessment were analysed to determine the repeatability associated with each appraiser and the reproducibility between appraisers. The statistical analysis detailed in Appendix 3 and summarised in Table 2.4 showed that the paint specialists (Group 2) were individually repeatable within 3 %, whereas a 9 % error could be expected for Group 1. More concerning was the 76 % error between appraisers for Group 1 which indicated poor agreement in what was deemed an acceptable surface. The 12 % error in reproducibility between the Group 2 appraisers was considered acceptable using the Six Sigma process [24] for this type of analysis.

Following these findings, it became obvious that background knowledge plays a major role in subjective assessment. Due to the low margin of error experienced by Group 2, it was decided that the average of their observations would be adopted as the visual assessment for the painted laminates (Table 2.5, Table 2.6). The prevailing defect observed was fibre strike-through.

Table 2.4: Statistical analysis of subjective assessment. Results show that Group 2 are more capable of reproducing their own results and have general agreement with each other on what is an acceptable painted surface.

	Percentage Error (%)	
	Within Appraiser	**Between appraiser**
Group 1 - inexperienced	9	76
Group 2 - experienced	3	12

Table 2.5: Laminates with *acceptable* paint quality as determined by subjective assessment.

Sample ID	Material	Moulding Process
C1	Uncoated $FeP0_4$	-
C2	Random E-glass preform - LS UP resin	RTM
C3	ST85 6K, 2x2 twill, CBS E-glass veil	RFI

Table 2.6: Laminates with *unacceptable* paint quality as determined by subjective assessment.

Sample ID	Material	Moulding Process
C4	6k, 2x2 twill carbon – ST85 (epoxy)	Vacuum bag
C5	Random carbon sheet compound	Compression
C6	6k, 2x2 twill carbon – DLS 1554-2 (epoxy)	Vacuum Infusion

Instrumented Waviness Detection

Surface waviness measurements were obtained using light reflectometry on the painted surfaces of the laminates used in subjective assessment. Results were unobtainable on the bare laminates due to low reflectivity. The wave spectra (W_{a-e}) and hybrid values for all the painted surfaces used throughout the study are supplied in Appendix 4. However, the results presented in this section relate to the shortwave, longwave and *Combined Ford* readings (Figure 2.25) as automotive standards for a (non-flattened) painted surface already existed. The laminates have been grouped into two categories in accordance with results obtained from subjective assessment, i.e. acceptable, unacceptable paint quality. Automotive industry limits for the three parameters have been included in Figure 2.25. Details of the automotive paint standards are found in Table 2.1.

The longwave measurements (Figure 2.25) show a slight increase as a progression is made from the subjective ranking of acceptable to unacceptable paint quality. However, all values still remain within industry tolerance. Most failures were due to short-term waviness, which was excessive for the (subjectively) unacceptable specimens. The laminates which were assessed to have acceptable paint quality (C1, C2 and C3) are well below industry tolerance whilst laminates C4, C5 and C6 show approximately 1.5 times the acceptable tolerance for short-term waviness. As indicated earlier, C4, C5 and C6 laminates showed visible evidence of fibre strike-through and other related surface features. The *Combined Ford* readings (Figure 2.25) also support the subjective assessment results and rate the 'unacceptable' painted surfaces as having excessive surface characteristics. It has been demonstrated that light reflectometry is able to detect the various defects and

rate the laminate paint quality accordingly. However, it has been demonstrated that more than one parameter is required to accurately report on the surface quality due to the nature of the surface characteristics.

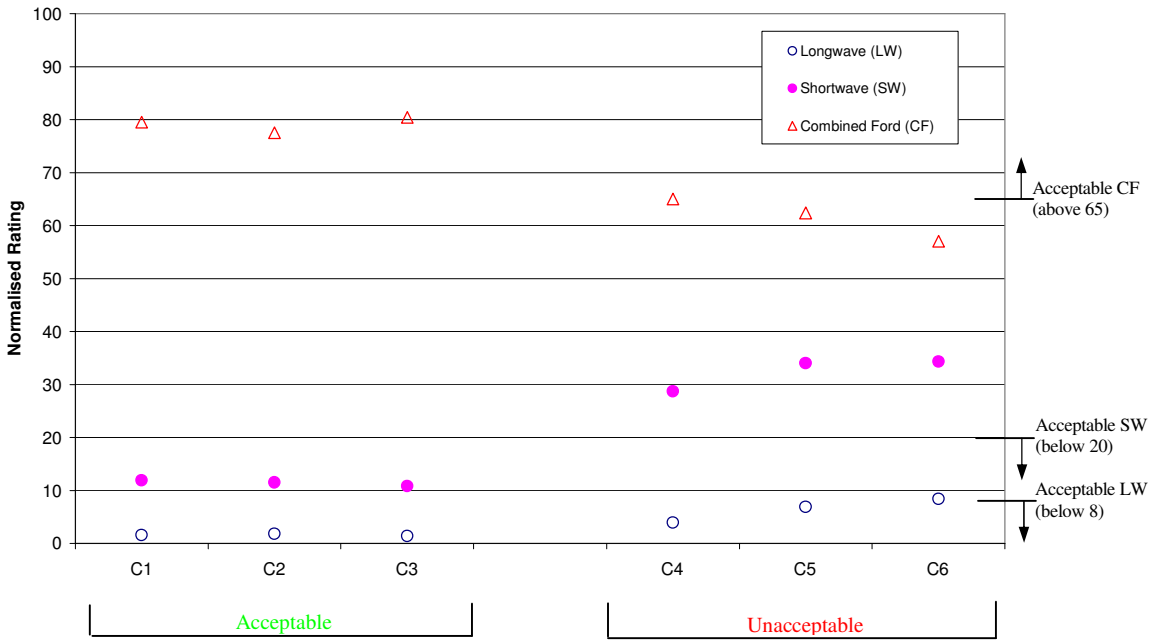

Figure 2.25: Longwave, shortwave and *Combined Ford* readings taken using light reflectometry on the painted laminates. Laminates have been grouped into two categories as determined by subjective assessment. Light reflectometry results complement the subjective study, with acceptable laminates falling within industry specified limits.

Surface Roughness Measurement

Surface roughness measurements were recorded using a 2D stylus profiler for the bare and painted laminates used in subjective assessment. A range of parameters were recorded to characterise the surface roughness, including *Ra, Rz, Rt, Pc, Rq, Rsk, Rku* (these parameters were described in Section 2.3.1).

The surface roughness measurements were analysed using Gaussian (normal) distribution and confidence intervals, revealing that *Kurtosis (Rku)* and *Skewness (Rsk)* of the bare laminates showed no correlation to the subjective or light reflectometry results for paint surface quality. *Rz, Rt, Pc, and Rq* showed major discrepancies upon statistical evaluation (results not presented). The arithmetic

mean (*Ra*) shown in Figure 2.26, gave the best correlation to the subjective and reflectometry results.

The laminates used in Figure 2.26 are grouped in accordance to the results presented for subjective assessment, i.e. acceptable or unacceptable paint quality. The *Ra* values for the 'acceptable' polymers were below 0.2 µm. This value is five times lower than that for acceptable strip steel (*C1*). The higher *Ra* value of 1 µm, for steel still offers an excellent surface for painting as its roughness profile is strictly periodic as opposed to a polymer composite which exhibits less regular characteristics (Figure 2.27).

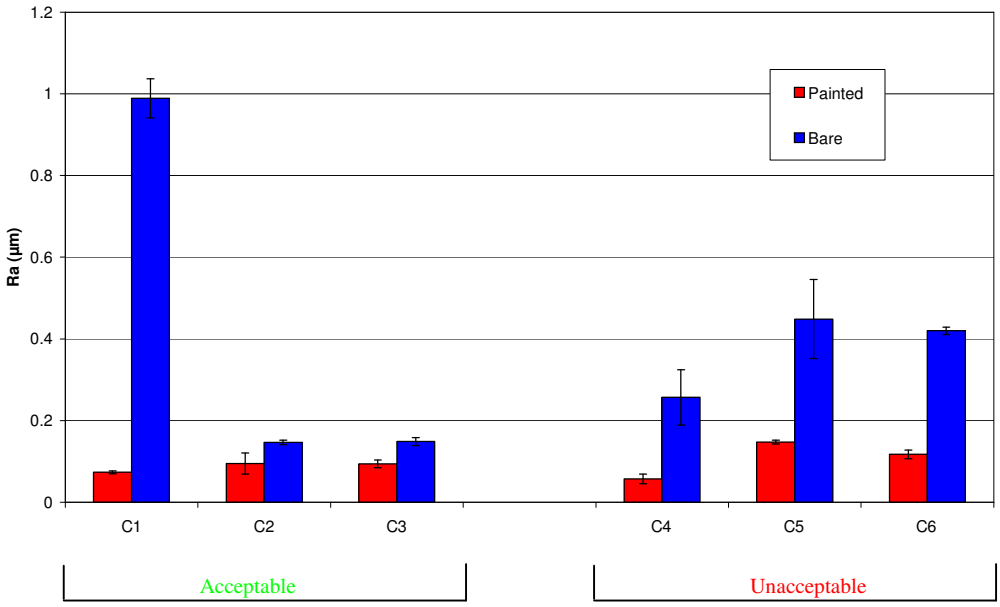

Figure 2.26: Arithmetic mean (*Ra*) of the bare and painted laminate surfaces conducted using stylus profilometry. Laminates have been grouped into two categories as determined by subjective assessment. The graph shows that bare laminates with low *Ra* values correlate to light reflectometry and subjective assessment results. Roughness readings on painted surfaces tend to show paint characteristics such as orange peel.

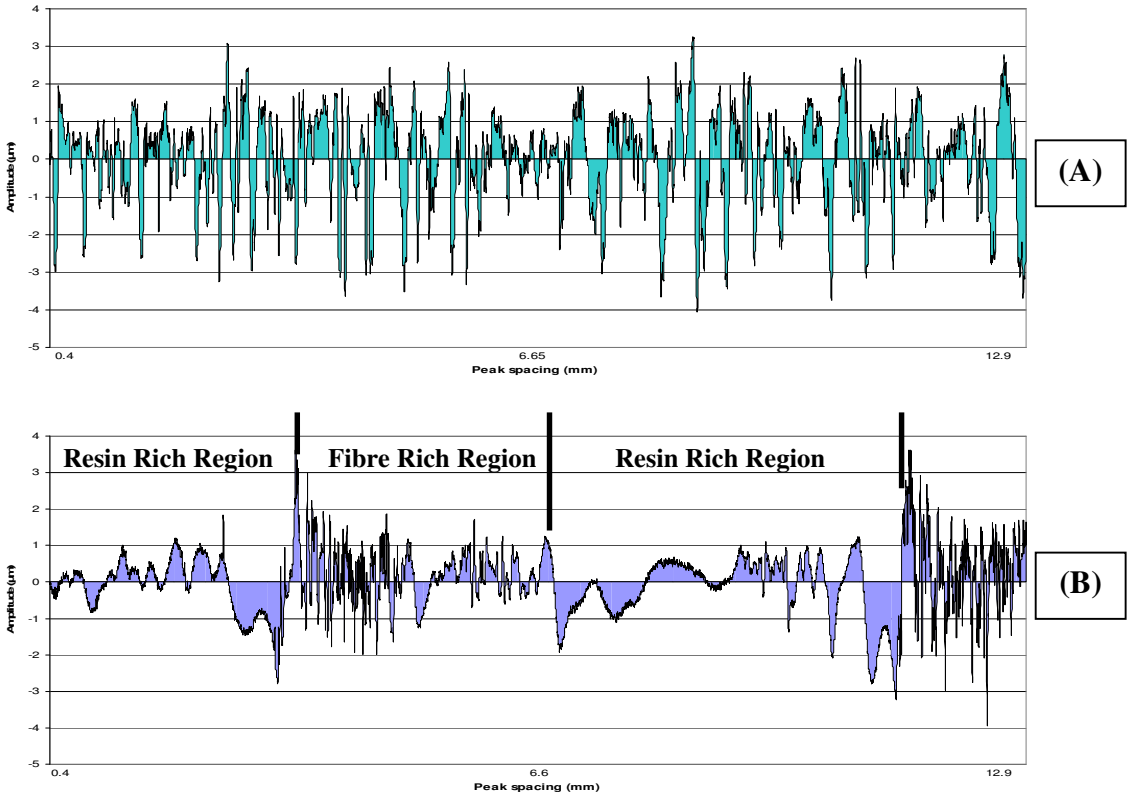

Figure 2.27: Roughness profiles for: (A) *C1* - Cold rolled strip steel, (B) *C6* - 6K 2x2 twill carbon with epoxy matrix moulded using a VI process. Both surfaces produce similar extremities in peak height. However, it was determined by subjective and light reflectometry assessment that the regional variation in profile "B" produced an unacceptable painted surface.

Figure 2.26 also indicates *Ra* values greater than 2 µm on the bare surfaces failed the subjective tests. A statistical analysis using a 95 % confidence interval was used to determine a threshold for acceptable bare surface roughness. It was revealed that a laminate resulting in a flawless paint finish had an unpainted surface roughness less than or equal to 0.16 µm *Ra* (Table 2.7). Above this value, it was highly probable that a defect would be visible on the painted laminate as a result of the bare laminate surface condition.

Table 2.7: 95% confidence interval and range for the two categories of *Ra* values for bare laminates. It has been shown that a bare laminate with a *Ra* equal to or below 0.16 µm will result in a suitable painted surface.

	95 % confidence interval (Ra)		
	Low	**High**	**Range (µm)**
No defects (acceptable)	0.15	0.16	≤ 0.16
Defects (unacceptable)	0.36	0.37	> 0.16

The surface roughness readings taken on the painted surfaces do not correlate with subjective assessment. Instead, it is believed that the readings show varying levels of roughness induced by the paint process. This is supported by the topography of the painted surface (Section 2.6.1), where surface defects such as fibre strike-through were evident, but were difficult to isolate and quantify when looking at a single profile trace. This suggests that profilometry is not suitable for characterising the range of potential structures on the surface of a painted polymer composite, although for bare substrates, it appears to be an accurate and repeatable technique.

2.6.3 *Tool Surface Study*

Semi-preg (C3) was moulded on four tool surfaces (Table 2.8) using the RFI process described in Section 2.5.2. Surface roughness profiles of the four tool surfaces (

) show the variation in surface geometry ranging from smooth and uniform for Tool 1 and 2, to irregular changes in amplitude and spacing for Tool 4. The *Ra* values of the laminates marginally increased over that of the tool surface roughness due to superposition of the fabric architecture and tool surface.

Table 2.8: Description of tool surfaces used for studies on surface quality. The surface roughness (*Ra)* of each laminate shows a marginal increase over that of the corresponding tool surface.

Tool ID (Sample ID)	Material Type	Surface Treatment	Surface Condition	Tool Surface *Ra* (µm)	Moulded laminate *Ra* (µm)
Tool 1	Glass	Tempered	Unmarked	0.07	0.15
Tool 2	Steel	Ground flat, polished, chromed	Unmarked	0.07	0.12
Tool 3	Steel	Ground flat	Light scratches	0.21	0.24
Tool 4	Steel	-	Heavy scratches, deep indentations	0.53	0.59

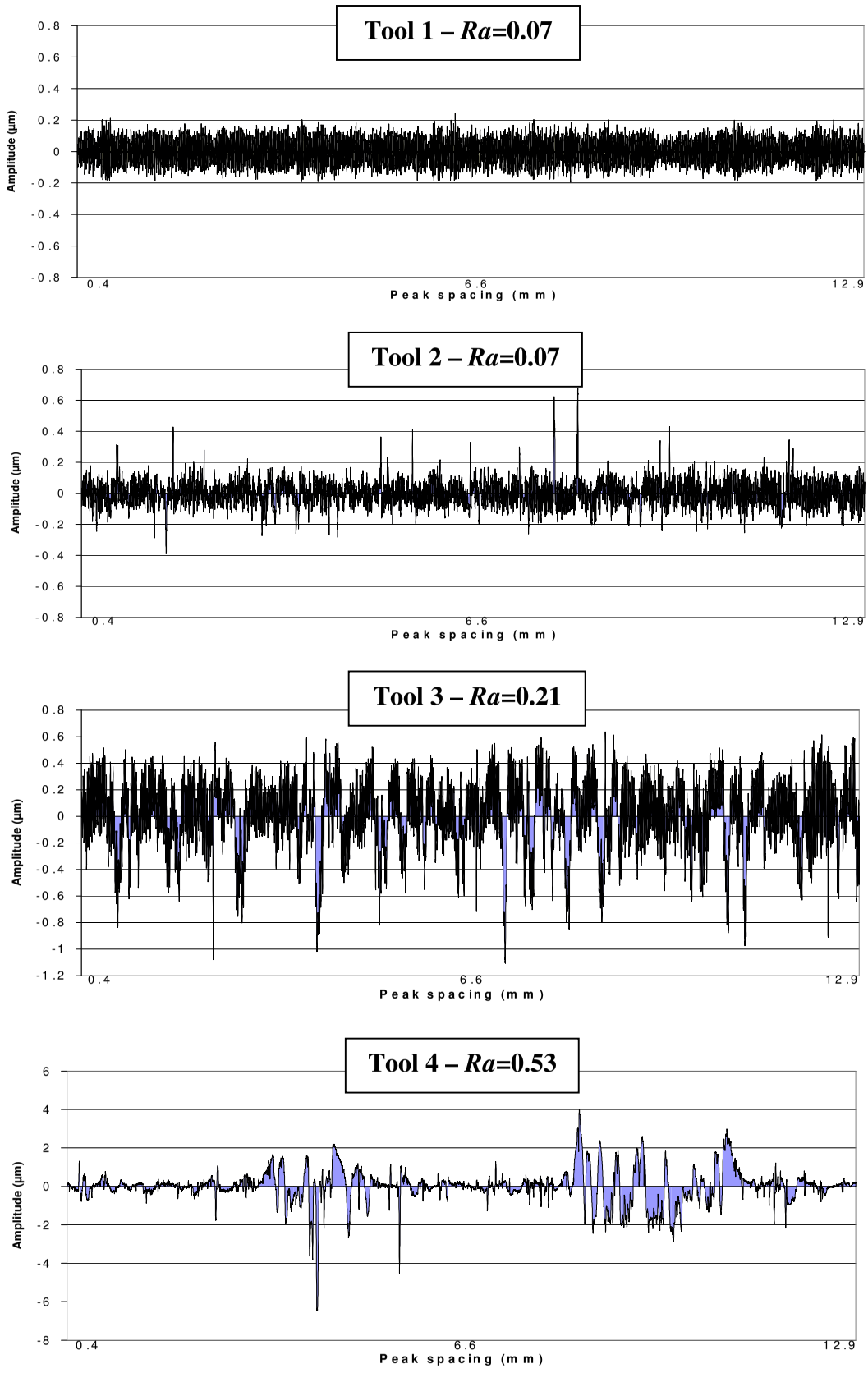

Figure 2.28: Roughness profiles of the four tool surfaces. Tool 1 to Tool 4 show a progressive increase in peak amplitude and spacing.

It has been shown in Figure 2.29 that the application of paint was able to mask defects associated with a tool surface roughness up to an *Ra* of 0.21 µm. All painted laminates show long-term waviness within industry standards. However, Tool 4 (*Ra* = 0.53 µm) has approximately double the allowable short-term waviness. Subjective assessment revealed that the painted laminate moulded on Tool 4 showed excessive scratches and indentations, which directly related to the tool surface and was therefore deemed to have unacceptable paint quality. *Combined Ford* readings also correlate with subjective assessment in indicating that a tool surface roughness of 0.53 µm results in an unacceptable paint quality. Geier's [1] suggestion of mould surface quality contributing to surface roughness holds true. However, it has been shown that the paint process is able to mask irregular patterns and light scratches up to a tool roughness of 0.21 µm *Ra*.

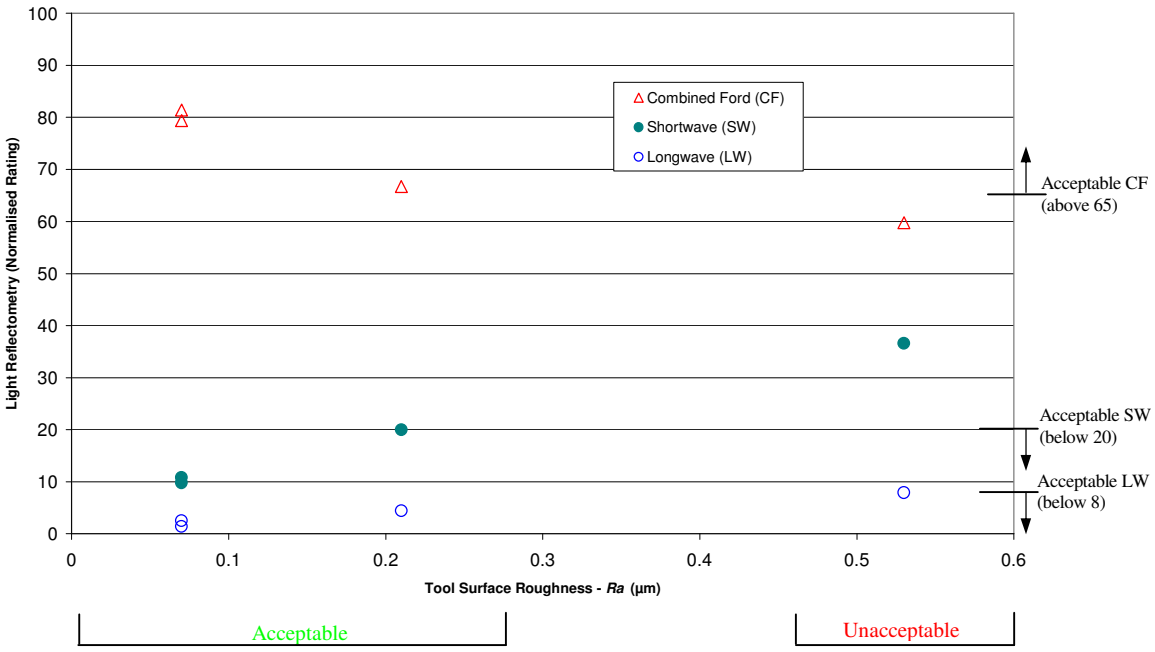

Figure 2.29: Light reflectometry results plotted against the respective tool surface roughness of the four painted laminates. It has been shown that excessive short-term waviness is obtained on the laminate moulded on Tool 4 with a surface roughness of 0.53 µm *Ra*.

2.6.4 *Effects of Tow Size and Resin Shrinkage on Surface Quality*

An unsaturated polyester (RT2557) and epoxy resin (DLS 1648) were used to mould a series of 2x2 twill carbon fabrics to simulate the effects of resin shrinkage and fabric architecture on the resulting surface quality. Chemical resin shrinkage for the resin systems (Table 2.9) was measure by a multipycnometer (Section 4.4.2).

Table 2.9: Volumetric resin shrinkage for epoxy and unsaturated polyester resin.

Resin Type	Sample ID	Chemical Shrinkage (%)	Standard Deviation
Epoxy	Low shrink (LS)	0.74	± 0.24
Unsat' polyester	High shrink (HS)	8.34	± 0.61

Figure 2.30 shows reflectometry results for *Combined Ford*, shortwave and longwave readings of the painted laminates. Subjective assessment and light reflectometry on the painted laminates show related trends and place the low shrink system (excluding the 12k fabric style) as exhibiting no visible surface defects. The 12k low shrink system is shown to have an acceptable *Combined Ford* reading but short and longwave measurements are marginally outside the acceptable region. All other systems exhibit at least 80 % additional short-term waviness over the industrial standard, with fibre strike-through as the prevailing defect.

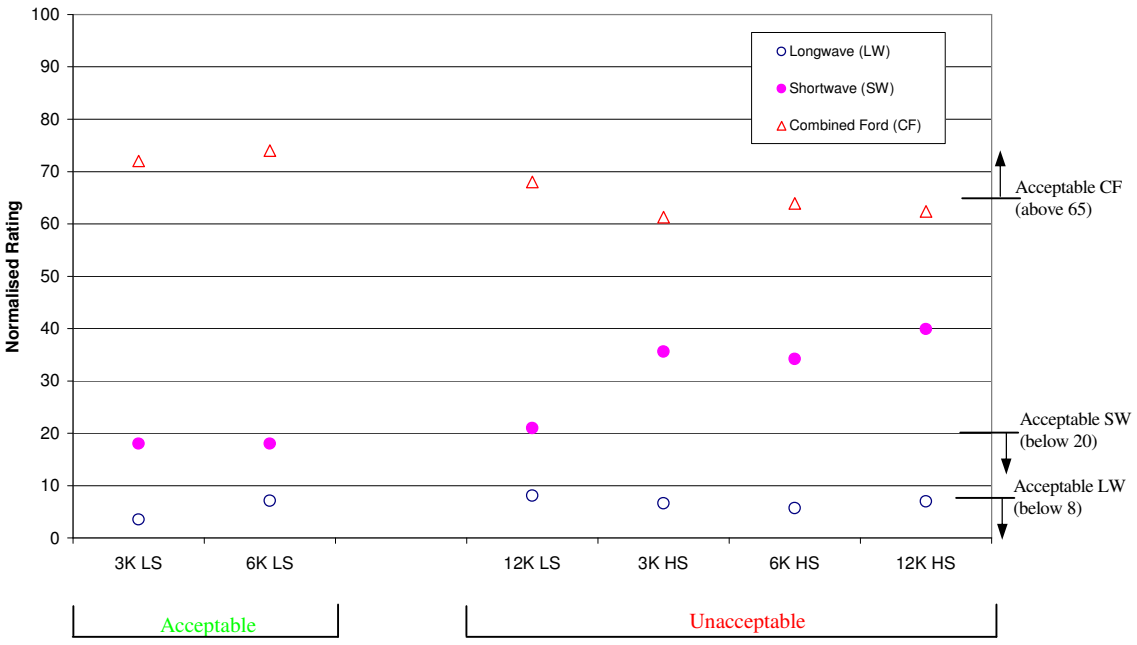

Figure 2.30: Light reflectometry results for laminates produced with various resin shrinkage and fabric architecture. Results show that the low shrink matrix coupled with the 3k and 6k fabric produced no visible defects on the painted surface.

Figure 2.31 shows that both fabric tow size and matrix shrinkage proportionally affect laminate surface roughness. For both the high and low shrink matrix, it has been shown that a 2-fold increase in *Ra* can be expected when comparing the effects of a 3k tow to a 12 k tow.

It was decided to model the effects of volumetric shrinkage and fabric architecture on surface roughness (Appendix 8) by applying a predetermined set of equations to a geometric model of a representative unit cell developed with the aid of TexGen software. The analysis returned a simulated topography of the surface plus an *Ra* value for each set of input parameters. Despite the various assumptions made to simplify the analysis, the simulated results show good correlation to experimental data (Figure A8.10).

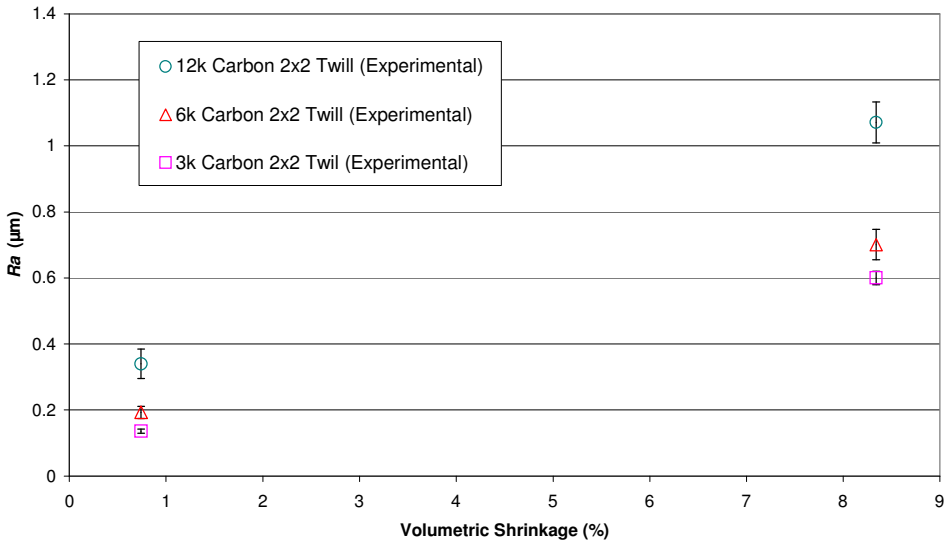

Figure 2.31: Relationship between volumetric resin shrinkage and surface roughness. This demonstrates an increase in *Ra* with change in volumetric shrinkage. Similarly, an increase in tow size creates a change in surface roughness.

2.7 Conclusions

It has been shown that the application of paint is able to significantly reduce surface roughness and short-term waviness due to the levelling effects of the successive coating layers. However, attenuation of defects with a wavelength greater than 10 mm (long-term waviness) were not possible using this coating process. Each layer in the coating process was shown to produce its own level of micro-scale surface roughness with minimal influence from the preceding layer.

Subjective assessment was statistically validated and shown to be an important tool in assessing paint quality. Instrumented assessment such as light reflectometry supports human visual perception of painted laminates, but expert visual assessment is still a necessary tool in assessing painted polymer laminates. The arithmetic mean (*Ra*) of the bare surface was found to be useful to predict the quality of the painted surface for a polymer composite.

The proven assessment methods: subjective, light reflectometry and stylus profilometry, assisted in further understanding the effects of material and process changes for polymer composite materials. Measured effects caused by tow size, resin shrinkage and tool surface roughness provide a valuable predictive tool for resulting surface quality. This helps to screen materials for surface quality requirements whilst minimising the overall costs. Creating a highly polished tooling surface has been shown to be an unnecessary process for the production of cosmetic laminates. However, increased tooling surface roughness may affect release of the component and increase residue build-up, which incurs increased production costs. The use of surfacing layers on the laminate provides a means to masking textile induced patterns and minor blemishes that have been reproduced from the tool surface.

2.8 References

1. Neitzel, M., Blinzler, M., Edelmann, K., and Hoecker, F., *Surface quality characterisation of textile-reinforced thermoplastics.* Polymer composite, 2000. **21**(4): p. 630-635.
2. Wenger, W., Dickson, G.R., McIlhagger, R., and Miller, P.P., *The surface-finish characteristics of composite components.* Materials Process Technology, 1992. **33**: p. 439-452.
3. Dickson, G.R. and McIlhagger, R., *Assessing the surface finish of polymer composite components.* Journal of Machine Tools Manufacture, 1992. **32**: p. 51-56.
4. Abraham, D. and McIlhagger, R., *Investigations into various methods of liquid injection to achieve mouldings with minimum void contents and full wet out.* Composites Part A: Applied Science and Manufacturing, 1998. **29**(5): p. 533-539.
5. Jeong, H., *Effects of voids on the mechanical strength ultrasonic attenuation of laminated composites.* Journal of Composite Materials, 1997. **31**(3): p. 276-292.
6. Sharkey, M., *Optical imaging has its place in the paint and coating industry.* Metal Finishing, 1998. **96**(2): p. 69-77.
7. Vu-khanh, T. and Do-thanh, V., *Predicting shrinkage in polyester reinforced by glass fabrics.* Journal of Composite Materials, 2000. **34**(12): p. 998-1008.
8. Fahy, E.J., *Modelling warpage in reinforced polymer disks.* Polymer Engineering Science, 1998. **38**(7): p. 1072-1084.
9. Choi, D.S. and Im, Y.T., *Prediction of shrinkage and warpage in consideration of residual stress in integrated simulation of injection moulding.* Composite Structures, 1999. **47**: p. 655-665.

10. Huang, C.K. and Yang, S.Y., *Warping in advanced composite tools with varying angles and radii.* Composite: Part A, 1997. **28**: p. 891-893.
11. Huang, M.C. and Tai, C.C., *The effective factors in the warpage problem of an injection-moulded part with a thin shell feature.* Journal of Material Process Technology, 2001. **110**: p. 1-9.
12. Kim, P.J. and Lee, D.G., *Surface quality and shrinkage of composite bus housing panel manufactured by RTM.* Composite Structures, 2002. **57**: p. 211-220.
13. Nauzin, J.P. and Jacobs, H., *Paint finish in automotive bodies.* Society of automotive engineers, 2002. **2002-01-0038**.
14. ISO, *Geometrical product specification (GPS) - Surface texture: Profile method - Terms, definitions and surface texture parameters.* 2002. **ISO 4287:2000**.
15. Geier, M.H., *Quality handbook for composite materials*. 1994, Chapman & Hall: London. p. 245-252.
16. Mitutoyo, *Surftest 211 - surface roughness tester users manual*. Vol. 4360M. 2000, Malaysia.
17. Halden, M., *Characterisation of steel sheet surfaces in order to predict surface appearance after painting.* IBEC, 1997: p. 115-120.
18. Scheers, J., Vermeulen, M., DeMare, C., and Meseure, K., *Assessment of steel surface roughness and waviness in relation with paint appearance.* Journal of Machine Tools Manufacting, 1998. **38**(5): p. 647-656.
19. Kigle-Bockler, *The new generation for understanding the appearance of coatings.* 2002(http://www.bykgardner.com/html/byk/index.html).
20. Coulthard, M. *On-line measurement of paint appearance on car bodies*. in *conference procedings from Surcar*. 1993. Cannes.
21. Corus, *53544 steel specification.* 2004.
22. Kendall, K., *Mould design for high volume resin transfer moulding*, in *Mech. Eng., PhD Thesis*. 1991, University of Nottingham: Nottingham.
23. Wilks, C.E., *Processing technologies for woven glass/polypropylene composites*, in *Mech. Eng., PhD Thesis*. 1999, University of Nottingham: Nottingham. p. 169.
24. Breyfogle, F.W., *Implementing Six Sigma: Smarter solutions using statistical methods*. 2nd ed. 1999, New York: John Wiley & Sons. 800.

3 Cure and Residual Volatile Assessment

3.1 Introduction

Organic compounds are released into the atmosphere before, during and after manufacture of polymer components, creating environmental and surface quality issues. Such compounds are present in the constituents of the matrix or are produced as a by-product of the polymerisation process. Unsaturated polyesters were studied here due to the high styrene content required to act as both a cross-linking agent and to control viscosity. This problem is compounded when thermoplastic additives, with styrene as a solvent, are used to reduce polymerisation shrinkage. Characteristics of low shrinkage polyester systems are associated with high residual volatile organic compounds, notably styrene and benzaldehyde.

The objectives of this study were to determine:

1. The effectiveness of residual reactivity detection as a means of measuring residual styrene levels.
2. The effects of formulation and process conditions on styrene conversion.
3. The factors that contribute to the formation of benzaldehyde.

Three initiators and one low profile additive were tested using different curing schedules and were characterised by differential scanning calorimetry (DSC), thermogravimetric analysis (TGA) and gas chromatography (GC). Process conditions that were investigated include the influence of:

1. Demould time.
2. Postcure temperature.
3. Ambient storage.

3.2 Theory and Review of Previous Work

The release of volatile organic compounds creates environmental and quality control problems, which affect both manufacturer and consumer. Residual styrene from unsaturated polyester laminates is a particular source of odour. It may also reduce paint quality due to the formation of blisters and voids at the elevated baking temperatures used in the curing of successive paint layers. For these reasons, the detection and control of residual compounds, such as styrene, are important to the development and future involvement of resin systems such as unsaturated polyester in the automotive industry.

Volatiles are a major concern to the automotive industry, with the Commonwealth Scientific and Industrial Research Organisation (CSIRO) [1] suggesting that high levels of toxic air emissions are causing new car owners to develop related illnesses. Toxic emissions include benzene, a category 1 cancer-causing toxin [2]; acetone, a mucosal irritant; and styrene, a central nervous system toxin. The literature indicates two dominant odour causing compounds in the use of polyester systems; styrene and benzaldehyde [3, 4]. Table 3.1 summarises the compounds and their physical properties.

Table 3.1: Compound identification and physical properties.

	***CAS No.**	**Molecular Formula**	**Molecular Mass**	**Relative Density**	**Boiling Point**
Styrene	100-42-5	C_8H_8	104.16	0.907	145ºC
Benzaldehyde	100-52-7	C_6H_5CHO	106.10	1.05	179ºC

* CAS number is assigned by the Chemical Abstracts Service to identify a specific chemical

Styrene monomer (Figure 3.1) is blended with unsaturated polyester to act both as a cross-linking agent and to control viscosity [5]. Styrene is the most frequently used monomer in polyesters, over methyl methacrylate or *n*-butyl methacrylate, due to its low viscosity, low cost and ready availability [6]. It readily undergoes polymerisation either when heated, exposed to light or to a peroxide. It is well known for its ability to polymerise with itself in the absence of an initiator. However, to prevent homopolymerisation, an inhibitor such as hydroquinone is

often used to obtain a suitable storage life. Styrene evaporates readily leaving a clear residue and has a distinctive odour.

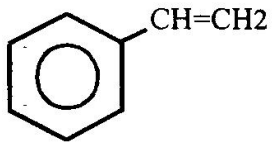

Figure 3.1: Molecular structure of pure styrene.

The use of styrene in the work place has caused much concern since the adoption of occupational exposure limits in 1975 headed by the National Institute of Occupational Safety and Health (NIOSH). The increased use of styrene-based polymers in the boat building industry during the mid 1970s prompted studies on effects and associated risks imposed on the workers. It was discovered that human exposure to styrene is highest in the production of fibreglass-reinforced plastics [7], where unsaturated polyester resin containing up to 40 wt% styrene as reactive diluent are commonly used. Styrene enters the human body by inhalation, ingestion or skin absorption and has one of the highest blood to air partition coefficients for industrially produced chemicals; 48 ± 7.6 at 37 ºC [8]. It is estimated that 60 to 70 % of the inhaled styrene penetrates into the circulatory system [9]. Studies have found that styrene accumulates in fat rich organs such as the central nervous system, which cause related illnesses such as; headaches, fatigue, nausea, weakness and dizziness [10]. Acute cases have been presented where long term exposure to styrene has shown evidence of neuropsychiatric symptoms [11, 12]. Styrene also affects the mucous membranes of the eyes, nose and upper airways.

Occupational exposure limits enforced by government law aim to minimise exposure to a specified substance for a full working day (8 hours), with reference to a time-weighted average concentration of 10 ppm. Occupational exposure limits for styrene have been continually revised as new information is presented highlighting more areas of concern. The further reduction on acceptable styrene concentration in the workplace was driven by the discovery of styrene genotoxic

effect on the blood, DNA strand rupture and the risk of cancer [13-15]. Discrepancies are also found between what individual countries are willing to accept (Table 3.2). To date, the U.K. has the highest acceptable styrene exposure limits for the countries listed in Table 3.2; set in 2000 at 100 ppm [16]. There is a strong push to limit open air moulding practices where styrene vapour easily enters the atmosphere. Moulding techniques such as vacuum bag moulding and closed tool moulding reduce workplace styrene emissions by up to 95 % [13].

Table 3.2: Occupational exposure limit value for styrene in various countries. Limit values are based on a standard working day [13].

	Country							
	Denmark	Finland	Germany	Netherlands	Norway	Sweden	U.K.	U.S.A
Concentration (ppm)	25	20	20	25	25	20	100	20

Benzaldehyde (Figure 3.2) is a colourless liquid with a characteristic bitter almond odour. It is formed by a double bond cleavage in the styrene side chain, and on oxidation forms benzoic acid [17, 18]. Benzaldehyde boils at 179 °C and is soluble in ethanol but is insoluble in water. Benzaldehyde serves no beneficial purpose in the polymerisation process and is purely a by-product from the oxidation of styrene.

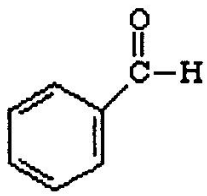

Figure 3.2: Molecular structure of pure benzaldehyde.

The environmental behaviour, ecological and human effects of benzaldehyde should be anticipated. However, few studies on its toxic effect are available. Occupational exposure limits have not been established by NIOSH despite strong evidence linking benzaldehyde exposure to central nervous system depression

[19]. The American Industrial Hygiene Association (AIHA) have realised the potential hazards of benzaldehyde and have published workplace environmental exposure limits for a full working day at 2 ppm [20]. The benzaldehyde threshold concentration is 10 times below that of the general styrene threshold, indicating the strong volatility of benzaldehyde. On-going research into the effects of long-term exposure to benzaldehyde will undoubtedly highlight the need for classification of the compound, allowing for regulated, safe exposure.

Environmental exposure limits are determined by monitoring organic compound vapours using activated charcoal tube or carbon cloth absorption at respiratory level during an 8 hour shift (ASTM D3686-95 and D3687-95). Thermal desorption techniques are commonly used to elute the organic compounds from the absorption medium, which are analysed by gas chromatography (GC) [21, 22]. This method is a fast and reliable means of environmental compound detection. However, it does not relate to the total residual compound content within the sample piece which may be released over the life of the part. A limited amount of research has been conducted into the effects of resin system, curing agent and reaction conditions on residual compounds in unsaturated polyesters [4, 23, 24]. Available methods to determine residual compounds (in particular styrene content) include gas chromatography [4, 23, 25, 26], nuclear magnetic resonance [27] and infrared spectroscopy [3, 28, 29]; gas chromatography has been the most commonly used among them. Solvent elution methods based around gas chromatography detection are primarily used for this purpose (ISO 4901:1985) [30].

Reported Factors Affecting Volatile Organic Content

The increasing push from the automotive industry to produce cheap polymer based materials with acceptable surface quality, has led manufacturers to introduce shrinkage control additives into unsaturated polyesters (Section 1.3.2). Low profile additives such as poly(vinyl acetate) (PVAc) can contain up to 60 % styrene as solvent and the use of these additives further increases the styrene content in the formulations. Also, the reaction exotherm may decrease because

LPA is a non-reactive component in the system. The presence of excess styrene is potentially a major source of volatile production in the moulded article. Literature has also shown the potential for benzaldehyde production through oxidation of excess styrene. This phenomenon was observed for 4 mm laminates containing 35 vol% random E-glass fibre and saturated polyester LPA [4]. Solvent desorption gas chromatography showed that the inclusion of a LPA such as saturated polyester (30 wt% styrene) increased the residual styrene two-fold and the residual benzaldehyde seven-fold over a storage period of one month (Figure 3.3). The increased benzaldehyde levels in the LPA based formulation were attributed to oxidation of excess styrene.

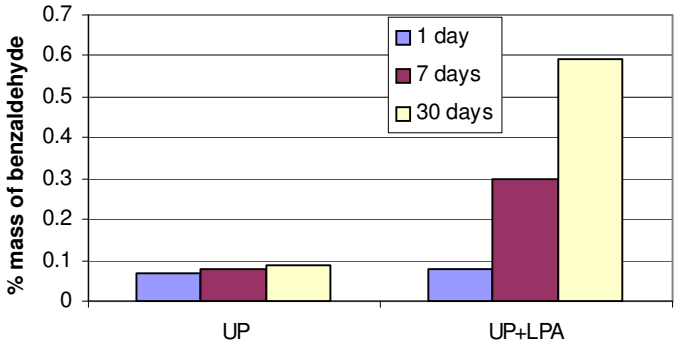

Figure 3.3: Influence of a saturated polyester LPA on the residual benzaldehyde levels of a maleic anhydride unsaturated polyester [4]. Measurements were recorded over a period of 30 days with the low profile system showing a dramatic increase in residual benzaldehyde levels as time progressed. Constituents are listed in Table 3.3.

Table 3.3: Constituents used by Reijnders [4] for the production of laminates in Figure 3.3.

	UP	UP+LPA
Maleic anhydride polyester (wt%)	100	75
LPA – saturated polyester (wt%)		25
Butanox M-50 (wt%)	2	2
Accelerator NL-49P (wt%)	1	1
Mould temp (°C)	70	70

Saturated polyester LPA has reduced levels of styrene as solvent compared to systems such as polystryrene, poly-methylmethacrylate or poly(vinyl acetate) (PVAc) (Table 3.4). The influence of elevated styrene loading used as solvent in these systems was shown to increase residual styrene levels. However, residual benzaldehyde levels remained relatively constant except for PVAc (Figure 3.4). The use of PVAc converted more styrene than poly-methylmethacrylate. In doing this, a two-fold increase in benzaldehyde was produced.

Table 3.4: Percentage weight of styrene in various LPAs used in the manufacture of low profile polyester resin.

Low Profile Additive	Acronym	Styrene (wt%)
Saturated Polyester	SP	30
Polyurethane	PUR	45
Poly-methylmethacrylate	PMMA	60
Poly(vinylacetate)	PVAc	60
Polystyrene	PS	65

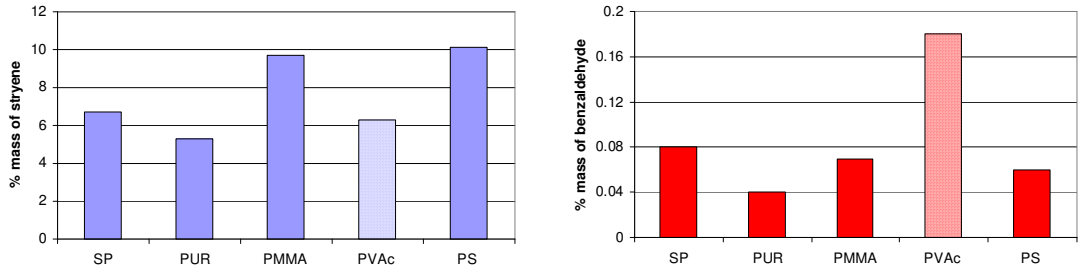

Figure 3.4: Effects of LPA type on residual styrene and benzaldehyde levels immediately after moulding [4]. The higher loading of styrene as solvent in LPA generally has an increased effect on residual styrene, with benzaldehyde production in PVAc increasing dramatically. Constituents are listed in Table 3.5.

Table 3.5: Constituents used by Reijnders [4] for the production of laminates in Figure 3.4.

	SP	PUR	PMMA	PVAc	PS
Maleic anhydride polyester (wt%)	75	75	75	75	75
LPA (wt%)	25	25	25	25	25
Butanox M-50 (wt%)	2	2	2	2	2
Accelerator NL-49P (wt%)	1	1	1	1	1
Mould temp (°C)	70	70	70	70	70

This section has outlined the residual compound issues associated with unsaturated polyester moulding and the potential effects it creates. Attention has been drawn to the presence of residual styrene and subsequent benzaldehyde production in moulded laminates utilising a low profile additive. As mentioned in Section 1.3.2, PVAc was the most efficient additive in unsaturated polyester for reducing resin shrinkage and producing a low profile effect. However, Reijnder suggests that the residual benzaldehyde associated with this system is more than double that of competing PMMA systems. Current theories of benzaldehyde production due to styrene oxidisation have been proven, but there is evidence to suggest there is an underpinning mechanism in LPA that influences the formation of residual benzaldehyde. Experimental evidence is required to show that LPA affects residual benzaldehyde content, over that of adding excess styrene. This will lay the basis to focus future research on the development of alternative low profiling systems which are inert to producing chemical by-products that are unpleasant and potentially harmful to human senses. Hence, it has been determined to study the influence of formulation and process variables and measure the resulting residual styrene and benzaldehyde content.

3.3 Experimental Method

A resin transfer moulding process (described in Section 2.5.2) was used to impregnate E-glass preforms with unsaturated polyester resin. The resin system was formulated to cure at 95 ºC, with initial surface quality results in Section 2.6.2 showing suitable paint quality resulting from a low profile unsaturated polyester system. There was no evidence of fibre strike-through or textile induced waviness and the measured surface characteristics were equivalent to semi-pregs and carbon/epoxy composites produced using RTM.

The base resin was Crystic® (RT2557) orthophthalic unsaturated polyester, supplied by Scott Bader Company and is described in Section 2.5.1 along with the reinforcement. Three initiators supplied by Akzo Nobel were used. Each was designed for moulding between 60 and 95 ºC.

1. Tertiary-Butyl peroxybenzoate initiator in 80% solution with acetylacetone (TBPB) (Trigonox® 93)
2. Acetyl acetone peroxide and tert-Butyl peroxybenzoate in solvents (AAP/TBPB) (Trigonox® 524)
3. Tertiary-Butyl peroxy-2-ethylhexanoate (TBPEH) (Trigonox® 21).

Cobalt accelerator G, supplied by Scott Bader Company, is a mix of 12 % cobalt-octoate solution in mineral oil, diluted to 1 % with styrene (AAO 17730). Calcium carbonate ($CaCO_3$) filler with a 5.7 µm nominal particle size was supplied by Omya UK Ltd and used at 30 wt% of resin. A summary of the test laminate constituents is set out in Table 3.6.

Table 3.6: Constituents

Constituent	Supplier	Product	Description
Base resin	Scott Bader	Crystic	Orthophthalic unsat' polyester
Low Profile additive	Dow Chemicals	PVAc with 60wt% styrene	Thermoplastic in styrene
Filler	Omya UK	BLR2	$CaCO_3$ @ 5.7µm
Initiator	Akzo Nobel	Trigonox 93	TBPB in solution
	Akzo Nobel	Trigonox 524	AAP/ TBPB
	Akzo Nobel	Trigonox 21	TBPEH
Accelerator	Scott Bader	Accelerator G	
Reinforcement	Owens Corning	OC R25H 1200 tex	
Veil	Owens Corning	OC 950A-AB 3307 tex	
Binder	Reichhold	Pretex 110	Bisphenol A 95% Dicyandiamide 5%

Isothermal DSC analysis was adopted to determine the residual reactivity of three unsaturated polyester matrices utilising different initiator systems. Analysis of resin flash from the laminates was performed using a Perkin Elmer Pyris 1 differential scanning calorimeter. ISO 11357-1:1997 was followed in order to estimate the degree of cure as follows. An initial baseline run was conducted by placing an empty pan in each sample holder and ramping the temperature at 10 ºC

/minute to 220 ºC under nitrogen. The baseline was then subtracted from each individual analysis to compensate for any change in detectable heat flow between the two heated chambers. 12 ± 1 mg of sample was contained in a hermetically sealed aluminium pan to prevent weight loss due to evaporation of volatiles. The temperature was then ramped to 220 ºC under the same settings and the exothermic heat of reaction was monitored. The degree of residual reactivity (1-α) at time *t* was determined from Equation 1.5 as:

$$1-\alpha(t)=\frac{1}{\Delta H_{tot}}\int_0^t\left(\frac{d\alpha}{dt}\right)dt \qquad [3.1]$$

where ($d\alpha/dt$) is the DSC output in J/g/min and ΔH_{tot} is the total heat of cure in J/g. The value of ΔH_{tot} was obtained by DSC analysis on an initially uncured sample of similar mass.

Thermogravimetric analysis (TGA) was performed on resin flash to determine mass loss due to residual volatile emission from the sample matrix. This process is commonly used in polymer matrices for determination of organic compounds, as it allows variable heating rates that can be manipulated to simulate the environment and application of intent. However, for the purpose of this experiment, TGA was used to evaporate all available surface compounds for detection using a Perkin Elmer Pyris 1 instrument. 10 to 20 mg of the sample was heated in air from ambient to 250 ºC at a rate of 10 ºC/ min. The composition of the exhaust was sampled using a Pfeiffer Thermostar mass spectrometer. Any gases detected could then be overlaid on the thermogravimetric trace to correlate weight loss with emission composition.

There were concerns that TGA only released surface volatiles and that the polymer matrix could potentially trap organic compounds within it. To determine whether this was occurring, a common method of organic compound detection was employed. Solvent elution gas chromatography (Figure 3.5) was used to determine the total residual compound content within the resin matrix. Solvent elution GC was chosen over thermal desorption GC, as solvent solution breaks

down the polymer, exposing all areas of the matrix for elution of the compounds, whereas thermal desorption and TGA are part of the same family, and rely on heating the sample to remove surface compounds. Detection of compounds and compound intensity was obtained on a Shimadzu GC 17A version 3 analyser with an automated sampler. A calibration curve was developed to enable the voltage response to be converted to a percentage mass of compound within the resin-fibre composite (Appendix 5). This allowed direct comparison of results to published work. Guidelines of ISO 4901:1985 were followed. Validation of experimental techniques (Appendix 6) was conducted to ensure suitable sample mass and solvent desorption time was allowed for sufficient elution of compounds. It was shown that the polymerised resin/filler/fibre composite cut into samples of 1.5 ± 0.1g and immersed in a sealed 15 mL glass vial containing dichloromethane for 15 hours resulted in optimal elution of styrene and benzaldehyde compounds. 0.5 μL of eluted solution was injected into the split injector for analysis. The injected solution was heated from 40 ºC to 270 ºC at a rate of 10 ºC/min and passed through a DB5 alumina silicate tubing of length 30 m and inner diameter of 0.25 mm. The column is coated with a stationary phase of 95 % dimethyl and 5 % diphenyl polysiloxane.

Due to the small sample size used in the experimental techniques (10 to 20 mg), there were concerns with samples not being representative of the entire test laminate due to their heterogeneous nature. To account for this, at least four samples were systematically taken from various locations on the plaque.

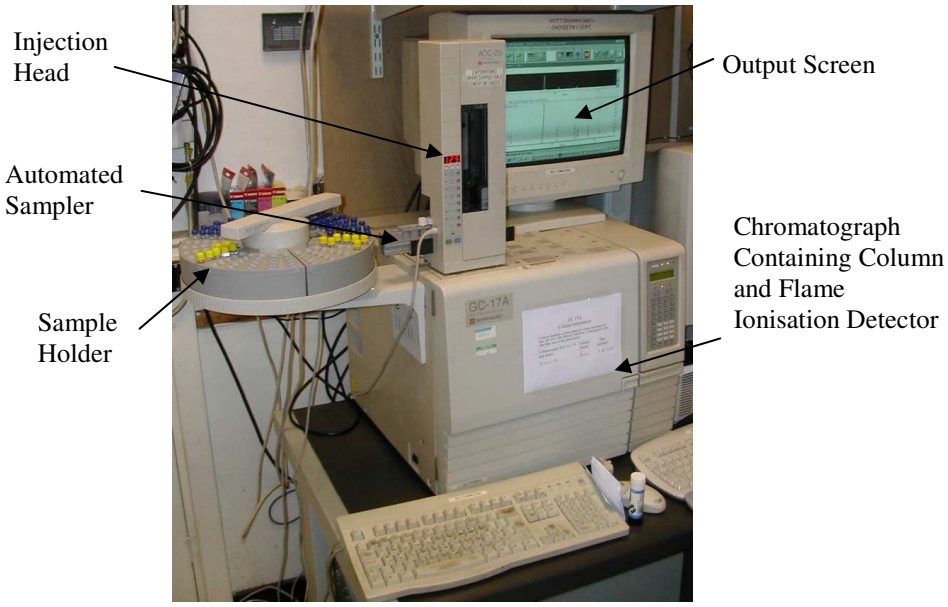

Figure 3.5: Gas chromatography equipment.

3.4 Results and Discussion

3.4.1 *Introduction*

The test matrix of samples seen in Table 3.7 were produced using as-moulded and postcured samples with three different initiators. The samples were chosen by degree and nature of odour being emitted. Subjective odour assessment rated AAP/TBPB the most disturbing odour, followed by TBPEH and TBPB. DSC, TGA and GC were conducted on these samples to determine cure characteristics, volatile emissions and total compound content. Table 3.8 is an overview of the parameter levels that were studied. The work can be split into formulation studies and process studies.

Table 3.7: Standard moulding constituents and parameters.

Resin	Initiator (%)	Accr (%)	Mould Temp (ºC)	Demould Time (min)
RT2557+30wt% PVAc	TBPEH (1.8)		95	30
RT2557+30wt% PVAc	AAP/TBPB (2)	G (1)	95	30
RT2557+30wt% PVAc	TBPB (2)	G (0.5)	95	30

Table 3.8: Matrix of variables used in the manufacture of test laminates.

	Variables	Description	Range
Formulation Variables	Initiator system	Trigonox 93	2%
		Trigonox 21	1.80%
		Trigonox 524	2%
	Low profile additive	PVAc	0 & 30%
	Cobalt loading	Accelerator G	0 - 2%
Process Variables	Demould time		10 - 60 mins
	Postcure rates		80 - 110 ºC
	Ambient storage		0 - 60 days

3.4.2 *Cure Efficiency*

Three laminates were moulded using the constituents in Table 3.7 with half of each laminate undergoing postcure. The residual reactivity of the three laminates was measured using DSC to determine conversion before and after postcure. DSC results shown in Figure 3.6 suggest greater than 94 % conversion with only a 3 % average increase upon postcure for all samples. Assuming that the resin mixture is not biased towards styrene, this would indicate that the cross-linking reaction has proceeded to a point where the rate-limiting step is the rate of diffusion of reactive species. There may be active sites available on the polyester chain but styrene radicals are unable to reach theses sites. The DSC analysis runs to temperatures much higher than the cure temperature of the resin (95 ºC) and since diffusion rates are temperature dependant this may push the cross-linking reaction closer to completion. However, the higher temperatures also increase the rate of styrene homopolymerisation and so the true residual reactivity is not clear.

TGA was used to monitor the evaporative loss of residual styrene from the three test samples. The derivative mass loss (Figure 3.7) shows a distinct decline for the TBPEH laminate at approximately 145 ºC, which corresponds to the boiling point of styrene. The total mass loss for the TBPEH sample at 145 ºC was 5.6 % with AAP/TBPB and TBPB producing smaller losses of 2.0 % and 1.3 % respectively. Mass spectrometry was ineffective due to the undetectable levels of volatiles being emitted at each sampling interval over the run period.

The total content of residual compounds in the three test samples was detected using GC to determine if the levels of residual styrene matched those via TGA. Figure 3.8 suggests residual styrene detected using GC was on average 20 % higher. The TBPEH initiated specimen exhibited a total 7.3 % residual styrene with a drop in levels for AAP/TBPB and TBPB to 2.5 % and 1.5 % respectively. Postcuring reduced residual styrene in each case. However, the reduction was not uniform. Only in the case of TBPB did postcuring reduce the residual styrene to a negligible level.

GC was conducted on TGA samples taken up to 150 ºC to determine if residual styrene remained within the samples. The results (Figure 3.8) show that residual styrene remained within all samples after undergoing the heat desorption of the TGA process. However, the residual styrene level for TBPB was negligible. A summation of the TGA and post TGA results from Figure 3.8, equate closely to the standard as-moulded results. It is unlikely that the discrepancies between the residual volatiles emitted in TGA and the total residual compound in GC are related to the variation in sample size, as all results are normalised to a unit mass. The discrepancies might be attributed to the compounds in the network structure being unable to evaporate due to physical entrapment (diffusion limited). This phenomenon has been reported [31, 32], with Zetterlund [31] discovering that significant trapping of radicals commences after a conversion of approximately 40 %.

The residual benzaldehyde levels of the three systems were monitored by GC (Figure 3.9). The AAP/TBPB system exhibited the highest residual benzaldehyde levels in the as-moulded state, with a 100 % increase upon postcure. Benzaldehyde increase upon postcure was not observed in the TBPEH and TBPB systems. Reijnders [4] noted an increase in residual benzaldehyde upon postcure when using a peroxide (Butanox M-50) accelerated with cobalt. The results for AAP/TBPB (accelerated by cobalt) support Reijnders findings. However, the TBPB (also accelerated by cobalt) does not. The reason for this is not obvious, but a study of the oxygen consumption rate for each system may help to explain the

differences, as increased reactivity with oxygen will promote oxidisation of residual styrene to form benzaldehyde upon additional heat input.

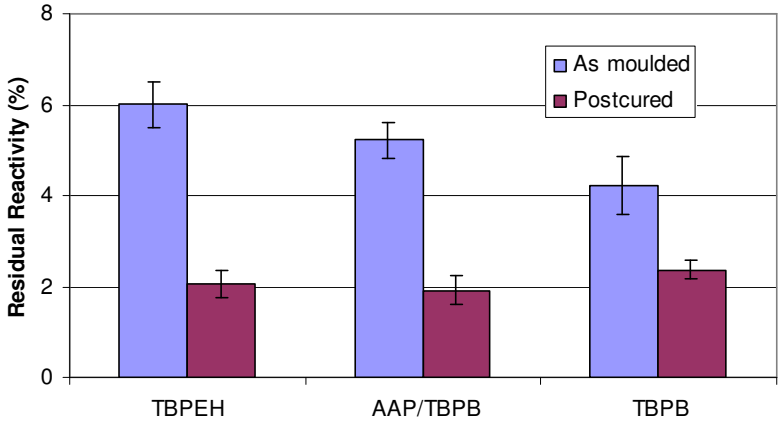

Figure 3.6: Residual reactivity detected by DSC of resin flash containing RT2557+30wt% PVAc+30wt% $CaCO_3$ with 3 initiator systems. All systems appear to be well cured with an average reduction of 3 % residual reactivity upon postcure.

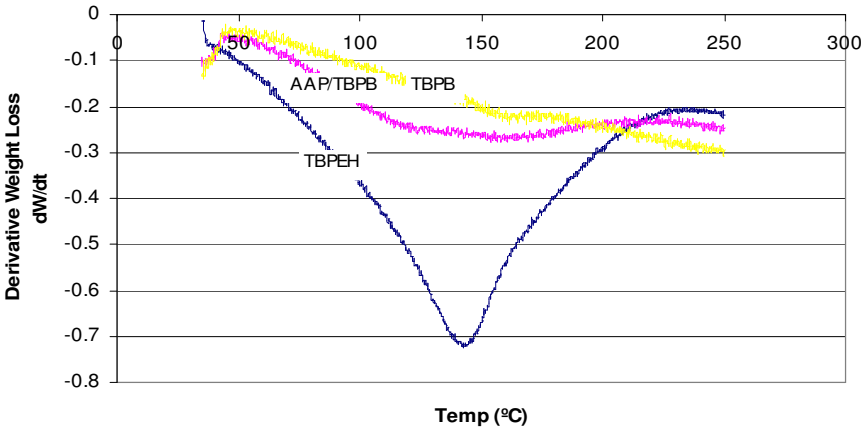

Figure 3.7: TGA on resin flash containing RT2557+30wt% PVAc+30wt% $CaCO_3$ with 3 initiator systems showing mass loss against temperature. The TBPEH system shows a 5.6 % mass loss corresponding to the evaporation point of styrene, with lower levels calculated for the other systems.

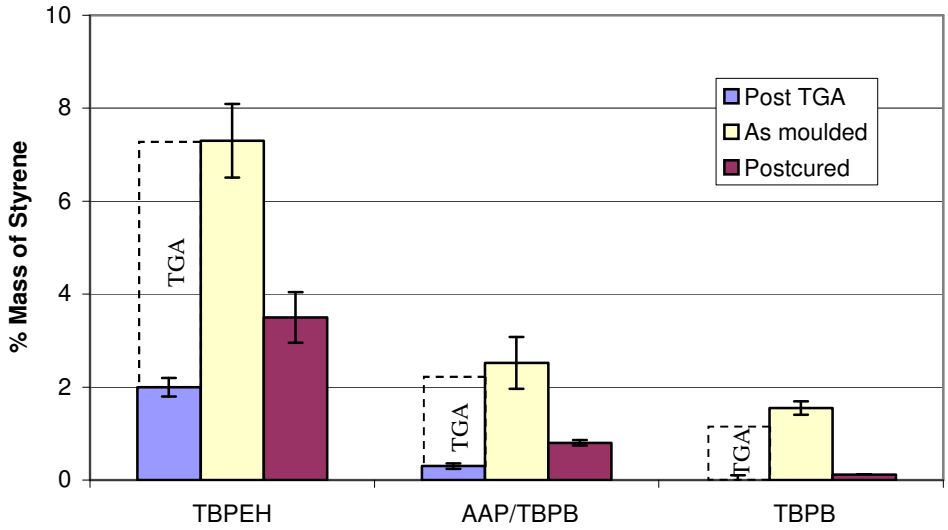

Figure 3.8: Residual styrene detected by GC from RT2557+30wt% PVAc+30wt% $CaCO_3$ +fibre with three initiator systems. Total residual styrene detection via GC shows a 20 % increase compared to TGA results. GC conducted on post TGA samples show that the heating process in TGA does not purge all of the residual styrene from the sample.

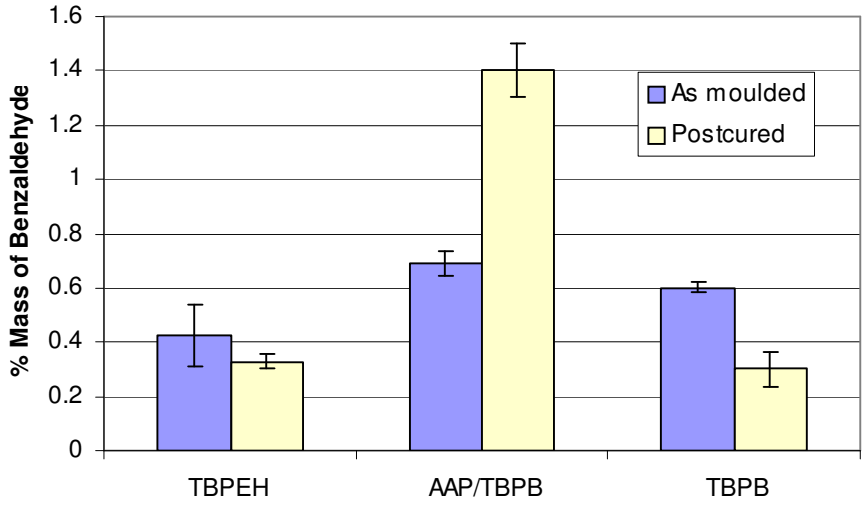

Figure 3.9: Residual benzaldehyde detected by GC from RT2557+30wt% PVAc+30wt% $CaCO_3$ +fibre with three initiator systems. TBPEH shows low residual benzaldehyde despite showing the highest residual styrene in Figure 3.8. AAP/TBPB resulted in a dramatic increase in benzaldehyde levels upon postcure whereas the TBPB system, which also uses a cobalt accelerator, showed a decrease in benzaldehyde levels upon postcure.

3.4.3 *Influence of a Low Profile Additive on Residual Content*

The effects of PVAc in styrene on residual volatiles were measured by GC and compared to a control sample with similar styrene levels. It was determined that adding 30 wt% PVAc solution to the liquid resin increased styrene concentration by 20 wt%. Table 3.9 shows the moulding conditions used for the samples.

Table 3.9: Mould conditions.

Resin	RT2557	Mould Temp (ºC)	95
Initiator (%)	TBPB (2)	Demould (min)	30
Accelerator (%)	G (0.5)		

Figure 3.10 shows that PVAc had no distinguishable effect on the residual styrene levels beyond that of adding excess styrene to RT2557. Postcuring reduced all systems to a negligible level.

The residual benzaldehyde levels seen in Figure 3.11 show that the addition of 20 wt % styrene to an unsaturated polyester system had a minor increase of 4 % on the as-moulded laminate. However, the inclusion of PVAc has been shown to promote residual benzaldehyde by 37 % compared to the control sample. Upon postcure all values fall to approximately half of their initial value for this particular cure system. Excess levels of styrene have been shown to increase the formation of residual benzaldehyde, but the dominant factor in this study has been shown to be the presence of PVAc.

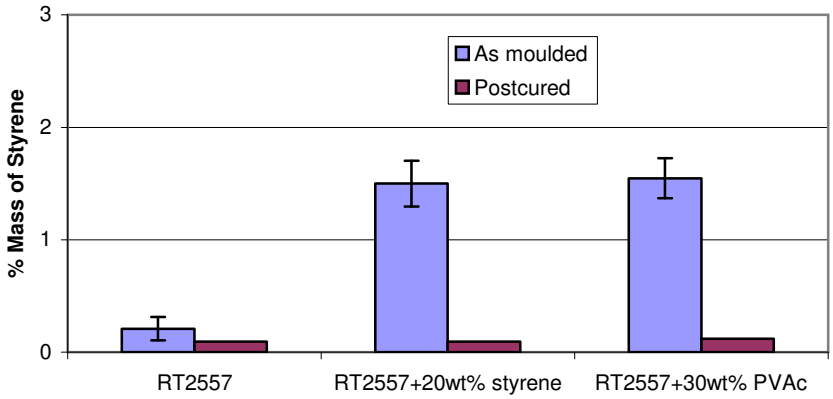

Figure 3.10: The influence of 20 wt% additional styrene and 30 wt% PVAc on the levels of residual styrene when compared to the base resin (RT2557), as detected by GC. The influence of PVAc has no more effect than the inclusion of 20 wt% styrene. Postcuring reduces all systems to a negligible level.

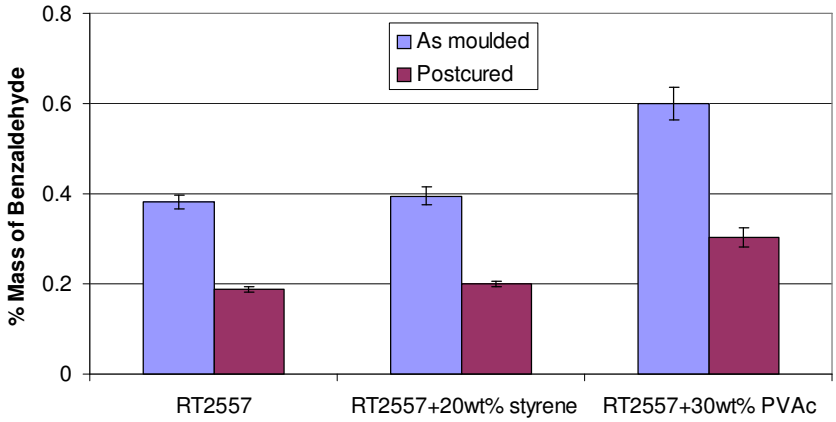

Figure 3.11: The influence of 20wt% additional styrene and 30wt% PVAc on the levels of residual benzaldehyde when compared to the base resin (RT2557), as detected by GC. Additional styrene had minimal affect on the residual benzaldehyde levels. However, the inclusion of PVAc increased benzaldehyde levels significantly. Postcuring reduced each system to half of its original value.

3.4.4 *Influence of Cobalt Levels on Residual Content*

Cobalt is used in unsaturated polyester to increase polymerisation rate and decrease residual reactivity. For this reason, the level of cobalt (Accelerator G) used throughout trials was thought likely to influence volatile levels. Trials were conducted to determine the effects of varying the accelerator loading between 0 to

2 wt% (the maximum recommended by the supplier). An unsaturated polyester/ TBPB system was used as a representative matrix (Table 3.10).

Table 3.10: Mould conditions.

Resin	RT2557 +30 wt% PVAc +30 wt% CaCO3	Mould Temp (ºC)	95
Initiator (%)	TBPB (2)	Demould (min)	30
Accelerator (%)	G (As specified)		

Figure 3.12 shows that residual styrene levels fell dramatically as accelerator loading increased to 1 %. Thereafter the residual styrene stabilised at 0.35 %, demonstrating that a stoichiometric loading was achieved. Upon postcure the residual styrene levels were negligible. The only exception here was the accelerator-free formulation. This maybe attributed to the two-stage reaction associated with this initiator, which requires a cobalt accelerator to promote the first stage. Once decomposition has started, an exotherm is produced which allows the second stage to complete the polymerisation process (Section 1.3).

Residual benzaldehyde (Figure 3.13) showed a steady increase with additional cobalt up to 1 wt% accelerator loading. At 0 wt% accelerator loading, the benzaldehyde levels increased upon postcure, demonstrating that the polymerisation process in the mould was incomplete and further heating in the postcure cycle continued the cure process to produce benzaldehyde.

The reaction rate will result in an increase in the reaction temperature Equation 1.1, which was seen when increasing the accelerator content (Figure 3.14). As the rate of the benzaldehyde side reaction is temperature dependant, we would expect the residual levels to increase with increased reaction rate. As a result, we see Figure 3.13 and Figure 3.14 showing related trends.

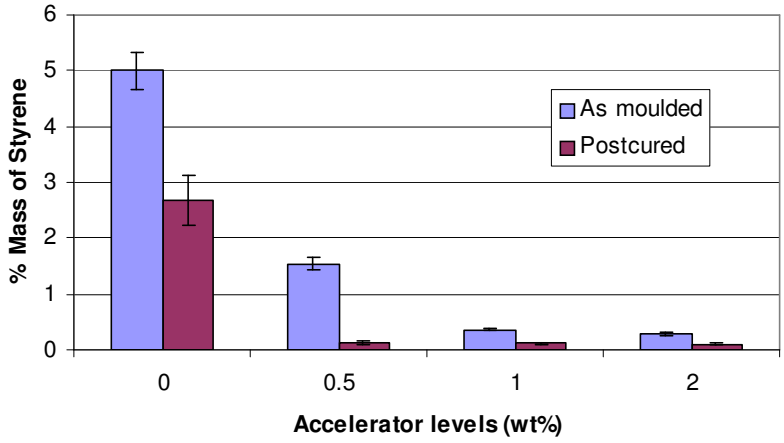

Figure 3.12: Varying accelerator loading between 0 and 2wt% to determine the effect on residual styrene levels, as detected by GC, for as-moulded and postcured samples. Increased accelerator loading reduces residual styrene content with a saturation point reached at 1 wt% accelerator. Postcuring reduces all systems (except 0 wt%) to a negligible level.

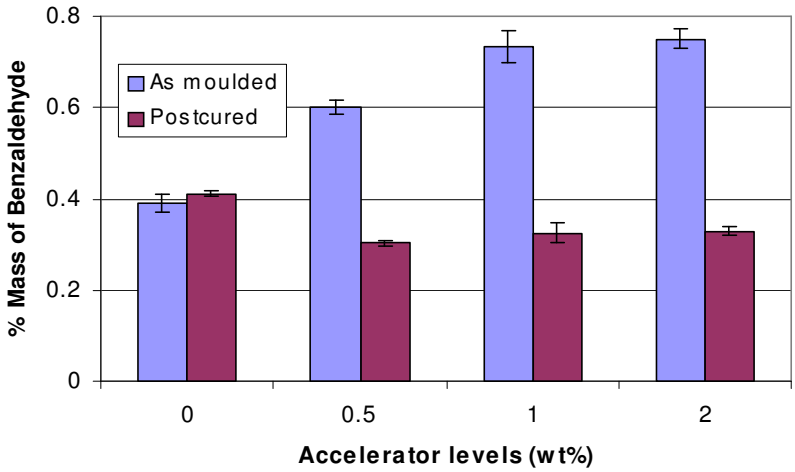

Figure 3.13: Varying accelerator loading between 0 and 2 wt% to determine the effect on residual benzaldehyde levels, as detected by GC, for as-moulded and postcured samples. Increasing accelerator loading creates an increase in residual benzaldehyde with stabilisation occurring at 1 wt% accelerator content.

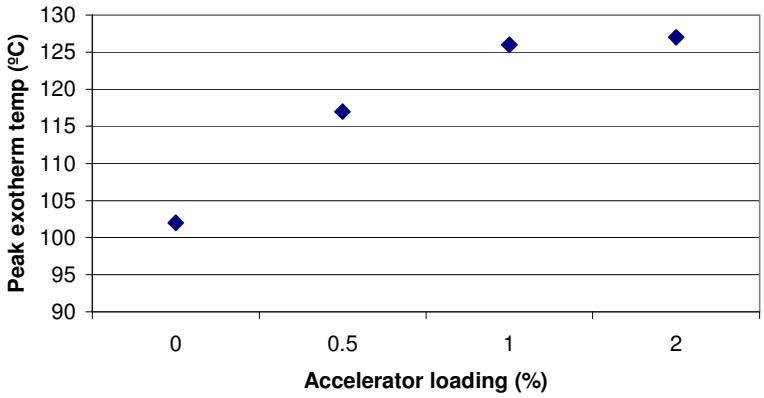

Figure 3.14: Peak exotherm temperature for accelerator loading ranging from 0 to 2 wt%.

3.4.5 *Influence of Demould Time on Residual Content*

Demould time was defined here as the elapse of time between the start of injection and the removal of the part from the mould. Clearly, it is desirable to minimise this. However, a balance must be reached to ensure that the polymerisation process is sufficiently complete for dimensional stability. Trials varied the demould time of the component from 10 to 60 minutes. An unsaturated polyester/ TBPB system with accelerator G was used as a representative matrix (Table 3.11).

Table 3.11: Mould conditions.

Resin	RT2557 +30 wt% PVAc +30 wt% CaCO3	Mould Temp (ºC)	95
Initiator (%)	TBPB (2)	Demould (min)	As specified
Accelerator (%)	G (0.5)		

Figure 3.15 shows an exponential decay in the residual styrene levels as demould time increased from 10 to 60 minutes for as-moulded samples. A 60 % reduction in residual styrene is achieved by delaying demould to 30 minutes with a further 8% reduction by extending to 60 minutes total. Postcuring the test laminates reduced styrene levels to a negligible value in all cases. DSC data (Figure 3.6) showed 96 % conversion at a demould time of 30 minutes for this particular system. Anecdotal evidence from industrial end users suggest that suitable

dimensional stability was achieved at this level. Dwell beyond 30 minutes would add unnecessary delay with minimal reduction of VOCs.

Figure 3.16 shows that residual benzaldehyde levels fell as demould time increased to 30 minutes with no discernable difference up to 60 mins. Postcuring the samples provoked a further 50 % reduction in each case for this particular system.

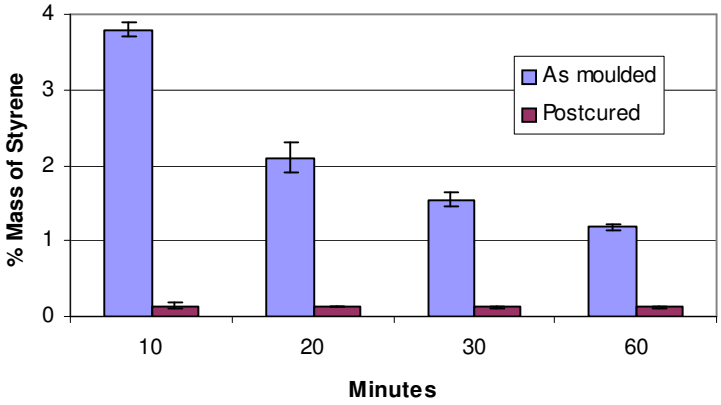

Figure 3.15: Varying demould time between 10 and 60 minutes to determine the effect on residual styrene levels by GC, for as-moulded and postcured samples of RT2557+30wt% PVAc+30wt% $CaCO_3$ +2wt% TBPB+0.5wt% Accl G. A decline in residual styrene content is seen when demould time is increased with all samples falling to negligible levels upon postcure.

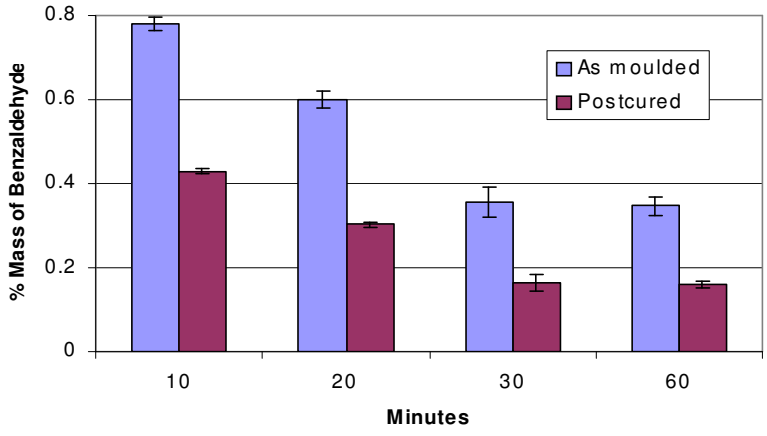

Figure 3.16: Varying demould time between 10 and 60 minutes to determine the effect on residual benzaldehyde levels by GC, for as-moulded and postcured samples of RT2557+30wt% PVAc+30wt% $CaCO_3$ +2wt% TBPB+0.5wt% Accl G.

3.4.6 *Influence of Postcure Temperature on Residual Content*

The standard postcure procedure described in Section 2.5.2 was varied from 80 to 110 ºC to determine the effects on residual volatiles. A polyester/ TBPB system with accelerator G was used as a representative matrix (Table 3.12).

Table 3.12: Mould conditions

Resin	RT2557 +30 wt% PVAc +30 wt% CaCO3	Mould Temp (ºC)	95
Initiator (%)	TBPB (2)	Demould (min)	30
Accelerator (%)	G (0.5)	Postcure (ºC)	As specified

Figure 3.17 shows that residual styrene levels fall exponentially as the postcure temperature is increased from 80 to 110 ºC. Levels at 90 ºC were four times greater than those produced at 100 ºC postcure and were undetectable via GC for the 110 ºC postcure cycle.

The residual benzaldehyde level (Figure 3.18) decreased as the postcure temperature increased. A reduction of 45 % in residual benzaldehyde was seen when increasing the temperature from 90 to 110 ºC. The curve suggests a possible benefit from postcuring above 110 ºC. However, structural integrity and dimensional stability of the composite may be compromised at temperatures near to the glass transition temperature (157 ºC via DSC).

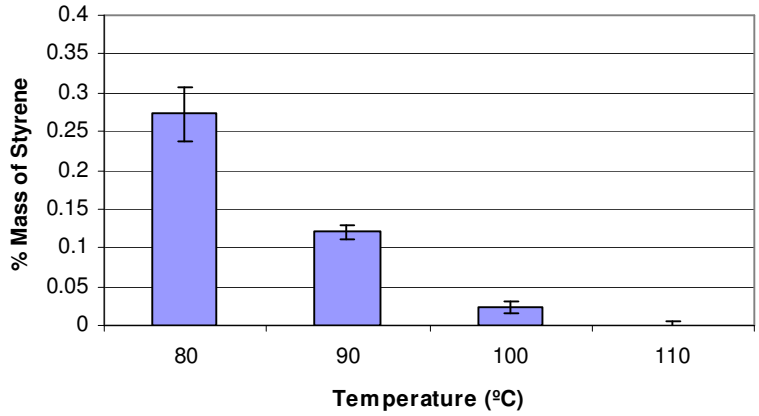

Figure 3.17: Residual styrene levels detected by GC for postcure temperatures between 80 to 110 ºC on RT2557+30wt% PVAc+30wt% $CaCO_3$ +2wt% TBPB+0.5wt% Accl G. A reduction in residual styrene content is seen as the postcure temperature is increased. Styrene was undetectable for a postcure process at 110 ºC.

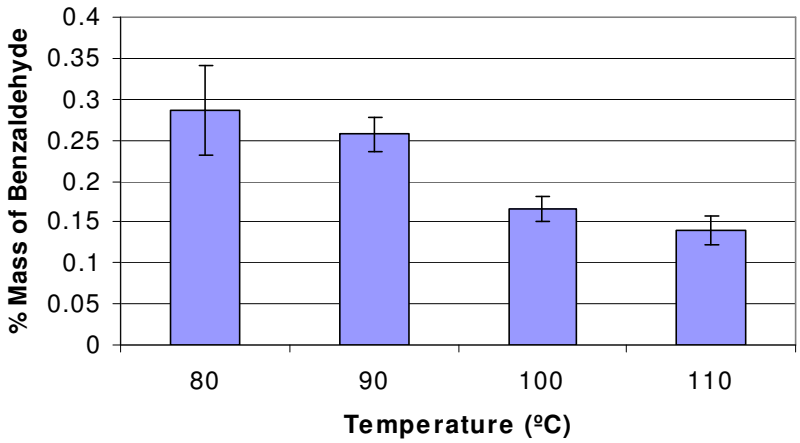

Figure 3.18: Residual benzaldehyde levels detected by GC for postcure temperatures between 80 to 110ºC on RT2557+30wt% PVAc+30wt% $CaCO_3$ +2wt% TBPB+0.5wt% Accl G. A steady decrease in residual benzaldehyde is seen with increasing postcure temperature.

3.4.7 *Influence of Ambient Storage on Residual Content*

Reijnders reported dramatic increases in residual benzaldehyde content at ambient conditions for laminates produced from low profile unsaturated polyester [4]. Previous trials have been run over a 30 day period with evidence to support that residual benzaldehyde levels had not stabilised. The current study investigates

residual styrene and benzaldehyde content over a 60 day period for RT2557+30wt% PVAc + 30wt% $CaCO_3$ with the three initiator systems (Table 3.13) at (20± 2) ºC and (50± 5) % relative humidity.

Table 3.13: Moulding conditions.

Resin	RT2557 +30 wt% PVAc +30 wt% CaCO3	Mould Temp (ºC)	95
Initiator (%)	As specified	Demould (min)	30
Accelerator (%)	G (as specified)		

Figure 3.19 shows that residual styrene levels fall in each case over the 60 days storage period for as-moulded laminates. The level of residual styrene in the as-moulded TBPB after 60 days was still four times greater than that of the sample immediately after postcuring (Figure 3.20). Postcured samples in Figure 3.20 show the same trend as mentioned for the as-moulded samples. However, the effect was reduced by the already exhausted levels of residual styrene. The TBPB system approached equilibrium after postcure and little emission was detected over the storage period.

Unlike Reijnders [4] trials, the benzaldehyde levels fell during ambient storage for all initiator types tested (Figure 3.21 and Figure 3.22). All as-moulded values fell below their respective postcured levels in each case after 60 days storage. This suggests that postcure promotes evaporation of benzaldehyde, but at the same time, diffusion limits the compound. It was observed that the benzaldehyde level directly after moulding matched Reijnders results after 30 days storage. The discrepancy with Reijnders results cannot be explained easily, but there is a possibility that high residual reactivity remained in the mouldings produced by Reijnders, which further polymerised upon storage. It would have been interesting to see the effects of postcure on residual compound levels in Reijnders trials, as this would have ruled out effects of an uncured system.

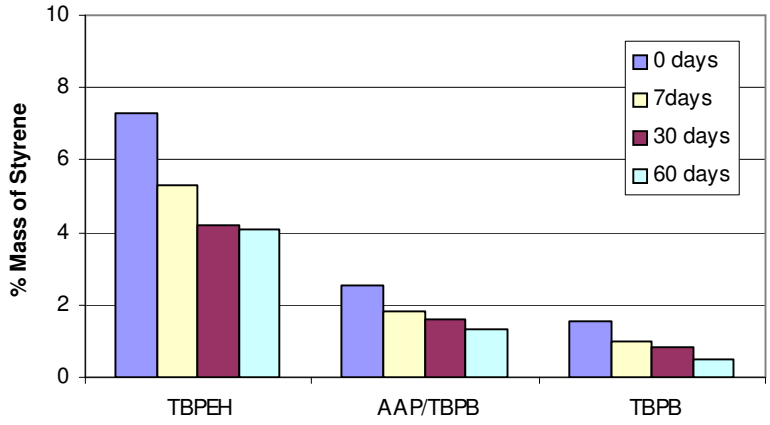

Figure 3.19: Residual styrene detected by GC for *as-moulded* RT2557+ 30wt% PVAc+30wt% $CaCO_3$ +fibre with various initiators during ambient aging. Each system shows a reduction in residual styrene content over the 60 day storage period.

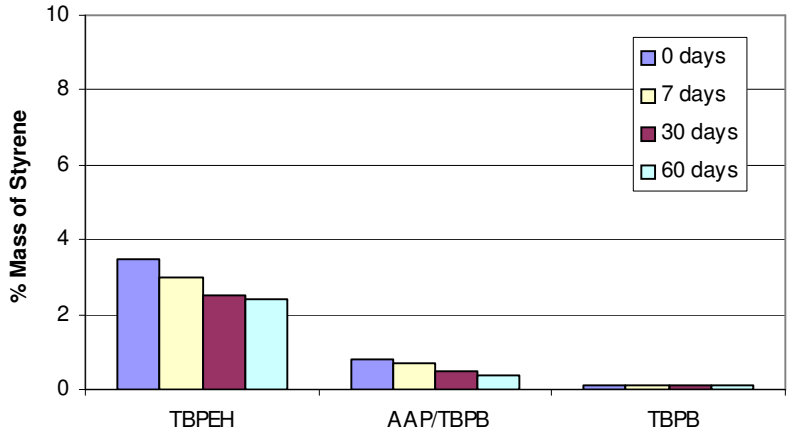

Figure 3.20: Residual styrene detected by GC for *postcured* RT2557+30wt% PVAc+30wt% $CaCO_3$ +fibre with various initiators during ambient aging. Each system shows a reduction in residual styrene content over the 60 day storage period, with TBPB reducing to a negligible level.

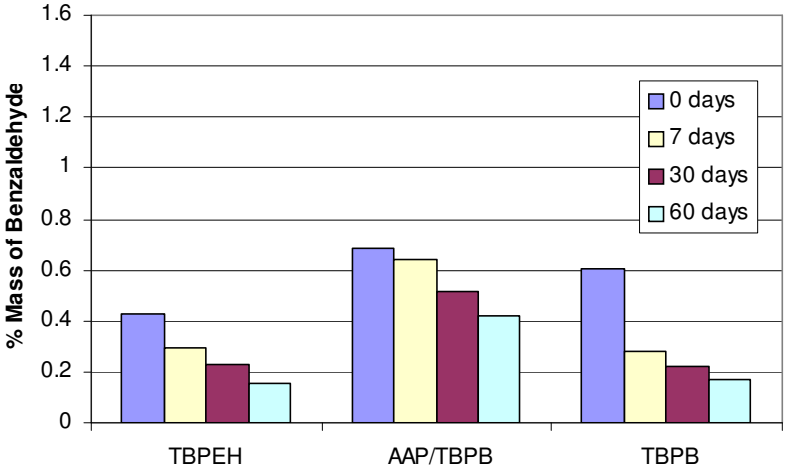

Figure 3.21: Residual benzaldehyde detected by GC for *as-moulded* RT2557+30wt% PVAc+30wt% $CaCO_3$ +fibre with various initiators during ambient aging. No increase in residual benzaldehyde was observed over the 60 day storage period.

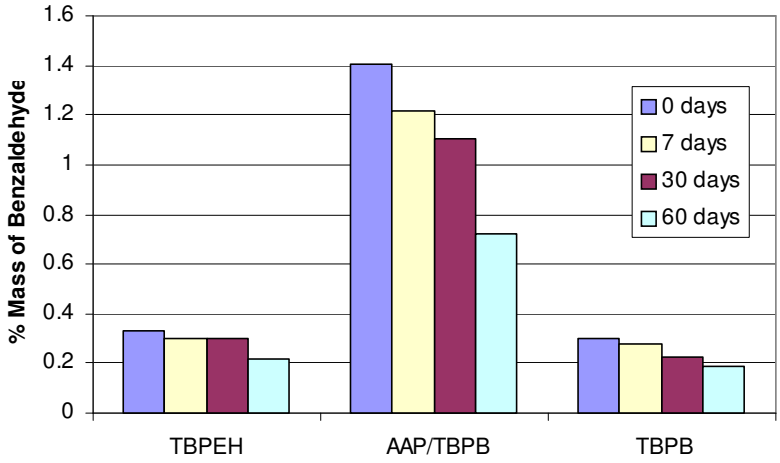

Figure 3.22: Residual benzaldehyde detected by GC for *postcured* RT2557+30wt% PVAc+30wt% $CaCO_3$ +fibre with various initiators during ambient aging. No increase in residual benzaldehyde was observed over the 60 day storage period. It was discovered that a greater reduction in residual benzaldehyde could be obtained over the 60 day storage period by not postcuring the samples.

3.5 Conclusions

The effects of system reactivity, thermal input and low profile additive on the residual organic compound levels (namely styrene and benzaldehyde) in unsaturated polyester matrix have been identified. The dominant variables for residual styrene and benzaldehyde production have been established.

The process of measuring the degree of cure determined by DSC uses temperatures three times greater than the cure temperature, which may push further polymerisation of active sites available on the polyester chain. However, the high temperatures also increase the rate of styrene homopolymerisation, affecting the true residual reactivity. Therefore, it is necessary to determine the residual styrene level by more direct methods before the level of residual reactivity can be accurately quoted. Residual styrene detection was best obtained by solvent-based gas chromatography as all compounds are eluted from the sample. Evaporative systems such as head-space analysis and the thermogravimetric analysis are limited by the availability of the volatile reaching the surface of the sample for desorption. This was demonstrated, as styrene monomer was diffusion limited within the unsaturated polyester matrix.

Solvent-based gas chromatography was effective for measuring conversion efficiency and monitoring volatile organic compounds. Styrene conversion using a peroxide initiator fluctuated depending on the reactivity of the system, which also affects the formation of benzaldehyde. The latter was influenced predominantly by the presence of PVAc. Other formulation variables affecting the production of styrene and benzaldehyde include the cobalt octoate accelerant.

Cure times and postcure temperatures showed a pronounced reduction in styrene and benzaldehyde over as-moulded laminates. A limit was observed in both situations where additional input had a negligible affect on compound detection and only served to extend the cycle.

Discrepancies with Reijnder's study concerning the ambient storage on benzaldehyde level suggests a need for further research into this field. An integrated modelling approach is required to relate cure kinetics and mechanistic models for the competing reactions to compound consumption. This would be a valuable tool in studying the affects of formulation and process variables on a range of polymer systems.

3.6 References

1. Manuel, D., *New car drivers exposed to toxic emissions.* CSIRO, 2001(http://www.csiro.au/index.asp?type=mediaRelease&id=newcars).
2. *National Toxicology Program.* Sixth Annual Report on Carcinogens, 1991(http://eagle.westnet.gr/~aesclep/carcinog.htm).
3. Cao, X. and Lee, J., *Control of shrinkage and residual styrene of unsaturated polyester resins cured at low temperatures: I Effects of curing agents.* Polymer, 2003. **44**: p. 1893-1902.
4. Reijnders, H., *The influence of cure systems on the formation of volatile components in RTM processed UP articles.* 2001(www.akzonobel.de/).
5. Owen, M.J., Middleton, V., and Jones, I.A., *Integrated design and manufacture using fibre-reinforced polymeric composites*. 2000, Cambridge: Woodhead publishing limited.
6. Weatherhead, R.G., *FRP technology - fibre reinforced resin systems*. 1998, Applied Science Publishing: London.
7. Miller, R.R., Newhook, R., and Poole, A., *Styrene production, use and human exposure.* Toxicology, 1994. **24**: p. S1-S10.
8. Sorsa, M., Peltonen, K., Vainio, H., and Hemminki, K., *Butadiene and styrene: Assessment of health hazards.* IARC Scientific Publications, 1993. **127**: p. 65-78.
9. Lof, A., Lundgren, E., Nydahl, E., and Nordqvist, M., *Biological monitoring of styrene metabolites in blood.* Journal of Work Environment & Health, 1986. **12**: p. 70-74.
10. Groth-Marnat, G., *Neuropsychological effects of styrene exposure: a review of current literature.* Journal of Perceptual and Motor Skills, 1993. **77**: p. 1139-1149.
11. White, D.M., Daniell, W.E., Maxwell, J.K., and Townes, B.D., *Psychosis following styrene exposure: case report of neuropsychological sequelae.* Journal of Clinical and Experimental Neuropsychology, 1990. **12**: p. 789-806.
12. Edling, C., Anundi, H., Johanson, G., and Nilsson, K., *Increase in neuropsychiatric symptoms after occupational exposure to low levels of styrene.* Journal of Internal Medicine, 1993. **50**(9): p. 843-850.
13. Frostling, H., *The occupational exposure limit value for styrene - a matter of life or death for the reinforced plastic industry.* Swedish work environment authority, 2002,(http://www.av.se/publikationer/rapporter/2002_02eng.pdf).

14. Somorovska, M., Jahnova, E., Tulinska, J., and Zamecnikova, M., *Biomonitoring of occupational exposure to styrene in a plastics lamination plant.* Mutation Research, 1999. **428**: p. 255-269.
15. Vodicka, P., Bastlova, T., Vodickova, L., Perterkova, K., Lambert, B., and Hemminki, K., *Biomarkers of styrene exposure in lamination workers: levels of O6-guanine DNA adducts, DNA strand breaks and mutant frequencies in the hypoxanthine guanine phosphoribosyltransferase gene in T-lymphocytes.* Carcinogenesis, 1995. **16**: p. 1473-1481.
16. *Occupational exposure limits 2000*, in *EH40/2000*. 2000.
17. Zhuang, J., Ma, D., Yan, Z., Liu, X., Han, X., Bao, X., Zhang, Y., Guo, X., and Wang, X., *Effect of acidity in TS-1 zeolites on product distribution of the styrene oxidation reaction.* Applied catalysis, 2004. **258**: p. 1-6.
18. Weir, N.A. and Ceccarelli, A., *Photodecomposition of polystyrene hydroperoxide: Part I - reactions in dilute solution.* Polymer Degradation and Stability, 1993. **41**(1): p. 37-44.
19. Russo, J., Chung, S., Contreras, K., Lian, B., Lorenz, J., Stevens, D., and Trousdell, W., *Identification of 4-(N,N-Dipropylamino) benzaldehyde as a potential reversible inhibitor of mouse and human class I aldehyde dehyrdogenase.* Biochemical Pharmacology, 1995. **50**(3): p. 399-406.
20. *Threshold limit values (TLVs) for chemical substances and physical agents and biological exposure indices (BEIs)*, in *American Conference of Government Industrial Hygienists*. 2001, ACGIH: Cincinnati, OH.
21. Inoue, O., Kanno, E., Kasai, K., Ukai, H., Okamoto, S., and Ikeda, M., *Benzylmercapturic acid is superior to hippuric acid and o-cresol as a urinary marker of occupational exposure to toluene.* Toxicology, 2004. **147**: p. 177-186.
22. Senzolo, C., Frignani, S., and Pavoni, B., *Environmental and biological monitoring of occupational exposure to organic micropollutants.* Chemosphere, 2001. **44**: p. 67-82.
23. Rodriguez, E.L., *Residual styrene monomer in cured unsaturated polyester resins.* Polymer Materials Science Engineering, 1988. **58**: p. 575-580.
24. Cao, X. and Lee, L.J., *Control of volume shrinkage and residual styrene of unsaturated polyester resins cured at low temperatures. II Effects of comonomer.* Polymer, 2003. **44**: p. 1507-1516.
25. Forrest, M.J., Jolly, A.M., Holding, S.R., and Richards, S.J., *Emissions from processing thermoplastics.* Annals of Occupational Hygiene, 1995. **39**(1): p. 35-53.
26. Yang, X., *Measurement of residual styrene content in unsaturated polyester resin by gas chromatography.* Huaxue Shijie, 1993. **34**(5): p. 220-223.
27. Newman, R.H. and Patterson, K.H., *Solid-state n.m.r determination of residual unsaturation in styrene-cured polyester resins.* Polymer, 1996. **37**(7): p. 1065-1069.
28. Tawfik, S.Y., Asaad, J.N., and Sabaa, M.W., *Effects of polyester backbone structure on the cured products properties.* Polymer Testing, 2003. **22**: p. 747-759.
29. Huang, Y.-J. and Liang, C.-M., *Volume shrinkage characteristics in the cure of low-shrink unsaturated polyester resins.* Polymer, 1996. **37**(3): p. 401-412.

30. Smith, R., *Before injection- modern methods of sample preparation for separation techniques.* Journal of Chromatography, 2003. **1000**: p. 3-27.
31. Zetterlund, P.B. and Johnson, A.F., *Free volume-based modelling of free radical crosslinking polymerisation of unsaturated polyesters.* Polymer, 2002. **43**: p. 2039-2048.
32. Hsu, C.P. and Lee, L.J., *Free-radical crosslinking copolymerization of styrene/unsaturated polyester resins: 2. Electron spin resonance study.* Polymer, 1993. **34**: p. 4506-4515.

4 Nano-Scale Silicates as an Alternative to Conventional LPAs

4.1 Introduction

It has been shown in Chapter 3 that LPAs used as modifier in polyester resin systems have an increasing effect on VOCs, namely residual styrene and benzaldehyde. LPA also increases the brittleness of the structure due to the formation of micro-cracking during phase separation. Here, an alternative to chemical based low profiling systems is studied in order to minimise changes to physical properties and to reduce residual VOCs without compromising the cosmetic laminate.

A novel approach is attempted using exfoliated clays to reduce resin shrinkage within styrene based unsaturated polyester resins via a so-called nanocomposite. Nanocomposites offer considerable promise for improving matrix functional properties especially fire retardancy and reduction of gas permeability. Work conducted in this chapter looks at:

- The feasibility of dispersing layered silicates in unsaturated polyester resin on a nanoscale.
- The feasibility of shrinkage control via nanoscale silicates.
- The potential for using silicates to replace some or all of the conventional LPA loading.
- Determination of the effectiveness of silicate clays to improve mechanical properties of existing LPA filled polyester resin.

4.2 Nano-Scaled Layered Silicates

Polymer based layered silicate nanocomposites are new hybrid materials that offer an interesting alternative to conventionally filled polymers. Nanocomposites utilise a reinforcement phase thickness of the order of a few nanometers, which is on the same scale as the radius of gyration of a polymer [1]. The polymer molecules at the surface of the nanoscale particles are completely immobilised,

with the neighbouring region being partially immobilised [2]. Due to the high surface area of the nanoscale particles, the effects from reduced molecular mobility become significant, leading to unique properties of the polymer nanocomposite [3, 4].

The high aspect ratio (10 to 2000) of the nano-scaled layered silicate plays a key role in the improvement of the properties of nanocomposites [5, 6]. Improvements in mechanical properties [7-10], thermal stability [11, 12] and dielectic properties [13] have been widely documented. Adding clay nanofillers to biodegradable polymers has also been shown to enhance compostability [14, 15]. Notably, low concentrations of silicate (1-5 wt%) result in the aforementioned improvements.

4.2.1 *Molecular Structure of Montmorillonite*

Clay mineral montmorillonite, a member of the dioctahdral 2:1 layered silicate smectite group, is widely used as a raw material over bentonite and hectorite due to its powerful catalytic and absorbent properties [16]. Two features of this material are the nearly unrestricted exchangeability of its intermediate layer cations and excellent swelling capacity in aqueous solutions. The expansion of the layers can lead to the disintegration of the crystal network [17]. Montmorillonite has a chemical structure of:

$$\mathbf{M_x(Al_{4-x}Mg_x)Si_8O_{20}(OH)_4} \qquad [4.1]$$

where M is the monovalent cation and x is the degree of isomorphous substitution (between 0.5 and 1.3).

The montmorillonite structure (Figure 4.1) consists of two fused silica tetrahedral sheets sandwiching an edge shared octahedral sheet. The layer thickness is around 1 nm and the lateral dimensions of these layers may vary from 10 nm to several microns depending on the particular silicate [18]. Isomorphous substitutions of Si^{4+} for Al^{3+} in the tetrahedral lattice and of Al^{3+} for Mg^{2+} in the octahedral sheet cause an excess of negative charges within the montmorillonite layers [19]. These

negative charges are counterbalanced by cations such as Ca^{2+} and Na^{+} situated between the clay layers. Montmorillonite's hydrophilic behaviour necessitates chemical treatment (sizing) in order to make an organophilic structure that is compatible with the polymer matrix in question [3]. An exchange of the Ca^{2+} and Na^{+} cations for alkylammonium ions renders the clay organophilic and lowers the surface energy of the clay layers [19]. This assists organic species to diffuse between the layers and eventually separate them i.e. intercalation or exfoliation.

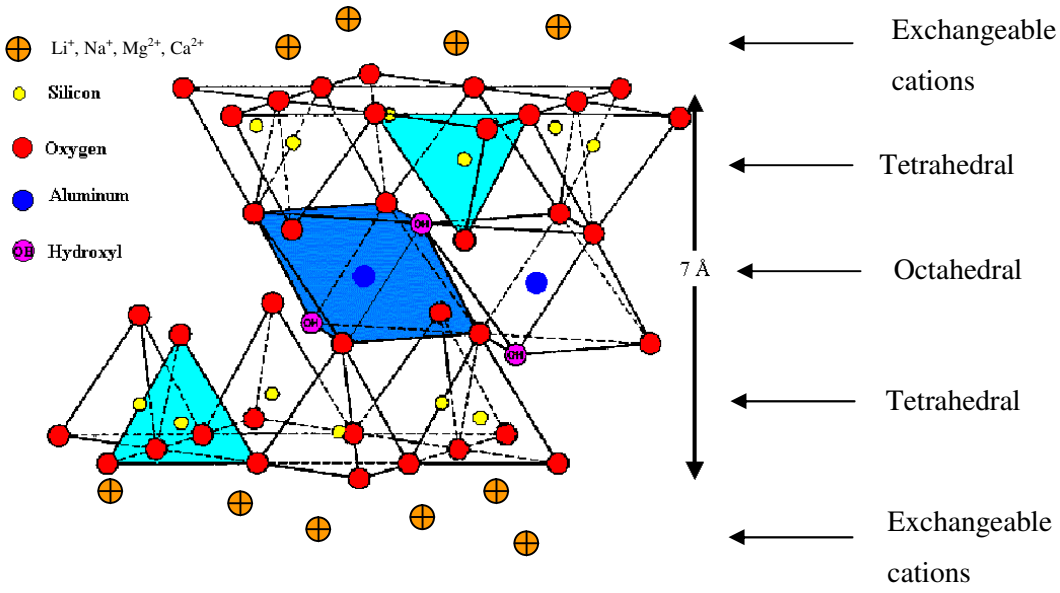

Figure 4.1: Structure model of dioctahedral 2:1 layer silicate.

4.2.2 *Dispersion*

The formation of a nanocomposite is dependent upon the matrix and its ability to penetrate the silicate layers. The so-called intercalation of polymers in layered silicates has proven to be a successful approach to synthesise several nanocomposites. The preparative methods are divided into three main categories according to the starting materials and processing techniques: Intercalation of polymer or pre-polymer from solution [20], In-situ intercalative polymerisation [3, 21-23] or melt intercalation [24, 25]. Nanocomposites developed from several thermoset polymers can be prepared by the in-situ intercalative polymerisation method [26] with phenol, epoxy and polyester resins all included in this category. In-situ intercalative polymerisation involves swelling the organophilic clay with a

compatible monomer followed by a crosslinking reaction. During swelling, the monomer diffuses from the bulk monomer into the galleries between the silicate layers. Different types of composites can be obtained depending on the degree of penetration of the monomer into the organo-layered silicate structure. Composites based on mica-type silicates can be divided into three distinctive morphologies (Figure 4.2)[3]:

a. *Immiscible,* mica-type silicate tactoids exist in their original aggregated state with no intercalation of the polymer matrix into the galleries [3]. For this case the particles act as micro-scale fillers.

b. *Intercalated nanocomposites* have the polymer matrix intercalated between the silicate layers and the expanded silicate layers are still in order.

c. *Exfoliated nanocomposites*, in which the individual 1 nm thick silicate layers are completely dispersed in a polymer matrix and the gallery structures are completely destroyed [27].

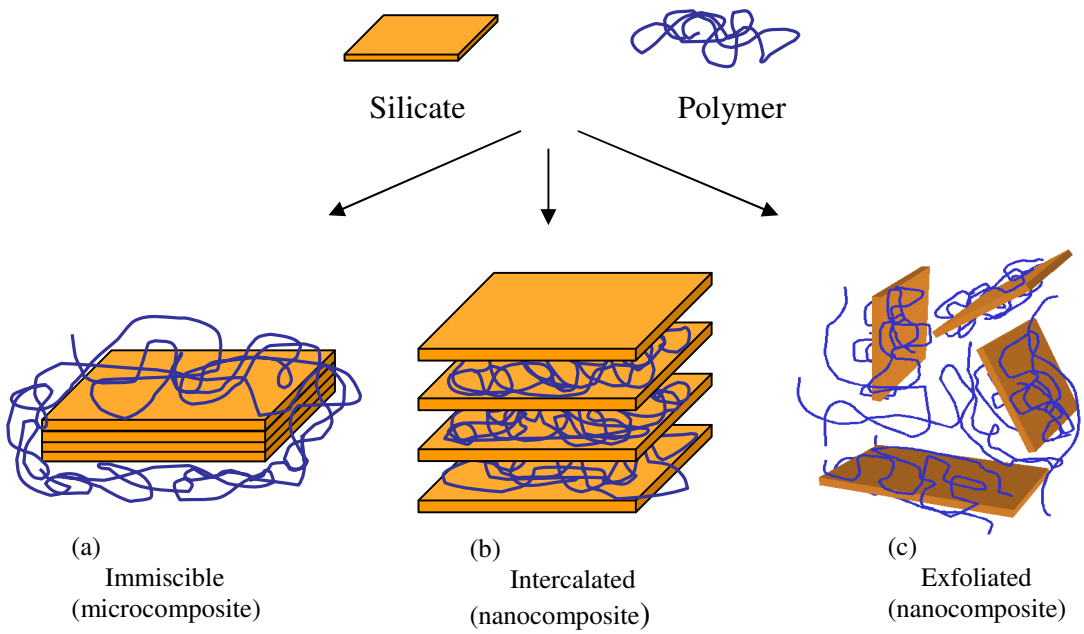

Figure 4.2: Scheme of composite structures arising from the interaction of layered silicates and polymers [3, 18].

The structure of nanocomposites has typically been established using X-ray diffraction (XRD) analysis and transmission electron microscopy (TEM). The two complimentary techniques are used for quantitative and qualitative analysis respectively. XRD is commonly used to probe the nanocomposite structure due to its ease and availability. By monitoring the position, shape and intensity of the basal reflections from the distributed silicate layers, the nanocomposite structure (intercalated or exfoliated) may be identified (Figure 4.3). The intercalation of polymer chains tends to increase the interlayer spacing in comparison with the spacing of the organoclay used. This leads to a shift of the diffraction peak towards lower angle values due to Bragg's law:

$$\mathbf{2}\boldsymbol{d}\mathbf{.}\ \mathbf{sin}\theta = \boldsymbol{n}\mathbf{.}\lambda \qquad [4.2]$$

where: d is the lattice spacing, θ is the angle of reflection, n is an integer and λ is the wavelength of the incident X-ray beam.

Extensive layer separation (d_{001} greater than 6-7 nm) and disordering associated with delamination of the silicate layers in the polymer matrix result in the eventual disappearance of any coherent diffraction peaks (Figure 4.3). This phenomenon is characteristic of a disordered, exfoliated nanocomposite. However, consideration must be given when using XRD to ensure that readings are representative of the bulk matrix and that grouped areas of disordered layers are not influencing results. TEM is traditionally used to complement XRD results and give real time visual analysis of the nanocomposite morphology.

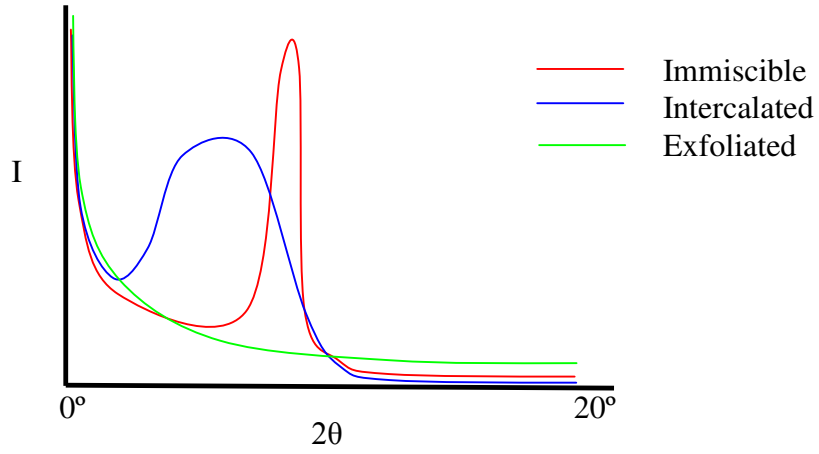

Figure 4.3: Schematic of XRD spectra for various polymer layered silicate composites [6].

The collective knowledge of morphology and heterogeneity of layered silicates [1, 28-31] indicates that the formation of an intercalated or exfoliated polymer layered nanocomposite occurs by a more complex process than simple sequential swelling and separation of individual layers starting from the surface of the primary particle. Defect structures, local chemical inhomogeneity, electrostatic forces, viscoelastic properties of the polymer and stress fields arising from interlayer swelling will all contribute to mediate polymer transport and layer mobility and thus final morphology.

The suggestion of using nano silicate particles to address the inherent problems associated with conventional low profiling systems, such as PVAc, is an attractive alternative, as monomer concentration will not be increased and benefits in mechanical properties with loadings as low as 1 wt% are reported. The use of silicates for retarding resin shrinkage is thought to be viable due to immobilisation of polymer molecules at the surface of the particles with neighbouring regions being partially immobilised. Upon polymerisation, residual forces should increase and restrict movement of the polymer molecules.

Numerous cases have been presented which suggest that intercalation of silicates in a polymer matrix is achievable but full exfoliation is desirable for optimal contact surface area. Thus, a study of the dispersion process and characterisation of the structure was planned. Volumetric shrinkage measurement and mechanical testing is required to determine the suggested effects of a low profile, nanocomposite matrix.

4.3 Experimental Methods

4.3.1 *Materials*

Two commercially available clays (Cloisite® 10A, Garamite® 1958) and a calcium carbonate filler were tested with an unsaturated polyester resin used in Chapter 2 (Summarised in Table 4.1). The calcium carbonate ($CaCO_3$) filler was supplied by Omya UK Ltd with a 5.7 µm nominal particle size. The clays (Table 4.2) were supplied by Southern Clay Products representing part of their additives range for polymer matrices.

Table 4.1: Constituents.

Constituent	Supplier	Product	Description
Base resin	Scott Bader	RT2557	Orthophthalic Unsat' Polyester
Low Profile additive	Dow Chemicals	PVAc with 60wt% styrene	Thermoplastic in styrene
Filler	Omya UK	BLR2	$CaCO_3$ @ 5.7µm
Initiator	Akzo Nobel	Trigonox® 93	TBPB in solution
Accelerator	Scott Bader	Accelerator G	60-80 ºC

Cloisite® 10A additive is a natural montmorillonite modified with a quaternary ammonium salt [32]. It consists of organically modified nanometer scale, layered magnesium aluminium silicate platelets, which are surface modified to assist inter-gallery absorption. Cloisite® 10A is reported to have a surface area in excess of 750 m^2/g with an aspect ratio in the range of 70 to 150 [32]. The typical dry

particle size is 6 µm with a specific gravity of 1.9 g/cc. This particular organically modified clay was chosen due to the presence of the benzyl group, which could be expected to encourage styrene into the gallery spacing.

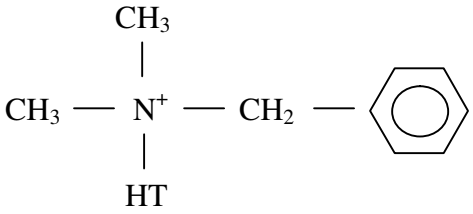

Where HT is Hydrogenated Tallow
(~65% C18; ~30% C16; ~5% C14)
Anion: Chloride

Figure 4.4: Cloisite® 10A chemical structure.

Garamite® 1958 is a proprietary blend of minerals that have been organically modified to provide thixotropic (shear thinning) advantages for use in applications with polymer resins such as unsaturated polyesters, epoxies and vinyl esters [33]. It has also been used to help with lowering monomer concentration. Garamite® 1958 is an alkyl quaternary ammonium clay organically modified with dimethyl dihydrogenated tallow with average particle size of 10 µm and specific gravity of 1.6 g/cc.

Table 4.2: Properties of silicate clay particles.

Property	**Cloisite® 10A**	**Garamite® 1958**
Modifier	Dimethyl, benzyl, hydrogenated tallow, quaternary ammonium	Dimethyl dihydrogenated tallow
Modifier (wt%)	39	20
Actual density (g/cc)	1.9	1.5-1.7
Particle size (µm)	~ 6	~ 10
X-ray result d_{001} (nm)	1.92	1.21

4.3.2 *Experimental Procedure*

The silicate was processed with unsaturated polyester resin using an in-situ intercalative polymerisation method. The silicate was dried at 110 ºC for one hour and then added to 1 kg of unsaturated polyester at loadings ranging from 1 to 10 wt%. Dispersion was by an air driven shear mixer with a 40 mm paddle at 1500 rpm. The speed was established in studies detailed in Appendix 7. Accelerator G and finally TBPB initiator were then added. The resin matrix was degassed at 700 mmHg for 10 minutes.

The resulting blend was cast using a 250 x 250 x 3 mm aluminium picture frame tool polished to an *Ra* of 0.15 µm (Figure 4.5). A 5 mm nitrile rubber seal was recessed around the perimeter of the upper and lower platen, which sealed against the picture frame using eight M12 bolts. Coupled to this was the shrinkage bar cast tool, which was manufactured from machined hydraulic tubing (Ø38.151 ID x 71.081 mm) capped at both ends and fastened by three M12 bolts. A Ø44 x 2.6 mm thick silicon o-ring was recessed into the tubing to provide a seal once assembled (Figure 4.6).

The tool was heated in an oven to 95 ºC prior to injection. The resin was injected at 50 kPa and the vent ball valve was closed after 20 sec of resin run-off. The chamber was pressurised to 500 kPa and then sealed by closing the injection ball valve. The tool was left to stand in the 95 ºC environment for a 30 min cure cycle (Table 4.3). Upon demould, the samples were postcured at 90 ºC using the cycle shown in Section 2.5.2.

Table 4.3: Conditions for moulding of samples

Resin	Initiator	Accelerator	Mould Temp (ºC)	Mould Pressure (kPa)	Demould Time (min)
RT2557	TBPB (2 wt%)	Accelerator G (0.5 wt%)	95	500	30

A concentric cylinder was used to measure the non-Newtonian viscosity over a shear rate of 0.15 to 67 s^{-1}. At shear rates less than 100 s^{-1}, the apparent viscosity increased with increased silicate concentration (Table 4.4). Thus loadings above 10 wt% were not used due to inherent problems when injecting into the mould. A decrease in viscosity was observed at shear rates greater than 100 s^{-1}.

Table 4.4: Peak viscosity of matrix with silicate loading varying between 0 to 10 wt%.

Silicate Loading (%)	Viscosity (Pas)
0	0.062
1	1.233
2	1.824
4	2.131
10	12.226

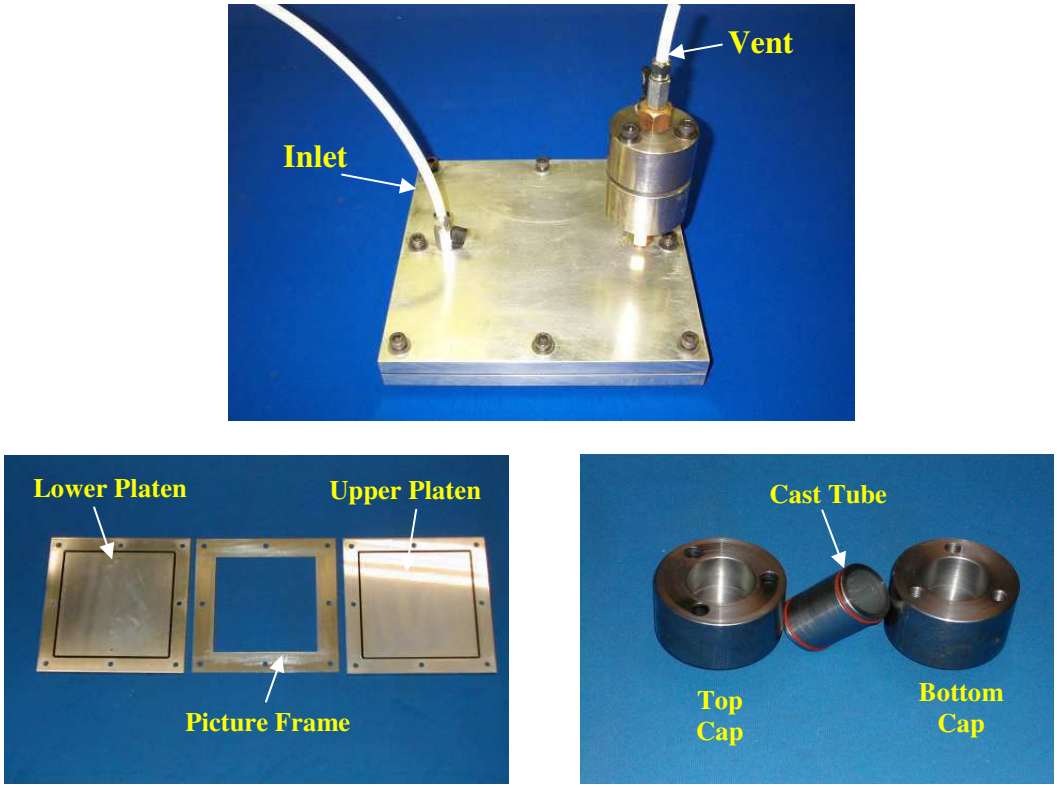

Figure 4.5: Aluminium resin casing tool and shrinkage bar tool.

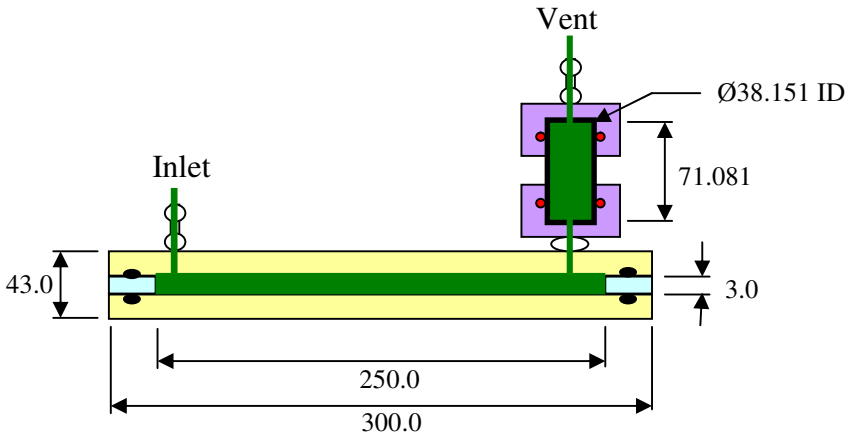

Figure 4.6: Cross section schematic of the cast tool and shrinkage bar tool.

X-ray Diffraction

X-ray diffraction (XRD) patterns were obtained using a Phillips PW 3710, equipped with Cu-K_α (λ = 1.5406 Å) radiation source and a Ni K_β filter. The X-ray generator operated at 40 kV and 40 mA. The diffraction angle 2θ was monitored from 2-12 degrees at a scanning speed and step size of 1 °/min and 0.02 degrees, respectively. Specimens were produced from polymerised castings measuring 50 x 20 x 3 mm. The top 100 µm of the specimens were ground with 1200 grit paper to ensure an even surface for diffraction and were held in position via a spring-loaded clip (Figure 4.7). The through-gradient effect was monitored (Appendix 7) revealing no variation in the level of dispersion

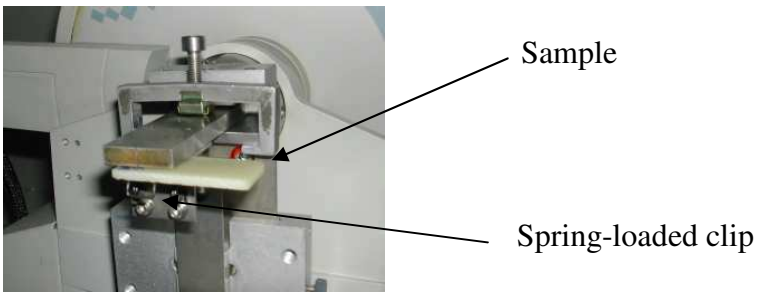

Figure 4.7: Sample held in the XRD armature using a spring-loaded clip.

Transmission Electron Microscopy

Transmission electron microscopy (TEM) was performed on ultramicrotomed samples prepared using a Reichert-Jung RACUT microtome equipped with a 45 degree diamond knife (Figure 4.8), and mounted on 200 mesh copper grids. The sections were cut to a thickness of 40 nm. TEM images were obtained using a JEOL 2000FX microscope with a LaB_6 filament operating at 120kV.

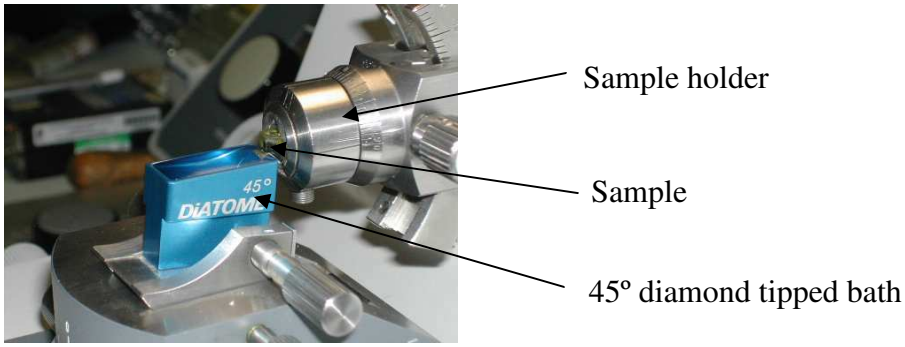

Figure 4.8: Ultramicrotomed cutter sample holder and diamond tipped bath.

Volumetric Shrinkage Measurement

The volumetric shrinkage of resin samples was determined using a Quantachrome Multipycnometer (Figure 4.9). Three test bars of the same resin composition were tested for repeatability. The true density of the solid sample was found by measuring the pressure difference, when a known quantity of nitrogen gas under pressure (approx 117 kPa) was allowed to flow from a reference volume (V_r) into a sample cell containing the solid material. The technique employs Archimedes principle of fluid displacement to determine the volume of the sample.

$$V_s = V_c - V_r\left[\left(P_1/P_2\right)-1\right] \qquad \textbf{[4.3]}$$

where V_s is the sample volume, V_c is the sample cell volume, P_1 is the pressure in the reference cell and P_2 is the pressure in the sample cell.

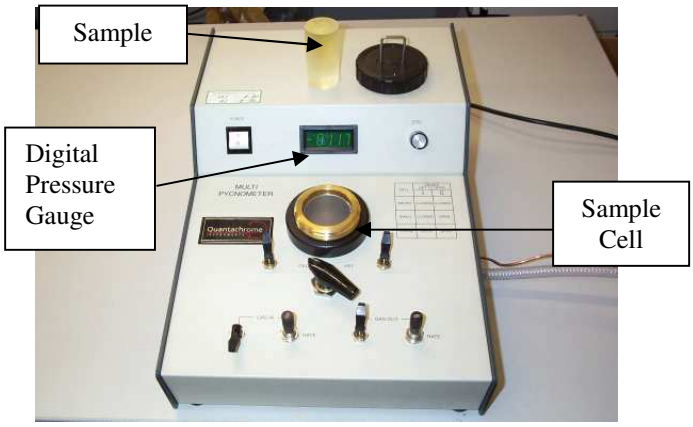

Figure 4.9: Multipycnometer used to measure resin sample volume via Archimedes principle.

Thermal Capacity

Isothermal analysis of cured nanocomposite was performed using a Perkin Elmer Pyris 1 differential scanning calorimeter to detect the glass transition (T_g). Each sample was heated from 50 to 250 ºC at a rate of 10 ºC/min under a nitrogen atmosphere.

Mechanical Testing

Preparing the samples proved difficult as standard diamond coated blades caused excessive chipping on the edges (Figure 4.10). The stress concentrations caused by chipped edges would serve to promote premature failure of the samples. To overcome this problem, the samples were prepared by a Buehler Petrotrim saw equipped with a 6" diameter, 0.025" thick Sunburst diamond blade (99-0371) supplied by MK Diamond Products, Inc. Tensile and flexural tests were conducted using a Hounsfield H25KS with a 100SC extensometer, following BS 2782-3 method 326f:1997 and BS EN ISO 178:1997 respectively. The tensile and flexural test specimens were loaded at a constant rate of 1 mm/min until failure. The tensile modulus was calculated as the slope in the stress-strain curve for strain values between 0.001 and 0.003. At least 15 specimens were taken from each sample.

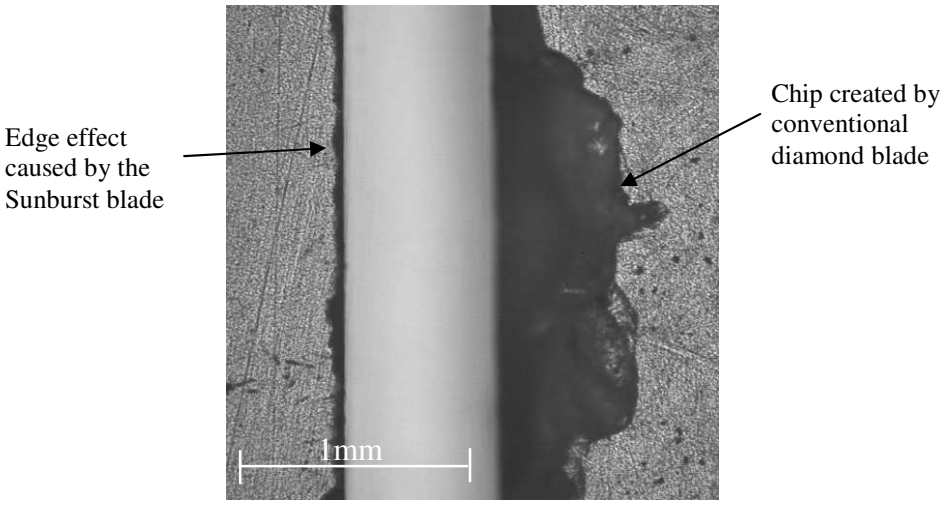

Figure 4.10: Edge effects on the neat resin samples caused by the Sunburst blade and conventional blade, respectively.

4.4 Results and Discussion

4.4.1 *Characterisation of Nanocomposite Structure*

XRD was used to characterise the structure of the clay composites. Figure 4.11 shows the X-ray diffraction spectra for the Cloisite® 10A composite, with clay loading between 1 and 10 wt%. A prominent peak corresponding to the basal spacing of pure Cloisite® 10A occurs at a *d*-spacing of 1.93 nm (4.52º 2θ). This reflection is absent for clay loadings between 1 wt% and 4 wt%, confirming the formation of a nanocomposite. A significant reflection remains for loading of 10 wt% with a corresponding *d*-spacing of 1.85 nm, indicating that limited exfoliation was achieved. This corresponds with previous work [22, 34, 35] that reported the presence of diffraction peaks for organoclay loadings above 5 wt%. Lepoittevin et al [34] stated that higher clay loadings limit the remaining space available for complete exfoliation of the silicate layers.

The Garamite® 1958 composites with 1 to 10 wt% loading exhibit a strong diffraction peak at a *d*-spacing of 1.21 nm, which corresponds to pure Garamite® 1958 (Figure 4.12). This indicates that a nanocomposite was not formed irrespective of clay concentration. The reduction in diffraction peak as clay

content decreased may be due to the clay being broken down in size during shear mixing. However, the particles do not appear to be intercalated on the nano-scale.

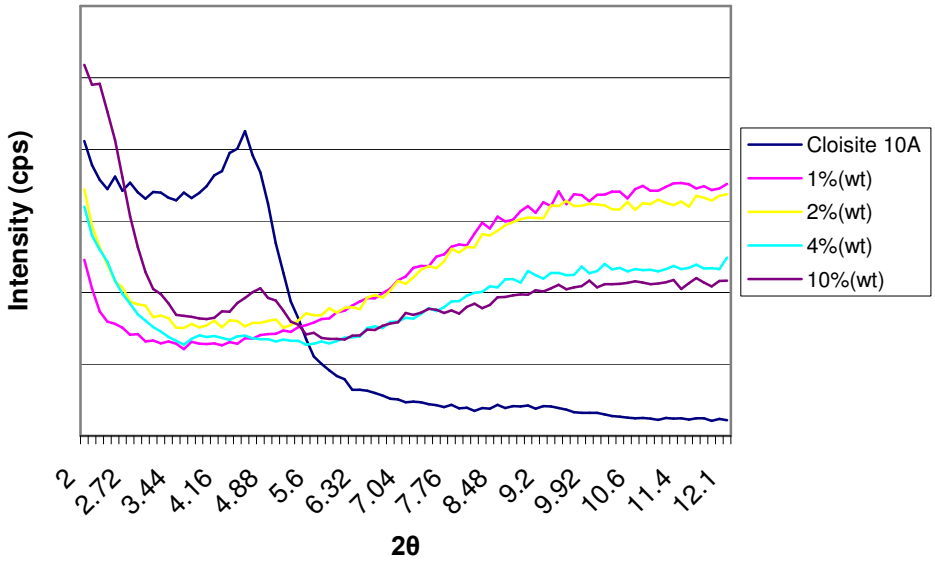

Figure 4.11: Cloisite® 10A composite with clay loading ranging from 1 to 10 wt%. Initial results indicate the formation of an exfoliated nano structure, which is evident by the disappearance of any coherent diffraction peaks for 1 to 4 wt% loadings.

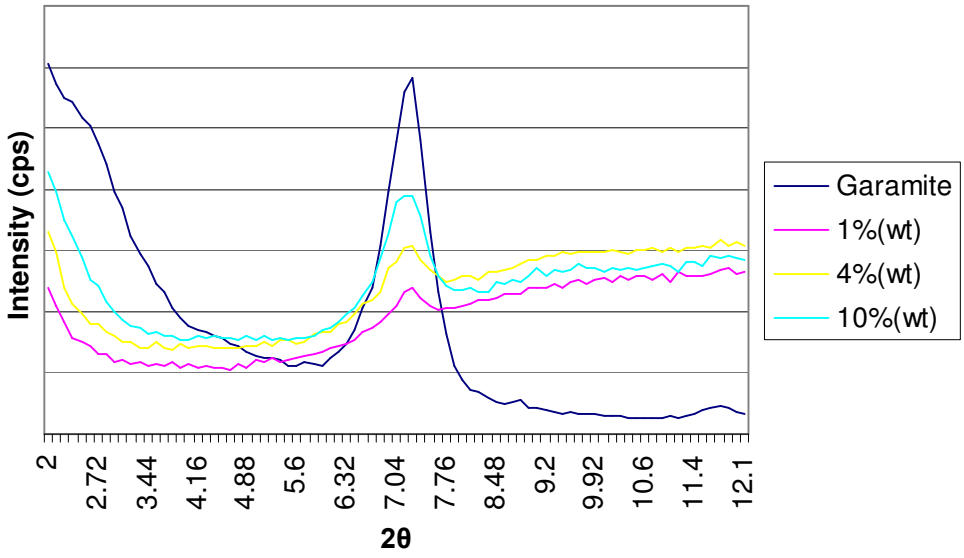

Figure 4.12: Garamite® 1958 composite with clay loading ranging from 1 to 10 wt%. Diffraction peaks corresponding to that of pure Garamite® indicate that intercalation or exfoliation was not achieved. Hence a nano structure was not formed.

Visual evidence for the formation of a true nanocomposite was provided by TEM of an ultramicrotomed section. The micrograph of 4 wt% Cloisite® 10A in unsaturated polyester resin (Figure 4.13) show individual silicate layers orientated perpendicular to the sample surface apparent as dark lines. The lateral size of the silicate plates was approximately 300 nm. At high magnification it is possible to see irregular dispersion of the silicate layers, confirming the XRD suggestion of an exfoliated structure.

Micrographs of 4 wt% Garamite® 1958 and unsaturated polyester resin (Figure 4.14) show the silicate layers maintaining in their original ordering with no exfoliation or intercalation. This supports the findings from XRD.

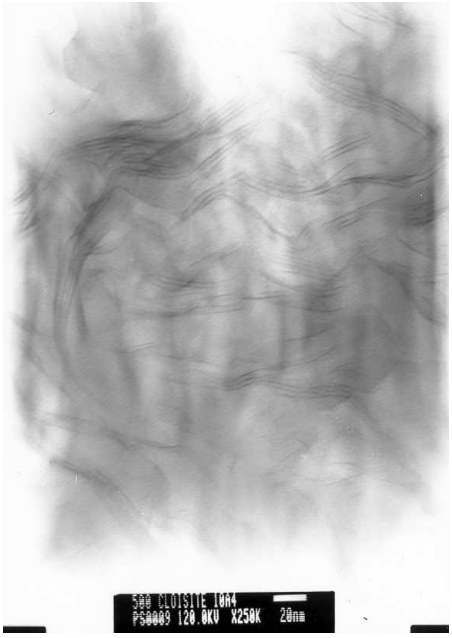

Figure 4.13: TEM micrograph of 4 wt% Cloisite® 10A in unsaturated polyester at high magnification (x250K). The disordered dark lines suggest an exfoliated nano structure.

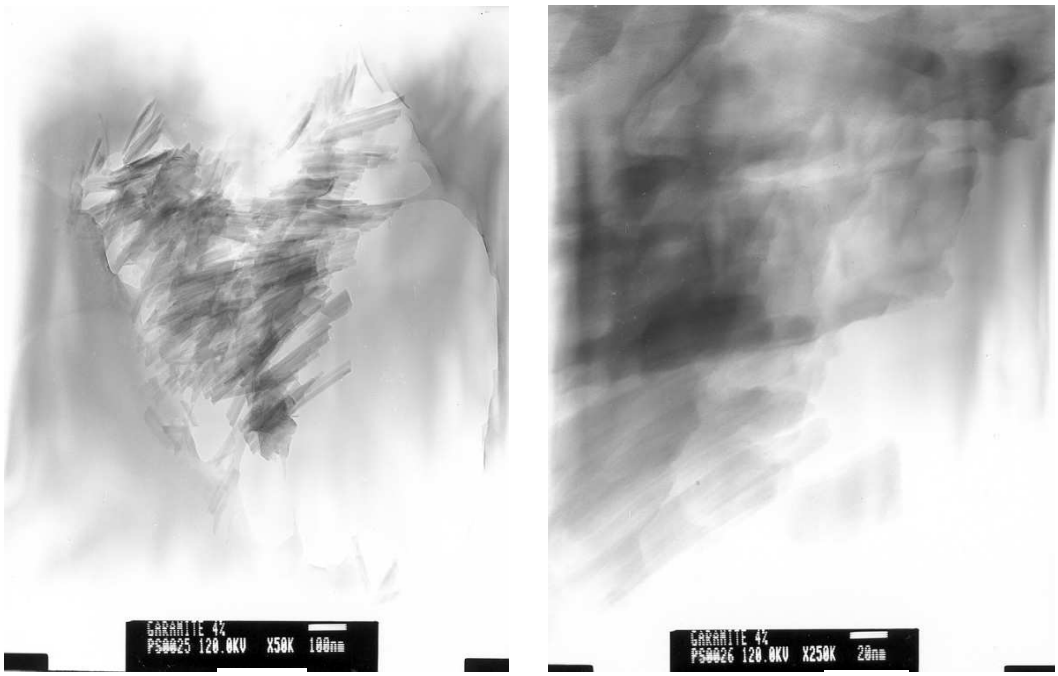

(a) **(b)**

Figure 4.14: TEM micrographs of 4 wt% Garamite® 1958 in unsaturated polyester: (a) low magnification (x50K) of large aggregate and (b) high magnification (x250K) within the aggregate. These micrographs show no exfoliation or intercalation due to the solid uniformity of the dark area.

4.4.2 *Material Physical Properties*

Volumetric Shrinkage

Volumetric resin shrinkage was monitored for the silicate composites (1 to 10 wt% clay) and compared to an inert filler ($CaCO_3$) and LPA (PVAc). The volumetric shrinkage of the base resin was 7.5 %. Figure 4.15 shows that $CaCO_3$ filler caused minimal reduction in volumetric shrinkage for loadings as high as 30 wt%. The reduction is attributed to the inert filler acting as a reactive volume diluent. PVAc provoked little reduction in shrinkage below 4 wt%. Thereafter, the resin shrinkage was reduced by 6.5 % for loadings up to 30 wt%. Using 30 wt% LPA is shown to reduce chemical resin shrinkage to the same magnitude seen in an epoxy system (Section 2.6.4), which produced acceptable surface quality.

Figure 4.15 suggest Garamite 1958 acts as a reactive volume diluent as it follows the same trend seen for $CaCO_3$. This is due to the ineffective intercalation and

exfoliation seen in the XRD data and TEM micrographs (Figure 4.12 and Figure 4.14 respectively).

The Cloisite® 10A exhibited a 1.8 % reduction in volumetric shrinkage for loadings as low as 1 wt%. A maximum mean reduction of 2.5 % was seen at 4 wt% clay loading. However, using a two-tailed, *t-test* [36] for statistical analysis of the data sets for the 2, 4 and 10 wt% loading, it was shown that the null hypothesis ($\mu_{2\%} = \mu_{4\%} = \mu_{10\%}$) was true at the 1 % significance level, i.e. no significant difference between the data sets could be concluded. Therefore, from 1 to 10 wt% loading of Cloisite 10A, a mean average of 2.5 % reduction in volumetric shrinkage could be expected.

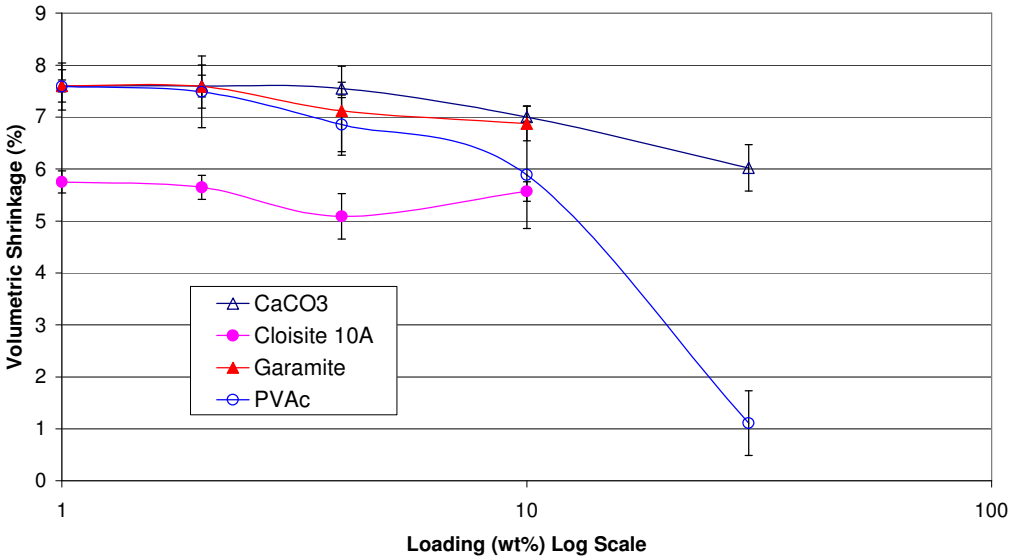

Figure 4.15: Percentage volumetric shrinkage for various loadings of $CaCO_3$, PVAc and montmorillonite composites in unsaturated polyester resin. Garamite® and $CaCO_3$ both act as a reactive mass diluent, where as the nano-structure of the Cloisite® 10A assist in reducing resin shrinkage by 2.5 % over that of the base system.

Glass Transition Temperature

The glass transition temperature of the nanocomposite and $CaCO_3$ filled unsaturated polyester resin was monitored for loadings ranging between 0 to 10 wt%. Figure 4.16 shows that base resin T_g increased for all concentrations of clay. A maximum of 11 ºC increase was seen for the nanocomposite structure

containing 4 wt% clay, with a 5 ºC drop seen for additional clay loading. Generally speaking, the addition of $CaCO_3$ shows no influence on the T_g. The increase of T_g due to clay dispersion is significant and potentially useful, not only from an application or industrial point of view, but also because it is difficult to achieve similar T_g enhancements by chemical modification or reinforcement by conventional filler.

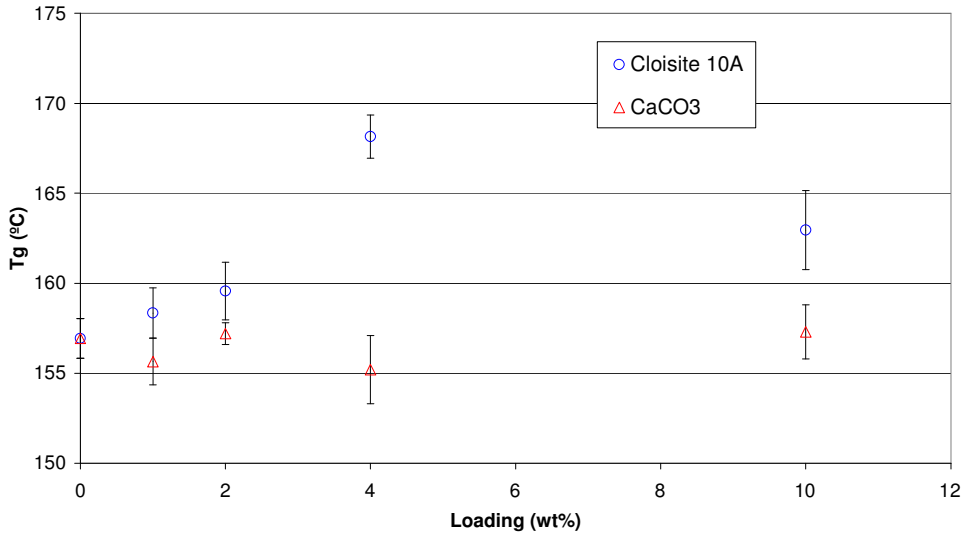

Figure 4.16: Glass transition temperature of Cloisite® 10A and $CaCO_3$ for loadings between 0 and 10 wt%. The nanocomposite shows significant increase in T_g for loads as low as 1 wt%. The system containing inert filler remains relatively unchanged for increased loadings.

The increase in T_g with the formation of a nanocomposite could be attributed to restricted motion near the organic-inorganic interface which may shorten polymer chains among the cross-linking points. However, some related studies have shown that the addition of clay to polyester decreases the curing reactivity [35, 37], which generally results in lower cross-link density and longer polymer chains among the cross-linking points. This would result in a decrease of glass transition temperature with additional clay content. More so, it would be expected that increased exfoliation levels would result in reduced reactive due to the consumption of free radicals by the clay particles. Increased mechanical performance of resin systems due to the formation of a nanocomposite have generally been associated with increased T_g levels [22], where as decreased T_g levels have been associated with a reduction in mechanical properties [35]. From

the results presented in Figure 4.16 it is predicted that additional benefits will be seen in mechanical performance studies for the nanocomposite.

Mechanical Properties

The dependence of mechanical properties on the clay concentration is shown in Figure 4.17 to Figure 4.20. It was decided not to present the mechanical results in a graphic form for Garamite® 1958, to make it easier to interpret the information presented on the true nanocomposite structure. It is seen in Table 4.5 that the Garamite® 1954 followed similar trends to $CaCO_3$ in each case.

Table 4.5: Mechanical properties of unsaturated polyester resin with organo-clay and inert filler. Garamite® and $CaCO_3$ show similar trends as no nanocomposite structure was observed in either case.

Filler type	Loading (wt%)	Tensile strength (MPa)	Young's modulus (GPa)	Flexural strength (MPa)	Flexural modulus (GPa)
	0	39.11	3.972	69.41	3.304
Cloisite® 10A	1	42.15	4.105	71.27	3.404
	2	44.01	4.827	68.26	3.315
	4	46.36	6.092	68.40	3.301
	10	41.98	6.250	63.83	3.200
Garamite® 1958	1	39.4	3.990	68.64	3.305
	2	37.66	4.010	68.01	3.378
	4	40.35	4.423	67.20	3.362
	10	40.49	4.231	64.10	3.390
$CaCO_3$	1	37.85	3.992	70.00	3.306
	2	37.95	3.984	70.01	3.307
	4	38.40	4.110	69.30	3.102
	10	30.58	4.300	62.02	3.350
	30	25.20	4.880	58.21	3.210

Figure 4.17 shows that the Young's modulus of the Cloisite® 10A increases with clay loading and peaks at 10 wt%. A 53 % increase over the base system is seen for clay loadings at 4 wt% and above. The levelling of results for high clay loading may be attributed to the lower degree of exfoliation and polymer-clay surface interactions at high clay contents. Through the use of DSC, Inceoglu et al. [38] inferred that clay acts as a free radical scavenger, adversely affecting the

crosslinking process and decreasing the cross-link density and the modulus at high clay contents. No significant benefits for the traditional filler could confidently be reported due to the standard deviations.

Clay concentration up to 4 wt% shows a general increase in tensile strength over the base unsaturated polyester resin (Figure 4.18), which indicates a suitable bond at the clay and polymer interface. Statistical analysis using a *t-test* [36] revealed that at the 1 % confidence level, a 15 % increase in UTS occurred at 4 wt% clay content. From 4 to 10 wt% clay concentration revealed a general decrease in properties, which may be attributed to the increased levels of stress concentrators formed by the lower degree of exfoliation. This creates an unstable matrix and the nanocomposite starts to behave in a similar fashion to the traditional filler.

The tensile results mimic that found by Lee et al. [15] who continued to show that the tensile strength peaked at 10 wt% and then dramatically fell to base level at 30 wt% Cloisite® 10A. The change corresponds to the passage from a totally exfoliated structure (below 10 wt%) to a partially intercalated-immiscible structure (greater than 10 wt%).

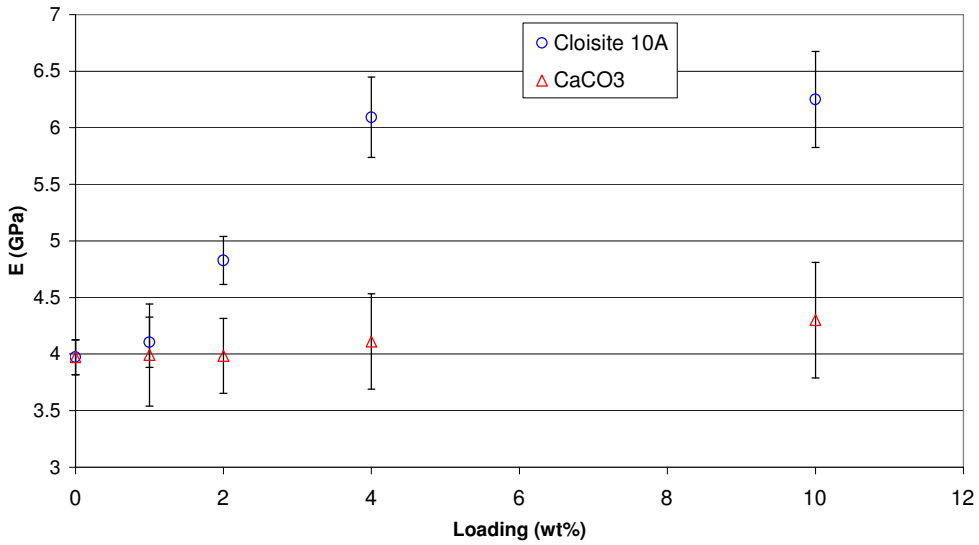

Figure 4.17: Young's modulus of an unsaturated polyester nanocomposite and traditionally filled resin at loadings ranging from 1 to 10 wt%. The nanocomposite shows significant improvement with addition clay loading up to 10 wt%. The addition of $CaCO_3$ shows no appreciable change.

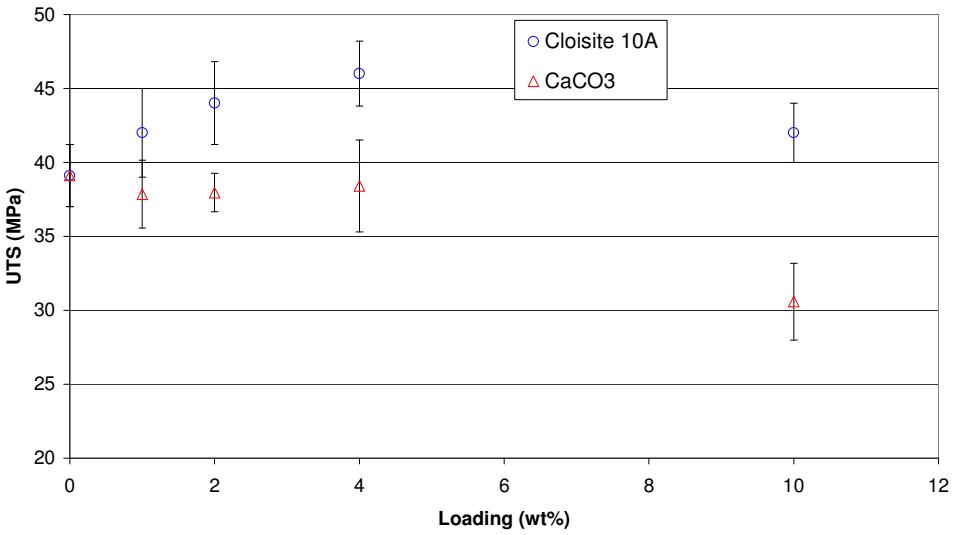

Figure 4.18: Tensile strength of an unsaturated polyester nanocomposite and traditionally filled resin at loadings ranging from 1 to 10 wt%. An increase in tensile strength is observed for clay loadings up to 4 wt%. Thereafter, the nanocomposite acts similar to a traditional filler and reduces tensile strength.

Figure 4.19 shows that the flexural modulus of the nanocomposite remains relatively unchanged for increased loadings of clay. An increase in flexural modulus was not seen in these experiments, unlike the reported 34 % increase claimed by Inceoglu et al. [22] when using unsaturated polyester and silicate clay (Cloisite® 30B). This could be due to the variation in clay surface treatment or orientation effects. Similarly, increased $CaCO_3$ levels showed relatively no effect on the flexural modulus.

The flexural strength of the nanocomposite and traditional filler (Figure 4.20) remained unchanged for loadings up to 4 wt%. Thereafter, both systems exhibit an approximate decrease of 7 % in flexural strength for 10 wt% loading. The reduction in exfoliation for high clay loadings promotes agglomeration of particles in the nanocomposite, which contribute towards stress concentrations. This may be one of the factors contributing to the trends seen in Figure 4.20. These results may also suggest that silicates exhibit poor shear strength as considerable shear forces are created during flexural testing.

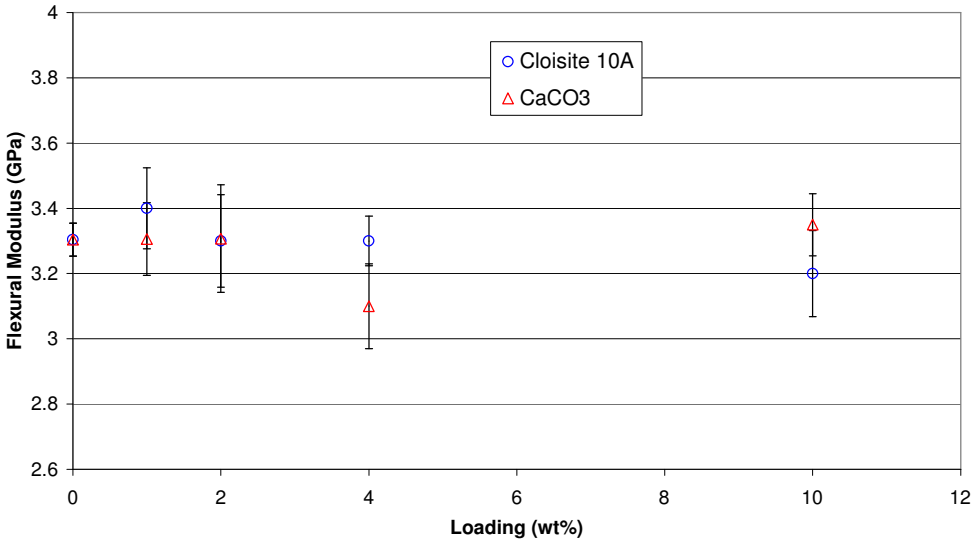

Figure 4.19: Flexural modulus of unsaturated polyester resin with clay and $CaCO_3$ loadings ranging from 1 to 10 wt%. No appreciable change is seen for either system irrespective of concentration.

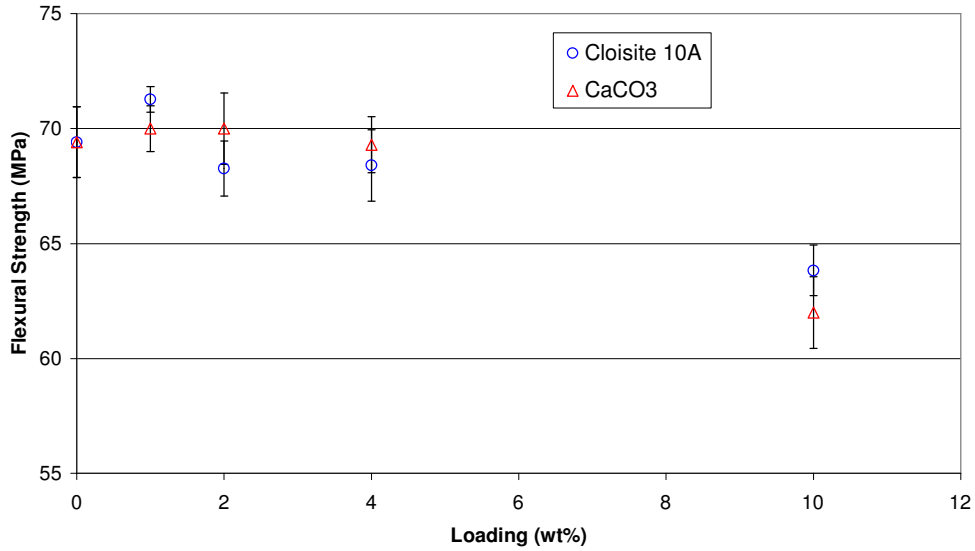

Figure 4.20: Flexural strength of unsaturated polyester resin with clay and $CaCO_3$ loadings ranging from 1 to 10 wt%. Both systems show similar trends with decreasing flexural strength associated with increasing additive content.

4.5 Conclusions

It has been demonstrated through changing surface reactant, that the level of exfoliation is influenced by the strong interaction or miscibility between the

polyester and clay surface type. It has been speculated that strong polar-type interactions such as hydrogen bonding, are critical for the formation of intercalated and especially exfoliated hybrids via in-situ intercalation [15]. However, Cloisite® 10A suffers from relatively weaker polarity due to the ammonium cation in the gallery. Through controlled processing, the intercalation of the monomer into the silicate layers has been shown to effectively exfoliate the silicate layers and create suitable interactions to form a true nanocomposite structure. 4 wt% of Cloisite® 10A was found to be the optimum loading in most test cases. This was due to high levels of exfoliation achieved through maximum swelling of the galleries from available monomer. Loadings higher than 4 wt% were starved of monomer and subsequent reduction in exfoliation was seen.

The use of nano-scale silicate clay in unsaturated polyester resin has been shown to be effective in reducing volumetric resin shrinkage due to the immobilisation of resin in the regions of contact with the silicate surface. However, the nanocomposite still needs to incorporate conventional methods of resin shrinkage control to obtain the level of resin shrinkage seen with epoxy resin (~1 %). Additional benefits were seen, including an increase in T_g, Young's modulus and tensile strength. However, adverse affects were seen to the flexural strength with negligible change to the flexural modulus.

4.6 References

1. Tolle, T.B. and Anderson, D.P., *Morphology development in layered silicate thermoset nanocomposites.* Composites Science and Technology, 2002. **62**: p. 1033-1041.
2. Tsagaropoulos, G. and Eisenberg, A., *Dynamic mechanical study of the factors affecting the two glass transition behavior of filled polymers. Similarities and differences with random ionomers.* Macromolecules, 1995. **28**: p. 6067-6077.
3. Kornmann, X., Berglund, L.A., Sterte, J., and Giannelis, E.P., *Nanocomposites based on montmorillonite and unsaturated polyester.* Polymer Engineering and Science, 1998. **38**: p. 1351-1361.
4. Agag, T., Koga, T., and Takeichi, T., *Studies on thermal and mechanical properties of polyimide-clay nanocomposites.* Polymer, 2001. **42**: p. 3399-3408.
5. Chen, C.G. and Curliss, D., *Resin matrix composites: organoclay-aerospace epoxy nanocomposites, Part II.* SAMPE, 2001(37): p. 11-18.

6. Pinnavaia, T.J. and Beall, G.W., *Polymer-clay nanocomposites*. 2000, New York: John Wiley & Sons.
7. Kojima, Y., Usuki, A., Kawasumi, M., Okada, A., and Fukushima, Y., *Mechanical properties of nylon 6-clay hybrid.* Materials Research, 1993. **8**: p. 1185-1189.
8. Messersmith, P. and Giannelis, E.P., *Synthesis and characterization of layered silicate-epoxy nanocomposites.* Chemistry of Materials, 1994. **6**: p. 1719-1725.
9. Giannelis, E.P., *Polymer layered silicate nanocomposites.* Advanced Materials, 1996. **8**: p. 29-35.
10. Lan, T. and Pinnavaia, T., *Clay-reinforced epoxy nanocomposites.* Chemistry of Materials, 1994. **6**: p. 2216-2219.
11. Lee, D.C. and Jang, L.W., *Characterisation of epoxy clay hybrid composite prepared by emulsion polymerisation.* Applied Polymer Science, 1998. **68**: p. 1997-2005.
12. Okada, A., *Nylon 6-clay hybrid.* MRS Proceedings, 1990. **171**: p. 45-50.
13. Bhattacharya, S.K. and Tummala, R.R., *Integral passives for next generation of electronic packaging: Application of epoxy/ceramic nanocomposites as integral capacitors.* Microelectronics, 2001. **32**: p. 11-19.
14. Qiaoling, H., Baoqiang, L., Mang, W., and Jiacong, S., *Preparation and characterization of biodegradable chitosan/hydroxyapatite nanocomposite rods via in situ hybridization: a potential material as internal fixation of bone fracture.* Biomaterials, 2004. **25**: p. 779-785.
15. Lee, S.R., Park, H.M., Lim, H., Kang, T., and Li, X., *Microstructure, tensile properties, and biodegradability of aliphatic polyester/clay nanocomposites.* Polymer, 2002. **43**: p. 2495-2500.
16. Moukarika, A., *Cation migration in alkali-saturated montmorillonites*. 2001, University of Loannina: Loannina. p. 103.
17. Beermann, T., *Structure determination at clay mineral single crystals of the smectite group by convergent beam electron diffraction (CBED): To the crystal chemistry of montmorillonite*. 2000, University of Bremen: Bremen.
18. Alexandre, M. and Dubois, P., *Polymer layered silicate nanocomposites: preparation, properties and uses of a new class of materials.* Materials Science and Engineering, 2000. **28**: p. 1-63.
19. Kornmann, X., Lindburg, H., and Berglund, L.A., *Synthesis of epoxy-clay nanocomposites: influence of the nature of the clay on structure.* Polymer 42, 2001: p. 1303-1310.
20. Musto, P., Ragosta, G., Scarinzi, G., and Mascia, L., *Polyimide-silica nanocomposites: spectroscopic, morphological and mechanical investigations.* Polymer, 2004. **45**: p. 1697-1706.
21. Suh, D.J., Lim, Y.T., and Park, O.O., *The property and formation mechanism of unsaturated polyester-layered silicate nanocomposite depending on the fabrication methods.* Polymer, 2000. **41**: p. 8557-8563.
22. Inceoglu, A.B. and Yilmazer, U., *Mechanical properties of unsaturated polyester/ montmorillonite composites.* Mat Res Soc, 2002. **703**: p. 387-392.

23. Benfarhi, S., Decker, C., Keller, L., and Zahouily, K., *Synthesis of clay nanocomposite materials by light-induced crosslinking polymerization.* European Polymer Journal, 2004. **40**: p. 493-501.
24. Lepoittevin, B., Pantoustier, N., Devalckenaere, M., Alexandre, M., Calberg, C., Jerome, R., and Dubois, P., *Polymer/layered silicate nanocomposites by combination intercalative polymerization and melt intercalation: a masterbatch process.* Polymer, 2003. **44**: p. 2033-3040.
25. Wang, S., Hu, Y., Zong, R., Tang, Y., Ghen, Z., and Fan, W., *Preparation and characterization of flame retardant ABS/montmorillonite nanocomposite.* Applied Clay Science, 2004. **25**: p. 49-55.
26. Sinha Ray, S. and Okamoto, M., *Polymer/layered silicate nanocomposites: a review from preparation to processing.* Progress in Polymer Science, 2003. **28**: p. 1539-1641.
27. Chen, D.Z., He, P.S., and Pan, L.J., *Cure kinetics of epoxy-based nanocomposites analyzed by Avrami theory of phase change.* Polymer Testing, 2003. **22**.
28. Shen, L., Phang, Y., Chen, L., Liu, T., and Zeng, K., *Nano indentation and morphological studies on nylon 66 nanocomposites. I. Effects of clay loading.* Polymer, 2004. **45**: p. 3341-3349.
29. Duk Yang, B., Hyun Yoon, K., and Woo Chung, K., *Dispersion effect of nanoparticles on the conjugated polymer-inorganic nanocomposites.* Materials Chemistry and Physics, 2004. **83**: p. 334-339.
30. Finnigan, B., Martin, D., Halley, P., Truss, R., and Campbell, K., *Morphology and properties of thermoplastic polyurethane nanocomposites incorporating hydrophilic layered silicates.* Polymer, 2004. **45**: p. 2249-2260.
31. Maiti, P., Nam, P., Okamoto, M., Kotaka, T., Hasegawa, N., and Usuki, A., *The effects of crystallization on the structure and morphology of polypropylene/clay nanocomposites.* Polymer Engineering Science, 2002. **42**: p. 1864-1871.
32. *Cloisite 10A data sheet.* Southern Clay Products, 2001(http://www.nanoclay.com/).
33. *Garamite data sheet.* Southern Clay Products, 2001(http://www.garamite.com/).
34. Lepoittevin, B., Pantoustier, N., Devalckenaere, M., Alexandre, M., Kubies, D., Calberg, C., Jerome, R., and Dubois, P., *Poly(caprolactone)/clay nanocomposites by in-situ intercalative polymerization catalyzed by dibutyltin dimethoxide.* Macromolecules, 2002. **35**: p. 8385-8390.
35. Bharadwaj, R.K., Mehrabi, A.R., Hamilton, C., Trujillo, C., and Murga, M., *Structure-property relationships in cross-linked polyester-clay nanocomposites.* Polymer, 2002. **43**: p. 3699-3705.
36. Chatfield, C., *Statistics for technology: A course in applied statistics, 3rd ed.* 1986, Chapman & Hall: New York. p. 142.
37. Gu, A. and Liang, G., *Thermal degradation behaviour and kinetic analysis of epoxy/montmorillonite nanocomposites.* Polymer Degradation and Stability, 2003. **80**: p. 383-391.
38. Inceoglu, A.B. and Yilmazer, U., *Synthesis and mechanical properties of unsaturated polyester based nanocomposites.* Polymer Engineering and Science, 2003. **43**(3): p. 661-669.

5 Characterisation of Low Profile Nanocomposite Laminates

5.1 Introduction

The use of nano scale silicate particles have been shown in Chapter 4 to assist in reducing polymerisation shrinkage with additional side benefits in mechanical properties. Although the main objective of creating a nanocomposite to reduce polymerisation shrinkage was achieved, it was also shown that the level of shrinkage control did not match that of a conventional low profiling system such as PVAc. It was envisaged that a hybrid nanocomposite-LPA system would produce suitable shrinkage control, resulting in a cosmetic polymer composite. The potential reduction in problematic residual VOCs due to lower LPA content and addition mechanical properties warranted further investigation.

5.2 Experimental Procedure

The materials used in this study were based on the low profile unsaturated polyester, E-glass system described in Section 2.5.1. The low profile and base resin systems were used as benchmarks throughout this study (Table 5.1). The preform was made from random E-glass fibres sandwiched between a chop-strand E-glass veil and moulded using RTM (Section 2.5.2) with unsaturated polyester (RT2557), initiated with TBPB and accelerated with a cobalt solution (Accelerator G). 4 wt% Cloisite 10A was included into the matrix using the in-situ intercalative polymerisation method described in Section 4.4.2. 4 wt% silicate clay loading was chosen as it was shown in Chapter 4 that a fully exfoliated structure was formed, the highest reduction in polymerisation shrinkage was obtained and the optimal improvements in mechanical properties were observed. PVAc was used as a LPA and added to the resin via shear mixing at loadings ranging from 0 to 30 wt%. All laminates were postcured in the process described in Section 2.5.2. The average fibre volume fraction of the composite samples was determined, by burn-off trials at 625 ºC, to be 25 %.

Table 5.1: Constituents used for experimental production of hybrid nanocomposites with LPA.

Sample ID	Resin	Silicate (wt%)	LPA (wt%)	Initiator (wt%)	Accel (wt%)	Reinforce-ment
Benchmark 1	Unsaturated Polyester	-	-	TBPB (2)	G (0.5)	Random E-glass, contin. surface veil
Benchmark 2	Unsaturated Polyester	-	PVAc (30)	TBPB (2)	G (0.5)	Random E-glass, contin. surface veil
Hybrid 0	Unsaturated Polyester	Cloisite 10A (4)	PVAc (0)	TBPB (2)	G (0.5)	Random E-glass, contin. surface veil
Hybrid 5	Unsaturated Polyester	Cloisite 10A (4)	PVAc (5)	TBPB (2)	G (0.5)	Random E-glass, contin. surface veil
Hybrid 10	Unsaturated Polyester	Cloisite 10A (4)	PVAc (10)	TBPB (2)	G (0.5)	Random E-glass, contin. surface veil
Hybrid 15	Unsaturated Polyester	Cloisite 10A (4)	PVAc (15)	TBPB (2)	G (0.5)	Random E-glass, contin. surface veil
Hybrid 20	Unsaturated Polyester	Cloisite 10A (4)	PVAc (20)	TBPB (2)	G (0.5)	Random E-glass, contin. surface veil
Hybrid 30	Unsaturated Polyester	Cloisite 10A (4)	PVAc (30)	TBPB (2)	G (0.5)	Random E-glass, contin. surface veil

Resin casts were produced for measurement of volumetric shrinkage using the procedure described in Section 4.4.2. Volumetric measurements of the resin casts were obtained using a multipycnometer (Section 4.4.2). Surface analysis techniques described in Section 2.5.4 were employed to characterise the bare and painted (Section 2.5.3) laminate surfaces. Residual VOCs of the composites were monitored by solvent elution gas chromatography (GC) on a Shimadzu GC 17A version 3 analyser with an automated sampler. Details of the method are found in Section 3.3. The tensile and flexural properties of the composites were measured using a Hounsfield H25KS with a 100SC extensometer following BS EN ISO 527-4:1997 and BS EN ISO 14125:1998 respectively. The tensile and flexural test specimens were loaded at a constant rate of 1 mm/min until failure. Tensile modulus was calculated as the slope in the stress-strain curve for strain values between 0.001 and 0.003. At least 5 specimens were taken from each sample to give an average reading. Impact strength was measured on an Avery-Denison Charpy impact tester with a 15 J capacity, following the ISO 179:1997 standard.

10 specimens each measuring 10x5 mm in cross-section were taken from each sample and tested in a normal (flatwise) impact with an unnotched edge.

5.3 Results and Discussion

5.3.1 *Surface Effects*

Stylus profilometry taken on the bare surface of the eight laminates (Figure 5.1) show a distinct decline in the surface roughness as LPA loading increases for the hybrid nanocomposites. The nanocomposite with 30 wt% LPA (Hybrid 30) is shown to reduce surface roughness by 61 % when compared to a conventional low profile composite (Benchmark 2).

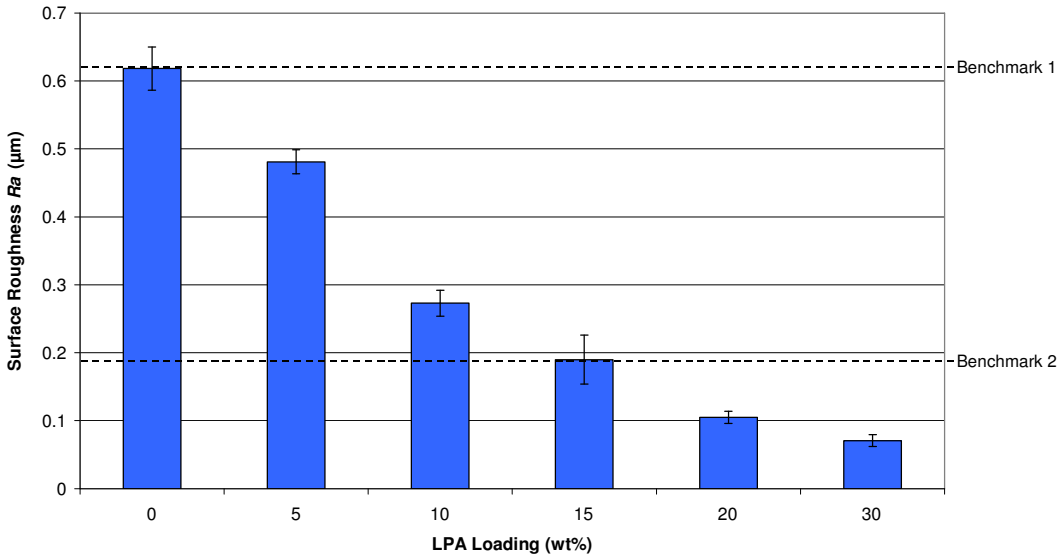

Figure 5.1: Surface roughness measurements of the nanocomposite hybrid systems with LPA. The formation of a nanocomposite is shown to reduce surface roughness when compared to a base resin system with similar LPA loading.

The reduced surface roughness seen when using silicate clay can be attributed to the reduction in polymerisation shrinkage (Figure 5.2) formed by the immobilisation of the resin molecules around the surface of the silicate clay particles. A comparison of the nanocomposite with 30 wt% LPA (Hybrid 30) to the conventional low shrinkage system (Benchmark 2), shows approximately 2 % reduction in volumetric shrinkage. The *Hybrid 30* sample was seen to exhibit an

expansion of 1 %, which adds to the initial positive pressure in the mould cavity created by thermal expansion during polymerisation (Section 1.3.1). This phenomenon resulted in the laminate surface duplicating the characteristics of the tooling surface. This is evident by similar surface roughness profiles (Figure 5.3) and *Ra* values (Tooling surface *Ra* = 0.07 µm, Section 2.6.3). The combination of 20 wt% LPA and 4 wt% silicate clay reduced volumetric shrinkage to levels seen in the low shrinkage unsaturated polyester system and $CaCO_3$ filler used in surface quality experiments detailed in Chapter 2.

Based on the findings from Section 2.6.2, the results from Figure 5.1 indicate that suitable paint quality will potentially be obtained from the nanocomposite laminates only with loadings of LPA greater than 15 wt%. However, 'Hybrid 15' is marginally over the roughness threshold of 0.16 µm.

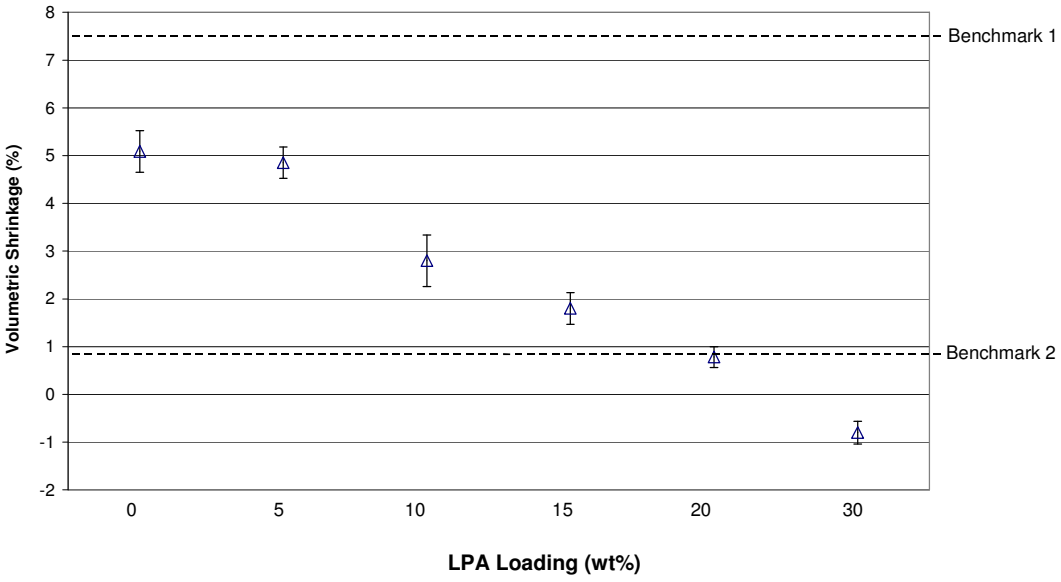

Figure 5.2: Volumetric shrinkage for hybrid composites of silicate clay and PVAc in unsaturated polyester resin. PVAc loadings range from 0 to 30 wt%. A nanocomposite with 20 wt% LPA is shown to have similar volumetric shrinkage to an unsaturated polyester with 30 wt% LPA (Benchmark 2).

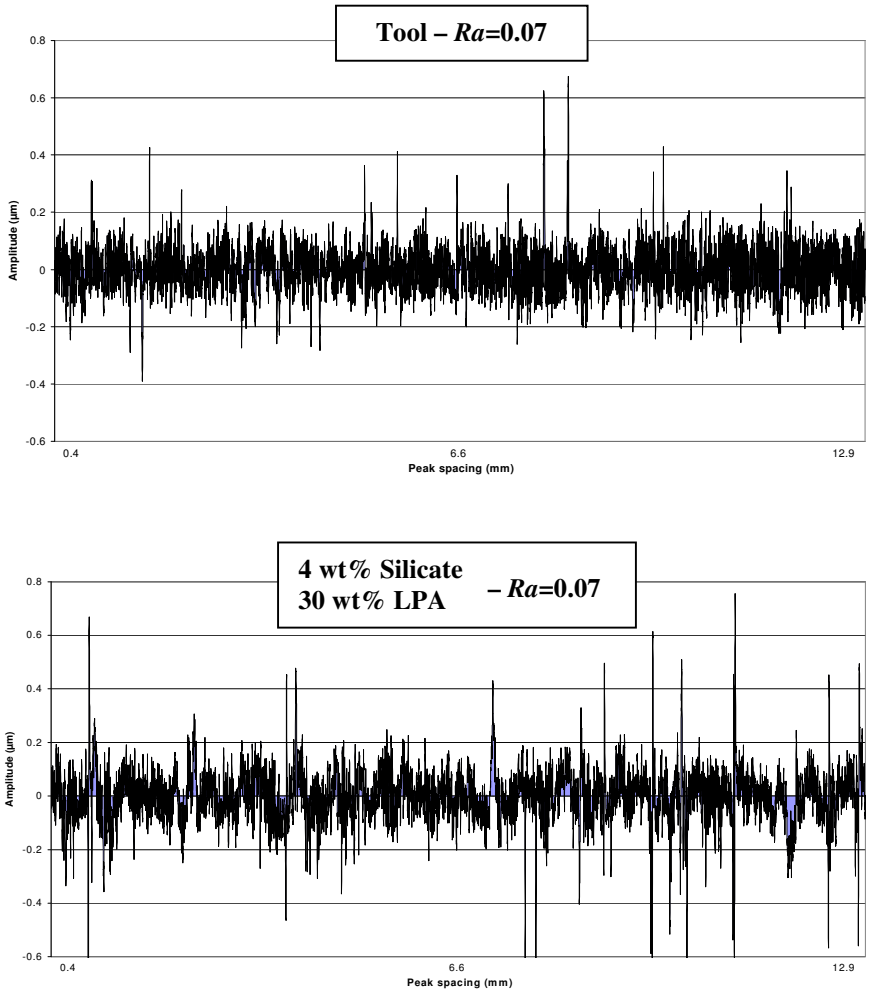

Figure 5.3: Surface roughness profiles for tooling surface and nanocomposite laminate. The expansion created by the nanocomposite with 30 wt% LPA produced a surface profile similar to that of the tooling surface, both with the same *Ra* value.

Light reflectometry analysis on the painted surfaces (Figure 5.4) confirmed that acceptable paint quality was achieved on the nanocomposites with LPA loading greater than 20 wt%. The nanocomposite samples with 20 and 30 wt% LPA plus the Benchmark 2 system are all shown to have shortwave, longwave and *Combined Ford* readings within specified tolerances. Surface roughness measurements had suggested that the nanocomposite with 15 wt% LPA may potentially result in acceptable paint quality. However, light reflectometry results show excessive short-term waviness which is associated with fibre strike-through. Fibre strike-through was the primary surface characteristic seen on the nanocomposite laminates with LPA loading ranging from 0 to 15 wt%. This characteristic is primarily associated with resin shrinkage values above 1 %

(Section 2.6.4). Subjective assessment of the painted laminates support light reflectometry results, in suggesting that acceptable paint quality was obtained on the nanocomposites with 20 and 30 wt% LPA plus the Benchmark 2 system.

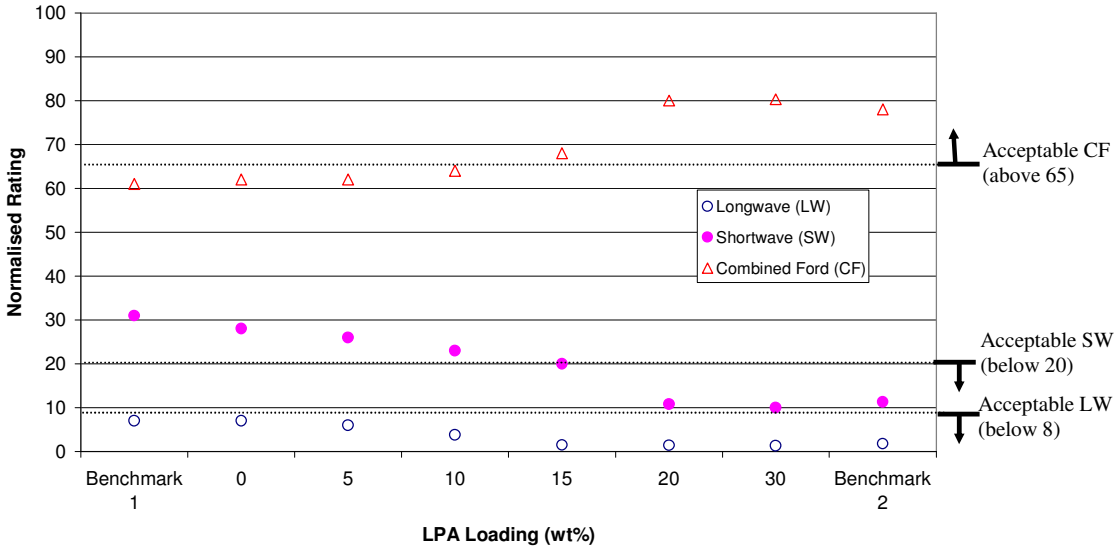

Figure 5.4: Light reflectometry results for the painted surfaces of the benchmark and nanocomposite laminates. Short-term waviness is the primary characteristic seen on laminates with less than 15 wt% LPA.

5.3.2 *Volatile Organic Compounds*

Gas chromatography was used on the samples listed in Table 5.1 to determine the residual styrene and benzaldehyde content for as moulded and postcured conditions. The residual styrene content of the benchmark systems (Figure 5.5) show similar results to the nanocomposites with the same LPA loading (0 and 30 wt%). An 8-fold increase in residual styrene is seen when LPA loading is increased from 0 to 30 wt%. A 0.44 % reduction in residual styrene is seen when reducing the LPA loading from 30 to 20 wt% in the nanocomposite system. However, postcuring reduces all systems to a negligible level.

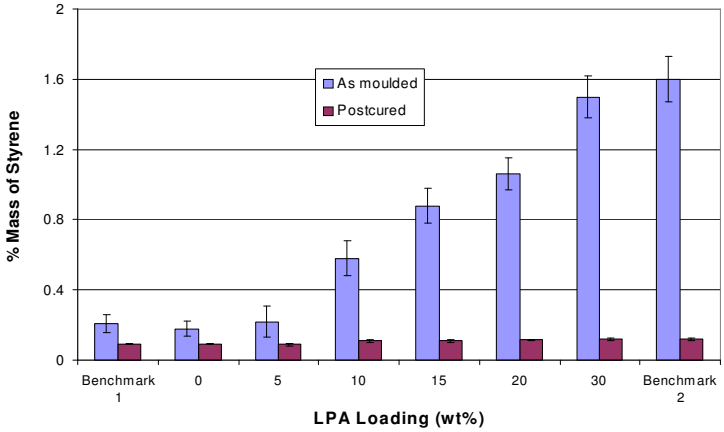

Figure 5.5: Percentage mass of residual styrene as detected by gas chromatography. The formation of a nanocomposite shows no discernable difference in residual styrene levels when compared to the benchmarking systems.

The formation of a nanocomposite showed no discernable difference in reducing residual benzaldehyde when compared to like benchmark systems (Figure 5.6). The residual benzaldehyde content of the nanocomposite doubled with the inclusion of 30 wt% LPA. The reduction from 30 to 20 wt% LPA in the nanocomposite showed a 0.09 % reduction in residual benzaldehyde content, with all systems reducing to approximately half their original value upon postcure. The formation of residual benzaldehyde has been shown in Section 3.4.3 to be directly related to LPA content.

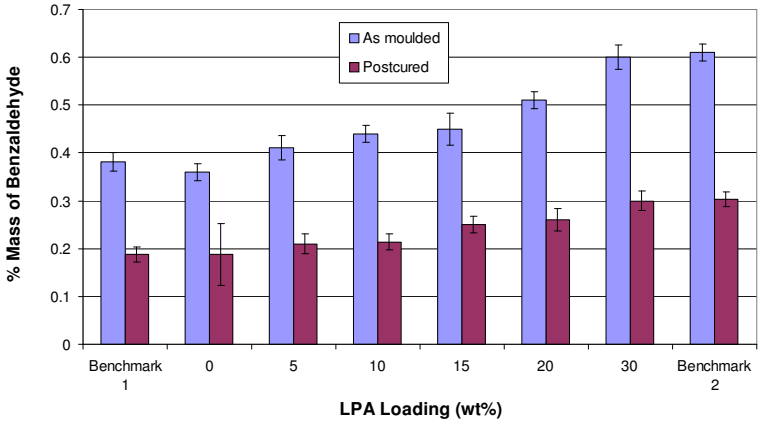

Figure 5.6: Percentage mass of residual benzaldehyde as detected by gas chromatography. The use of clay shows no discernable difference in residual benzaldehyde levels when compared to the benchmarking systems. Increased LPA loading in the nanocomposite increased residual benzaldehyde levels.

5.3.3 *Mechanical Properties*

Tensile tests (Figure 5.7 and Figure 5.8) on the materials listed in Table 5.1 revealed that LPA in the base unsaturated polyester system produced a 25 % reduction in Young's modulus. The use of silicate clay to form a nanocomposite increased the stiffness 2-fold for all levels of LPA loading. Similar trends in tensile strength were observed, where the UTS of the unsaturated polyester composite fell by 7 % with the inclusion of 30 wt% LPA (Benchmark 1 and 2). However, the formation of a nanocomposite increased the UTS by an average of 53 % for all cases. The rule of mixtures [1] was used to calculate the theoretical Young's modulus of the unsaturated polyester composite (Benchmark 1) and of the nanocomposite (Hybrid 0). Calculated properties were based on the Young's modulus of the resin cases presented in Table 4.5 with the Young's modulus of E-glass being taken as 70 GPa. Predicted values are shown in Figure 5.8 and show good agreement with experimental data, falling just outside the bounds of the error bars in each case.

The area under the curves in Figure 5.7 indicate that the formation of a nanocomposite resulted in higher strain energy at failure over that of the base or low profile unsaturated polyester system. Measurement of impact strength via Charpy analysis (Figure 5.9) showed an average of 3 % decrease when using LPA in unsaturated polyester (Benchmark 1 and 2). The loss of impact strength is easily compensated by the inclusion of clay, which is shown to improve the impact strength by an average of 28 %.

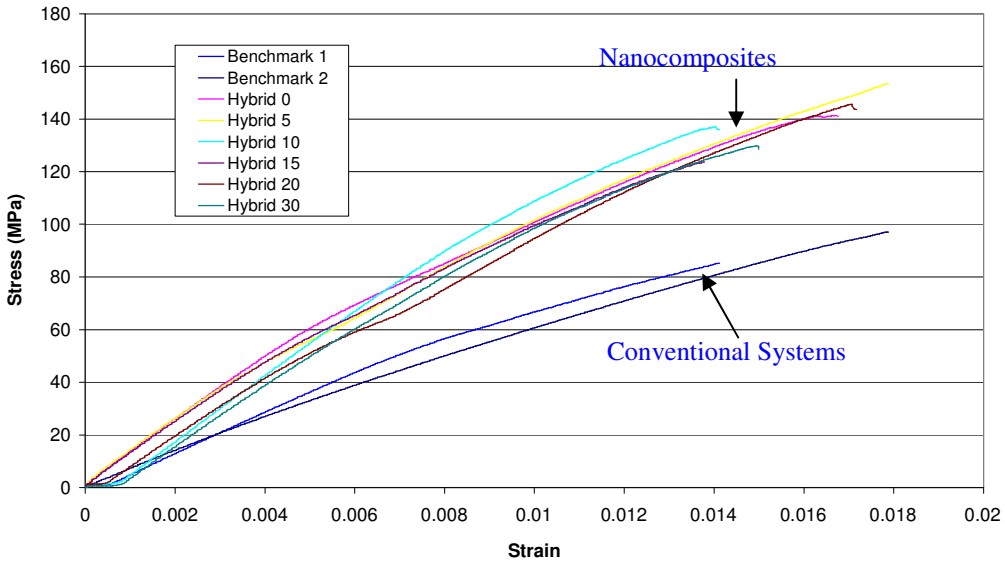

Figure 5.7: Stress-strain curves for the benchmark and nanocomposite materials listed in Table 5.1. The nanocomposite structures create a stiffer material over that of the compliant benchmark systems made from unsaturated polyester resin.

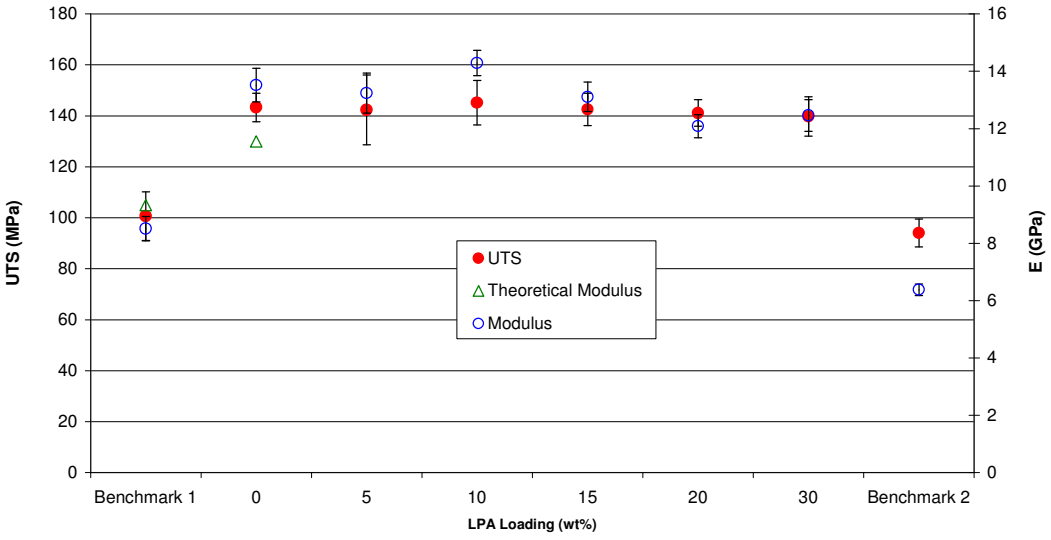

Figure 5.8: Tensile properties of the benchmark and nanocomposite materials listed in Table 5.1. The increase in properties seen with the nanocomposites is independent of the LPA loading.

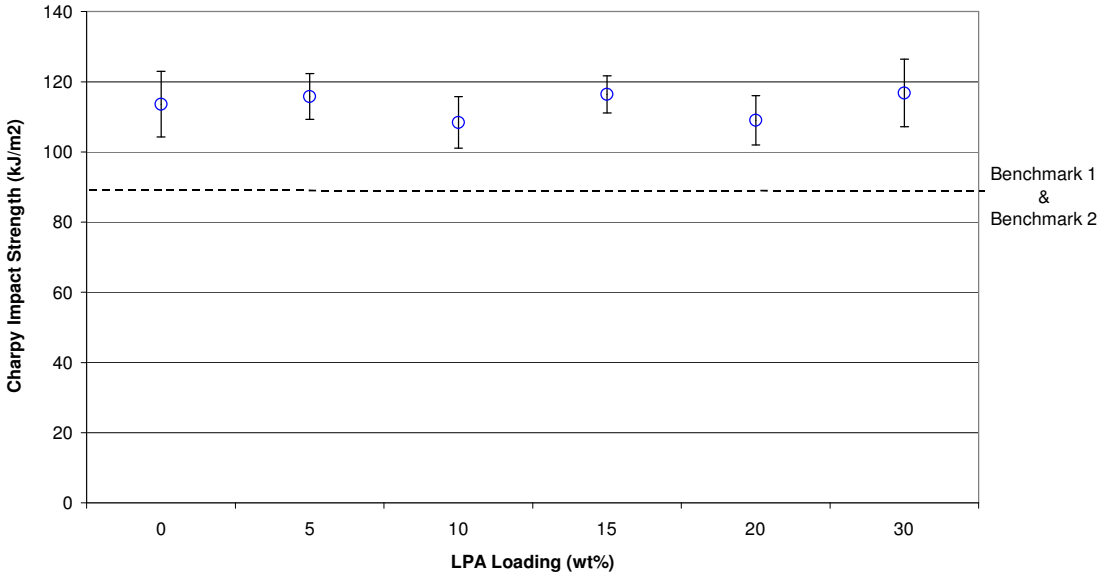

Figure 5.9: Effect of clay on unnotched, Charpy impact energy of unsaturated polyester composites. The formation of a nanocomposite structure improves impact strength above that of a base or LPA loaded unsaturated polyester matrix.

Figure 5.10 shows that flexural strength and modulus of the base unsaturated polyester composite is reduced by 24 and 30 % respectively with the inclusion of 30 wt% LPA. The use of silicate clay to form a nanocomposite has also been shown to reduce flexural strength and modulus by 20 and 14 % respectively, over that of the base unsaturated polyester system (Benchmark 1). The flexural properties of a composite material with LPA were improved with the use of silicate nanocomposites, but it was not possible here to restore these to the levels of a conventional (i.e. non-low profile) resin.

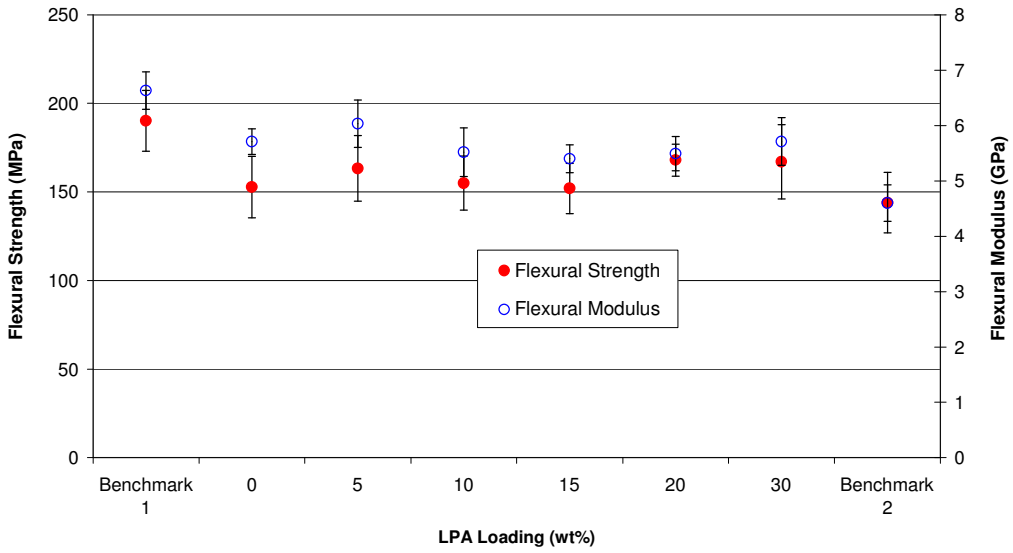

Figure 5.10: Flexural properties of the benchmark and nanocomposite materials listed in Table 5.1. Silicate clay improves flexural properties above that of a low profile polyester system. However, it is unable to restore the flexural properties to those of the base unsaturated polyester system.

5.4 Conclusions

A hybrid nanocomposite system utilising organophilic silicate clay and LPA can be used to form a cosmetic polymer composite based on unsaturated polyester resin. The resistance to polymerisation shrinkage formed by the nano clay particles has been shown to assist the LPA in forming a low profile matrix to create an acceptable cosmetic surface. The assistance of the nano structure in impeding polymerisation shrinkage allowed a reduction in LPA loading, which reduced inorganic additives and lowered residual volatiles, namely styrene and benzaldehyde.

The formation of a nanocomposite structure in a low profile unsaturated polyester matrix restored tensile properties lost through microvoid formation in the phase separation of the LPA and polymer. An increase in UTS and Young's modulus of 53 % and 108 % respectively could be expected due to the formation of a nanocomposite. Hence, a stiffer structure was formed with an average increase of 28 % in Charpy impact strength. The use of silicate clay was unable to fully

restore flexural properties lost when using a LPA in the polyester matrix. However, a minor increase in flexural modulus was obtainable.

5.5 Reference

1. Hull, D. and Clyne, T.W., *An introduction to composite materials. 2nd Edition*. 1996, Cambridge University Press: Cambridge.

6 Discussion and Conclusions

6.1 Introduction

This chapter discusses the work included in the main body of this thesis, with reference to the overall theme described in Chapter 1. The contents of each chapter are summarised and assessed to evaluate their implications in the manufacture of cosmetic polymer composites for the automotive industry. Several recommendations for further work are made, and the overall conclusions are presented.

6.2 General Discussion

This thesis is mainly concerned with matrix selection for low cost, cosmetic, automotive body panelling. The overall objective of this research was to identify the parameters that affect residual VOCs and to use this information to optimise the curing process and subsequent mechanical properties.

6.2.1 *Surface Quality*

A repeatable and reliable process for detection of surface characteristics on bare and painted polymer substrates was presented in Chapter 2. The use of stylus profilometry for measuring the surface roughness via the roughness parameter *Ra*, provided a reliable predictive tool for determining final paint quality. This technique was found to be useful in measuring surface roughness of bare polymer substrates but not that of painted substrates. Through the use of microscopy, the paint process was seen to include its own level of surface roughness, which influenced the true representation of the paint quality when using profilometry. To overcome this, light reflectometry was used to measure short and long-term waviness. This allowed for accurate determination of paint quality and detection of specific characteristics such as fibre strike-through and textile induced waviness. These results showed good correlation with subjective assessment of the painted substrates. An extensive study was undertaken to verify the subjective

assessment, which utilised appraisers with no experience in assessing surface quality (Group 1) and a second group with extensive experience in assessing surface quality (Group 2). A Sigma Six process and MiniTab software analysis revealed that the choice of appraisers influenced subjective results and showed that Group 2 could be statistically justified as an acceptable means for qualitative assessment of a painted surface. The development of the surface analysis techniques, allowed further investigation into the effects of tool surface roughness, chemical resin shrinkage and tow size.

The surface roughness model (Appendix 8) demonstrates potential to simulate the surface behaviour of laminates by accounting for thermal and polymerisation shrinkage. There were a number of assumptions made to simplify the analysis, which inherently add limitations to the accuracy of the model. An interesting future study could be to expand the thermal analysis in two-dimensions to account for the strain induced by neighbouring regions. Also, the current simulation has only been developed for use where the fabric has not suffered any shear deformation. Utilising the existing analysis principles to model the surface roughness of a draped fabric with localised shear deformation would be a likely next step. Despite the clear need for further development, the surface roughness model presented produces encouraging results.

6.2.2 *Residual VOCs*

The identified residual VOCs of styrene and benzaldehyde emitted from low profile unsaturated polyester laminates were investigated in Chapter 3. Initial investigations utilising a thermal desorption technique (TGA) were proven to be inadequate for extraction of all available compounds when compared to results from a solvent elution technique (GC). This highlighted the inability of the monomer to fully terminate due to physical entrapment. Residual thermal activity studies using DSC revealed that the substrates were essentially fully cured despite having measurable levels of residual monomer. This posed the question as to whether DSC is an accurate means of measuring the residual reactivity of a polymer composite due to the elevated temperatures used in DSC trials and the

ability for homopolymerisation of residual styrene. The development of a suitable GC method allowed residual VOCs to be monitored for changes to formulation and process parameters. Various situations were investigated to assist in optimisation of the cure process with an emphasis placed on the increase in VOCs produced when using PVAc as a means for controlling shrinkage in the polyester matrix.

6.2.3 *Nanocomposites*

A novel approach to reducing the polymerisation shrinkage of unsaturated polyester resin was presented in Chapter 4 following the discovery of the problems associated with the use of PVAc as an additive. A variation of the in-situ intercalative polymerisation method was devised and used to disperse nano-scale silicate clay in an unsaturated polyester matrix. Characterisation of the structure via XRD and TEM confirmed the formation of a nanocomposite with full exfoliation of the silicate particles. A reduction in polymerisation shrinkage was seen for loadings of clay as low as 1 wt%. The reduction in polymerisation shrinkage obtained from the formation of a nano structure was not able to meet the requirements of a cosmetic composite. However, evaluation of an E-glass preform moulded by RTM with a hybrid matrix of silicate clay and PVAc was trialled in Chapter 5, which resulted in acceptable surface quality and a reduction of residual VOCs due to the reduced amount of thermoplastic additive. As well as reducing residual VOCs, the nanocomposite was found to improve other areas of physical and mechanical properties that are generally problematic with low profile unsaturated polyester systems. Tensile properties were improved with the formation of a nanocomposite. The two-fold increase in Young's modulus and 53 % improvement in UTS exceeded most reported values in related literature. A slight improvement in flexural properties and impact energy absorption was also demonstrated, with a notable increase in the glass transition temperature.

6.3 Recommendations for Future Work

In light of the work performed, some important improvements or studies that could be undertaken when measuring the surface quality aspects of a polymer composite are:

- Investigate the effect that surface roughness has on paint adhesion (ASTM D3359, ASTM D 3170-01, SAE J400)
- Analyse variations in the paint process for changes to the masking ability of paint on surface defects. Initial parameters to look at would include: paint type (solvent or waterborne), paint thickness, baking temperatures, surface conditioning and spraying pressure.

From the surface roughness modelling the following refinements are suggested:

- Derive the true reaction rates and obtain thermal parameters of the polymer composite for accurate determination of thermal heat conduction throughout the cure process. This will allow the surface characteristics of the laminate to be determined at any time interval during the mould cycle.
- Build on the basic principles used for the current model and formulate an iterative two-dimensional thermal analysis to account for the strain induced by neighbouring regions.
- Apply the existing modelling principles to investigate the effects that fabric shear angle has on surface roughness.

Some suggested future improvements and studies that could be performed with the residual VOC detection are as follows:

- An integrated modelling approach is required to relate cure kinetics of a system to compound consumption/production. This will require a detailed understanding of the reaction scheme and mechanism of the polymerisation process. In any free-radical reaction there are a wide variety of potential products and detailed information on component reactivity ratios and reaction kinetics are required. In a multi-component,

two-stage reacting thermoset matrix, this becomes extremely complex and merits significant further investigation. Modelling the system is made particularly difficult by the volatile compounds involved and the variation in diffusion rate of these compounds through the matrix as the reaction proceeds (as well as the loss of volatiles during open-air post curing). The system may also be complicated by the potential for radical termination on the walls of the metal mould, thus component morphology could affect the composition of the final product. The aforementioned suggestions are potentially suited to the polymer chemistry discipline.

The development of nanocomposites for reducing volumetric shrinkage of unsaturated polyester would benefit from the following research:

- An investigation into the influence that sizing agent on the silicate clay has on the exfoliation and final mechanical properties of the nanocomposite. A silane (3-(Trimethoxysilyl)propyl methacrylate) or amine ([2-(Methacryloyloxy)ethyl] trimethylammonium chloride) solution have been identified as potential modifiers for improving compatibility of silicate to polyester resin.

6.4 Major Conclusion

This section includes a summary of the major conclusions arising from the work described in this thesis.

1. The surface quality of polymer composites can be effectively analysed using instrumented techniques such as stylus profilometry, with thresholds being developed for each technique. The use of the arithmetic mean roughness parameter (*Ra*) provides accurate representation of the laminate roughness in relation to the final paint quality.
2. Material characteristics such as thermal contraction, polymerisation shrinkage and fibre architecture influence laminate surface roughness, as relative matrix rich regions change volume in relation to the reinforcement during polymerisation. Matrices with high coefficients of thermal

expansion and high polymerisation shrinkage produce greater surface roughness.

3. A good basis for analytical modelling of the surface roughness is to start from a geometric description of the reinforcement and matrix and produce a general output, which is independent of the manufacturing process.
4. Paint layers progressively reduce defects associated with short-term waviness, but is unable to mask features attributed to long-term waviness.
5. The process of measuring the degree of cure determined by DSC increases the rate of styrene homopolymerisation, affecting the true residual reactivity. Residual styrene content needs to be measured and accounted for in the determination of true residual reactivity.
6. Solvent elution techniques are better suited to eluting total residual content as evaporative techniques are limited by the diffusion rate and compound entrapment.
7. Process and formulation variables such as postcure rate, initiator type and cobalt loading influence residual VOCs to varying levels. However, the dominant variable was found to be the inclusion of PVAc used as a low profile additive, which increases VOCs over that of just adding additional styrene.
8. The in-situ intercalative polymerisation method provides an appropriate means to forming an exfoliated nanocomposite structure within an unsaturated polyester matrix. A significant influence in reducing polymerisation shrinkage and increasing glass transition temperature is achievable with the formation of a nanocomposite due to the immobilisation of the matrix surrounding the interface of the nano-scale silicate.
9. The formation of a hybrid nanocomposite with PVAc permits the reduction of residual VOCs as a result of the decreased levels of LPA needed to form a cosmetic surface.
10. Tensile and impact strength lost through the use of an LPA are compensated for with the formation of a nanocomposite. Component

thickness can possibly be reduced for a nanocomposite due to a significant increase in tensile properties over that of a standard or low profile unsaturated polyester matrix.

Appendix 1 Publications Arising from Thesis

Schubel, P.J., Harper, L.T., Turner, T.A., Warrior, N.A., Rudd, C.D., Kendall, K.N. *Surface analysis of "Class A" polymer composite substrates for the automotive industry.* in 4th Asian-Australasian Conference on Composite Materials, 2004, Sydney, Woodhead Publishing, Paper No. E-712, Session PS-32.

Warrior, N., Harper, L., Turner, T., Schubel, P., Rudd, C., Kendall, K. *Affordable Lightweight Body Structures (ALBOS) Dti/DfT Foresight Vehicle Programme*. in JSAE Japan Society of Automotive Engineers Annual Congress, May, 2004, Yokohama, Paper No. 20045470, Session Material II No 86.

Warrior, N.A., Rudd, C.D., Turner, T.A., Schubel, P.J., Harper, L.T. *Affordable Lightweight Body Structures*. in IOM3 Materials Congress, 2004, London, Session 6B.

Appendix 2 Paint Thickness Distribution

Paint thickness was measured using a Krautkramer CTM20 ultrasonic pulse echo meter. It operates using a constant sound velocity principle with an active polyvenylidenfluorid (PVDF) polymer probe and resolution of 1 µm.

Table A2.1 shows the paint thickness for successive coats on all experimental substrates. On average the clear coat, base and primer are 53, 28 and 80 µm respectively. The Gaussian distribution (Figure A2.1) shows the total paint thickness average ranged between 156 and 165 µm with a 1st order standard deviation between 138 and 183 µm.

Table A2.1: Paint thickness measured by ultrasonic pulse echo.

	C1	C2	C3	C4	C5	C6	3K UP	6K UP	12K UP	3K EP	6K EP	12K EP
Clear	54	56	69	46	52	35	43	47	72	48	47	52
Base	17	38	40	38	32	22	21	25	27	22	22	29
Primer	124	52	77	77	68	90	81	109	55	91	98	91
Total	*195*	*146*	*186*	*161*	*152*	*147*	*145*	*181*	*154*	*161*	*167*	*172*

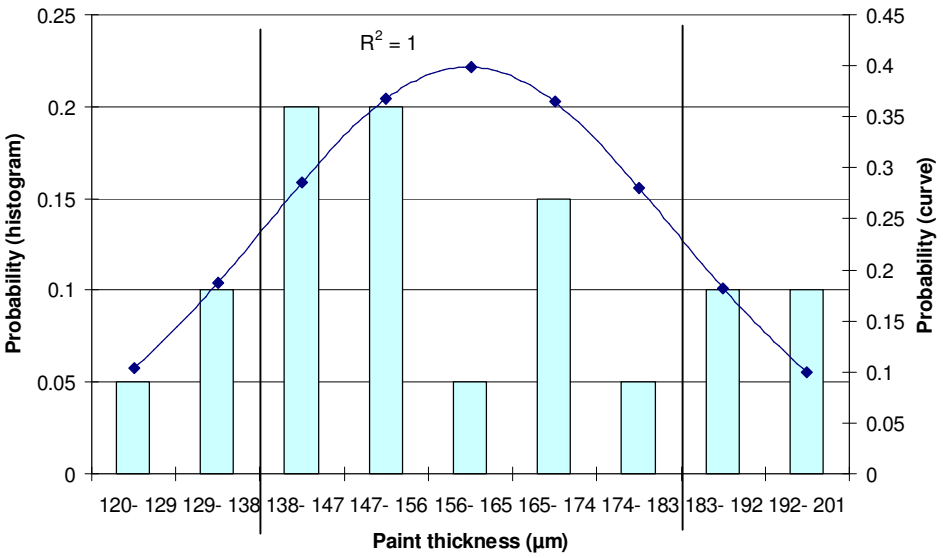

$$\phi(z) = \frac{1}{\sqrt{2\pi}} \exp\left(-\frac{z^2}{2}\right)$$

Figure A2.1: Gaussian distribution for total paint thickness.

Appendix 3 Statistical Evaluation on Subjective Surface Quality Trials

The reproducibility and repeatability (R&R) study on the painted substrates was conducted using the Six Sigma process and MiniTab® software. The appraisers were chosen due to their extensive experience in the field of automotive paint processes. The statistical analysis was conducted by comparing the observations of the 3 paint specialists to Appraiser 0, who showed 100% reproducibility.

Table A3.1: Personal details of appraisers

ID	Name	Occupation	Company
Appraiser 0	Andrew Hawtin	Lead Technician	Aston Martin Lagonda
Appraiser 1	Alan Berwick	Lead Technician	Aston Martin Lagonda
Appraiser 2	Terry Gilbert	Technical Advisor	PPG Industries
Appraiser 3	Richard Bailey	Technical Advisor	PPG Industries

Table A3.2: Observations made by the appraisers for 25 substrates.

	Appraiser 0	**Appraiser 1**		**Appraiser 2**		**Appraiser 3**	
Panels	*Attribute*	*Trial 1*	*Trial 2*	*Trial 1*	*Trial 2*	*Trial 1*	*Trial 2*
1	A	A	A	A	A	A	A
2	A	A	A	A	A	A	A
3	A	A	A	A	A	A	A
4	R	R	R	R	R	R	R
5	R	R	R	R	R	R	R
6	A	A	R	A	A	A	A
7	A	A	R	A	A	A	A
8	R	R	R	R	R	R	R
9	R	R	R	R	A	A	A
10	R	R	R	R	R	R	R
11	R	R	R	R	R	R	R
12	R	R	R	R	R	R	R
13	R	R	R	R	R	R	R
14	R	R	R	R	R	R	R
15	R	R	R	R	R	R	R
16	R	R	R	R	R	R	R
17	R	R	R	R	R	R	R
18	R	R	R	R	R	R	R
19	R	R	R	R	R	R	R
20	A	A	A	A	A	A	A
21	A	A	A	A	A	A	A
22	A	A	A	A	A	A	A
23	R	R	R	R	R	R	R
24	R	R	R	R	R	R	R
25	A	A	A	A	A	A	A

A = Accept surface quality
R = Reject surface quality

A3.1 Within Appraiser

Table A3.3: Assessment agreement within appraiser.

Appraiser ID	N.o. Inspected	* N.o. Matched	Percent (%)	95 % confidence interval	
1	25	23	92	74	99
2	25	24	96	79.6	99.9
3	25	25	100	88.7	100

*** Appraiser agrees with himself across trials.**

Table A3.4: Assessment agreement of appraiser versus the standard.

Appraiser ID	N.o. Inspected	* N.o. Matched	Percent (%)	95 % confidence interval	
1	25	23	92	74	99
2	25	24	96	79.6	99.9
3	25	25	96	79.6	99.9

*** Appraisers assessment across trials agrees with standard.**

Table A3.5: Assessment disagreement of appraiser versus the standard.

Appraiser ID	N.o. R/A	Percent (%)	N.o. Matched	Percent (%)	N.o. Mixed	Percent (%)
1	0	0	0	0	2	8
2	0	0	0	0	1	4
3	0	0	1	6.3	0	0

N.o. R/A: Assessments across trials = R / standard = A.
N.o. A/R: Assessments across trials = A / standard = R.
N.o. Mixed: Assessments across trials are not identical.

A3.2 Between Appraisers

Table A3.6: Assessment Agreement.

N.o. Inspected	* N.o. Matched	Percent (%)	95 % confidence interval	
25	22	88	68.8	97.5

*** All appraisers' assessments agree with each other.**

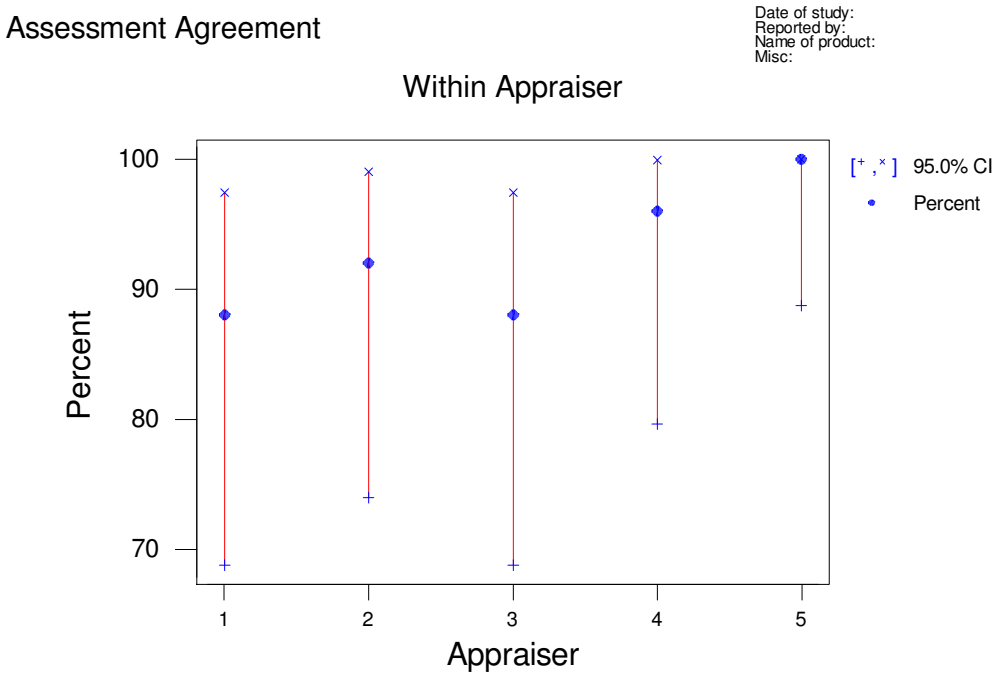

Figure A3.1: Repeatability within each appraiser

A3.3 Conclusions

It has been shown in Table A3.3 that on average, each appraiser from Group 2 can reproduce their own results to an accuracy of 97 % when asked to reassess the laminates. Table A3.6 shows that 88 % of the observations matched the standard (Appraiser 0) observation. This shows that the measurement error within Group 2 is 12 %. Statistically this measurement error is acceptable as denoted by the Six Sigma process.

Appendix 4 Surface Waviness Characterisation

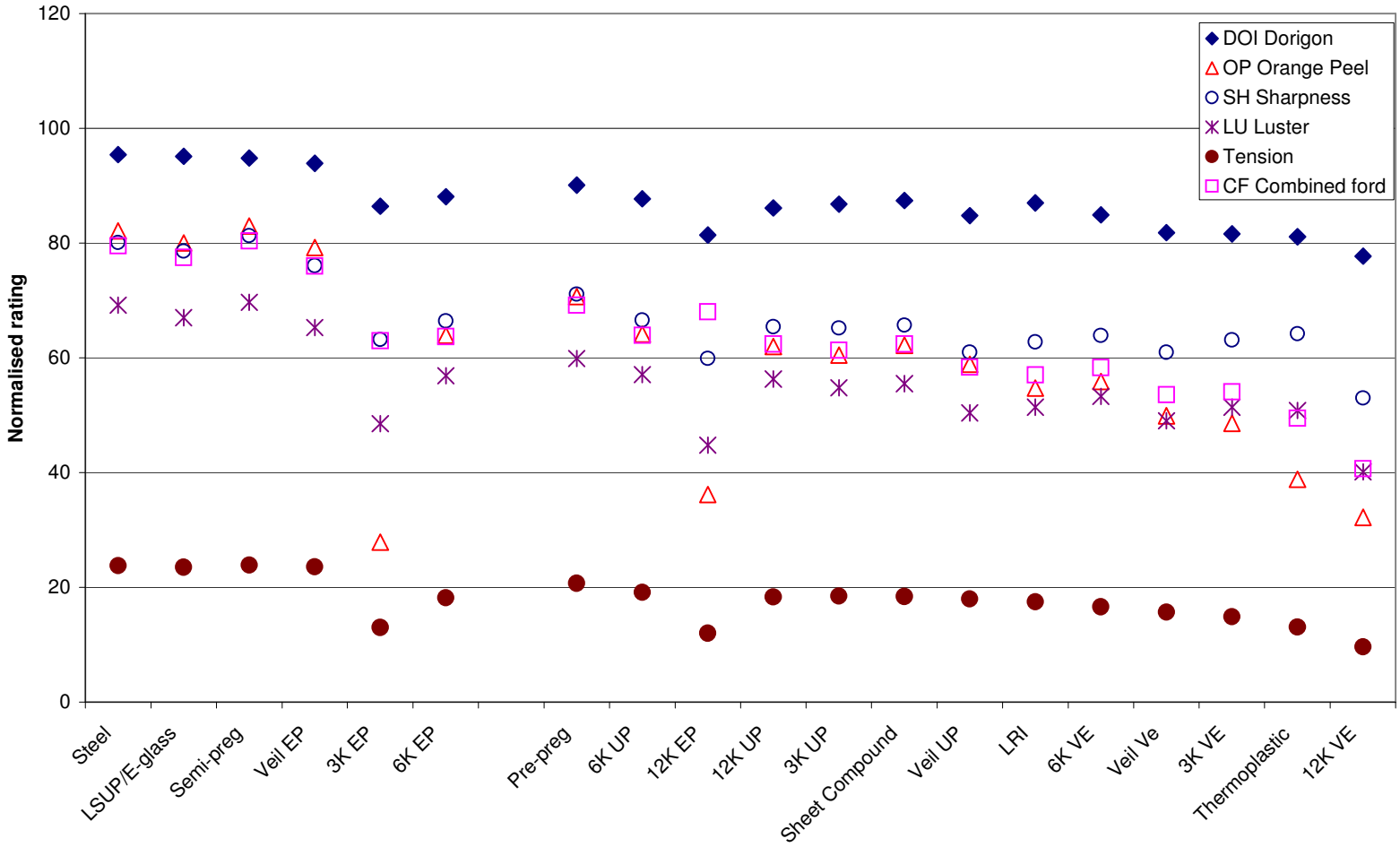

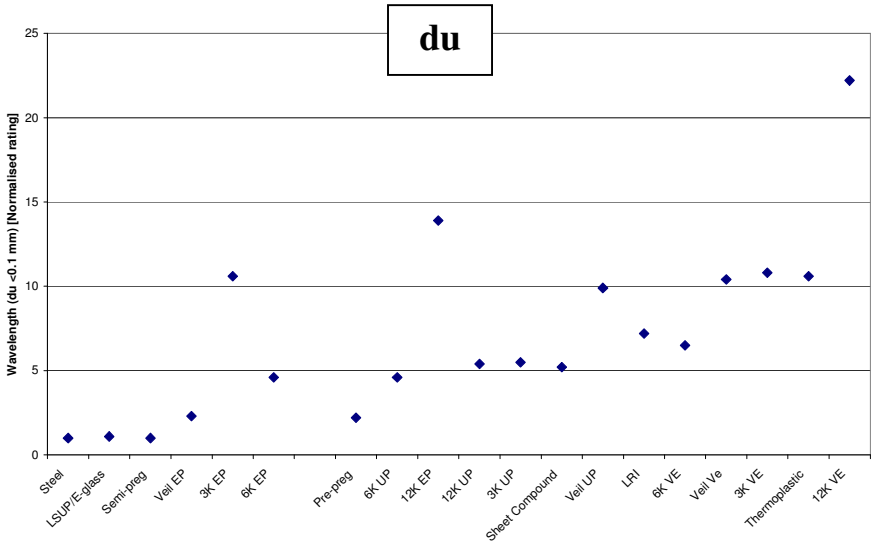
du
Wavelength (du <0.1 mm) [Normalised rating]
0
5
10
15
20
25
Steel
LSUP/E-glass
Semi-preg
Veil EP
3K EP
6K EP
Pre-preg
6K UP
12K EP
12K UP
3K UP
Sheet Compound
Veil UP
LRI
6K VE
Veil Ve
3K VE
Thermoplastic
12K VE

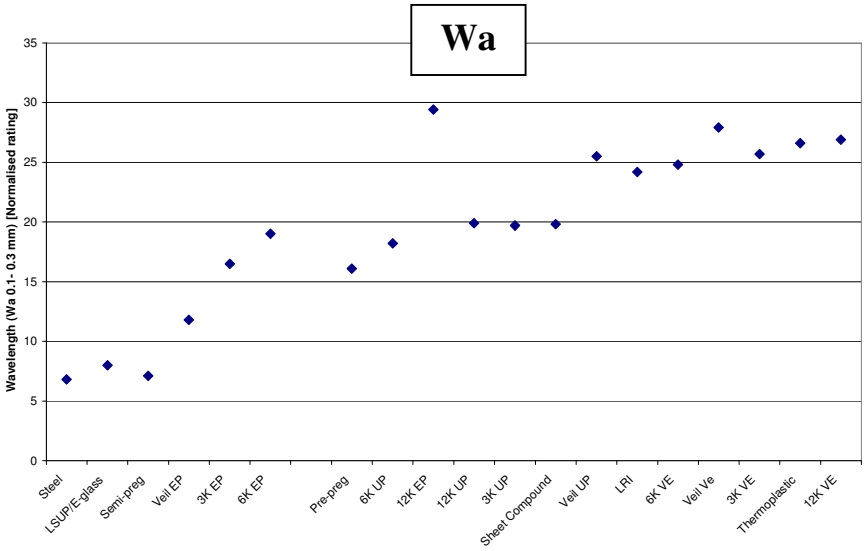
Wa
Wavelength (Wa 0.1- 0.3 mm) [Normalised rating]
0
5
10
15
20
25
30
35
Steel
LSUP/E-glass
Semi-preg
Veil EP
3K EP
6K EP
Pre-preg
6K UP
12K EP
12K UP
3K UP
Sheet Compound
Veil UP
LRI
6K VE
Veil Ve
3K VE
Thermoplastic
12K VE

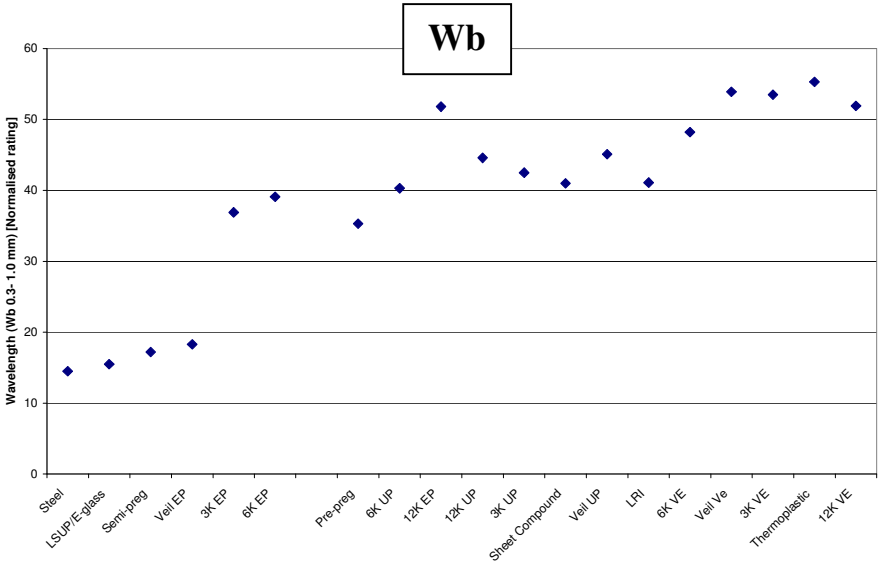
Wb
Wavelength (Wb 0.3- 1.0 mm) [Normalised rating]
0
10
20
30
40
50
60
Steel
LSUP/E-glass
Semi-preg
Veil EP
3K EP
6K EP
Pre-preg
6K UP
12K EP
12K UP
3K UP
Sheet Compound
Veil UP
LRI
6K VE
Veil Ve
3K VE
Thermoplastic
12K VE

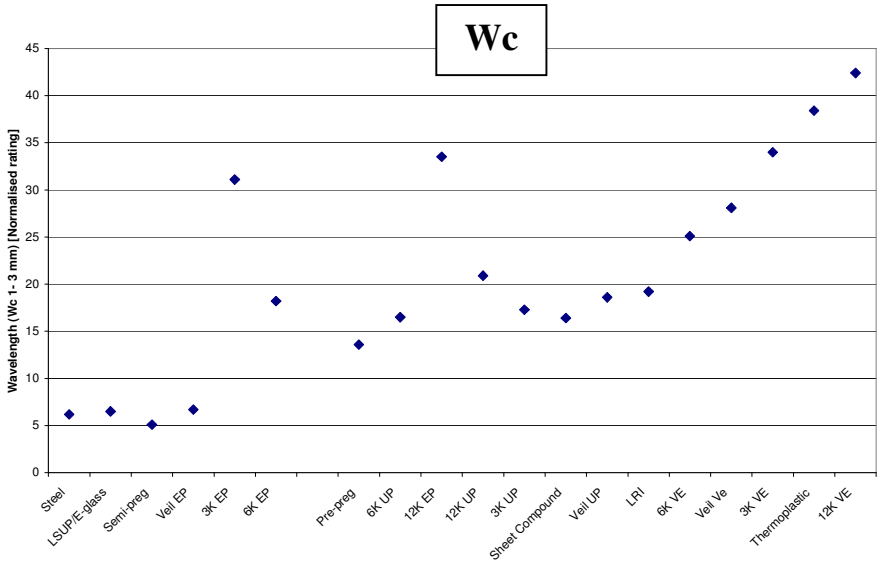
Wc
Wavelength (Wc 1 - 3 mm) [Normalised rating]
0
5
10
15
20
25
30
35
40
45
Steel
LSUP/E-glass
Semi-preg
Veil EP
3K EP
6K EP
Pre-preg
6K UP
12K EP
12K UP
3K UP
Sheet Compound
Veil UP
LRI
6K VE
Veil Ve
3K VE
Thermoplastic
12K VE

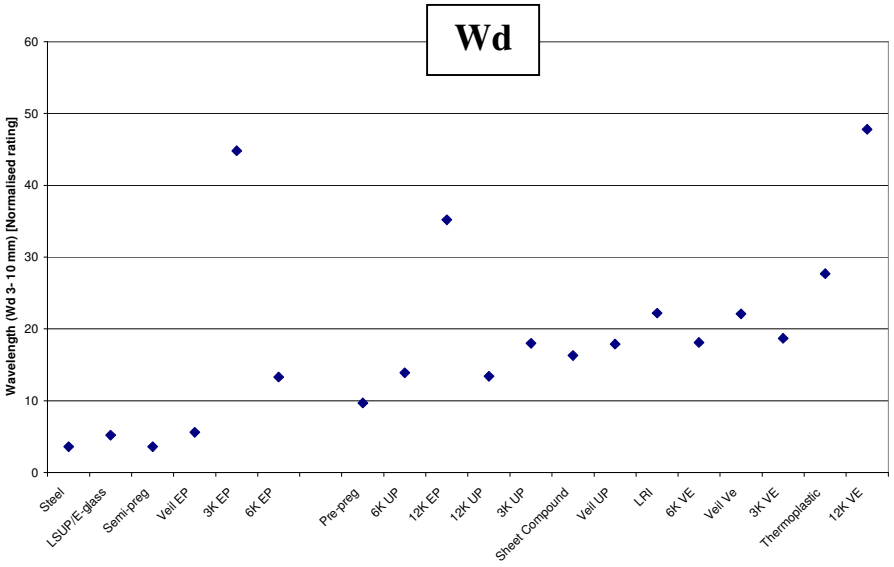
Wd
Wavelength (Wd 3- 10 mm) [Normalised rating]
0
10
20
30
40
50
60
Steel
LSUP/E-glass
Semi-preg
Veil EP
3K EP
6K EP
Pre-preg
6K UP
12K EP
12K UP
3K UP
Sheet Compound
Veil UP
LRI
6K VE
Veil Ve
3K VE
Thermoplastic
12K VE

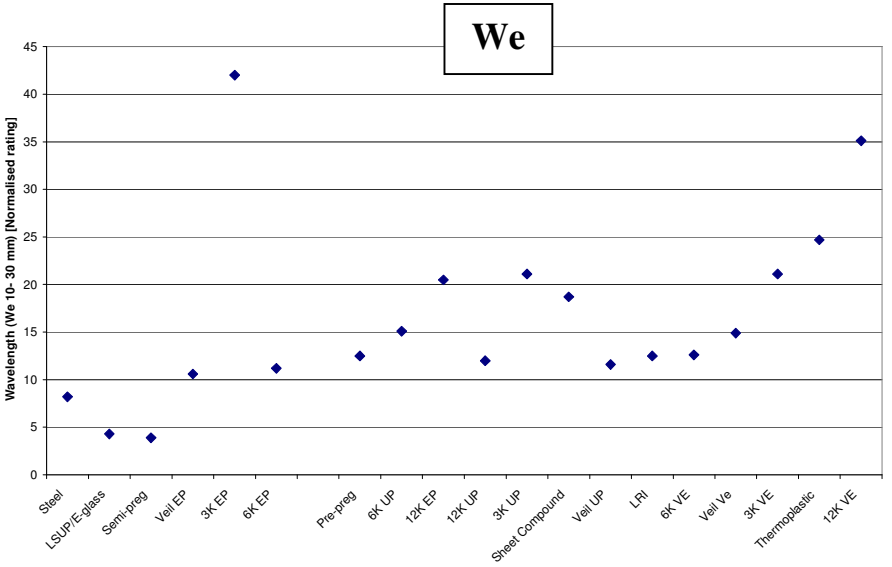
We
Wavelength (We 10- 30 mm) [Normalised rating]
0
5
10
15
20
25
30
35
40
45
Steel
LSUP/E-glass
Semi-preg
Veil EP
3K EP
6K EP
Pre-preg
6K UP
12K EP
12K UP
3K UP
Sheet Compound
Veil UP
LRI
6K VE
Veil Ve
3K VE
Thermoplastic
12K VE

Appendix 5 Calculation of Percentage Mass Compound for Gas Chromatography

A5.1 Introduction

It was desirable to convert the response area of a GC plot into a value directly related to a unit mass of compound. This allowed a direct comparison between samples and relevant literature. The number of moles of any substance is related to the area of the distribution. For this reason it is possible to create a calibration curve for a know substance from which all detected values can be based.

A5.2 Calibration

A known quantity of pure concentration (styrene/ benzaldehyde) was injected into the GC to return the response area. The concentration was varied from 1 to 10 µL/10mL of solution, resulting in linear response (Figure A5.1). The plot of the number of moles injected against response area was used to calculate the equation of the line. The subsequent calibration factor was found for the particular compound with respect to the GC instrument used.

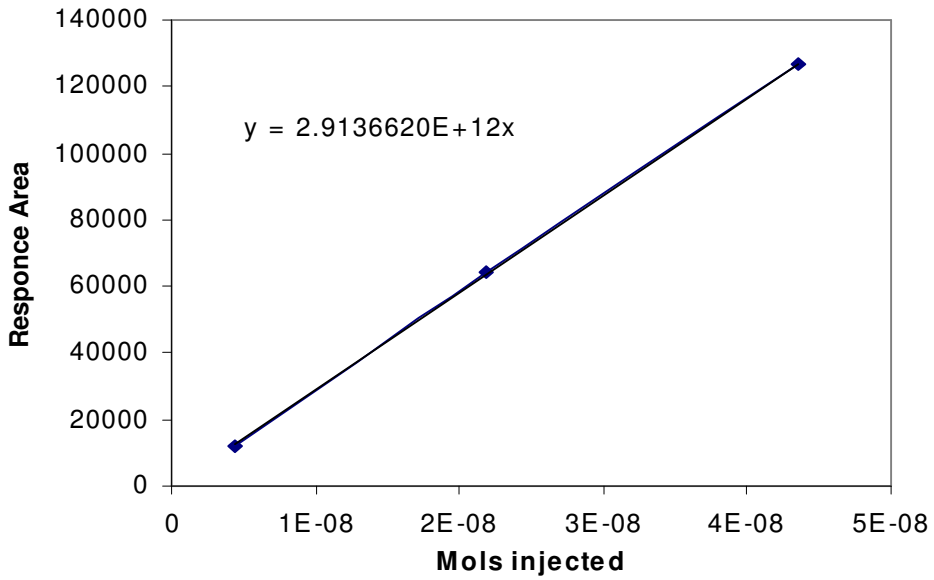

Figure A5.1: Response area of 1 to 10 uL/10mL of styrene solution.

A calculation of the number of moles injected is given by:

$$M_i = \left(\frac{C_v \cdot \rho}{M_r} \right) . V_i \qquad \text{[A5.1]}$$

where

M_i is the known amount of moles injected into the solution

C_v is the calibration volume in mL/10mL

ρ is the density of the compound

M_r is the molecular weight of the compound

V_i is the injection volume expressed in mL

The calibration factor (C_f) was calculated directly from the gradient of the calibration graph (Figure A5.1). The number of moles are then calculated by:

$$moles = \frac{A_r}{C_f} \qquad \text{[A5.2]}$$

where

A_r is the response area of the compound

C_f is the calibration factor

The bulk mass of the compound is calculated by:

$$m_b = \left(moles . M_r \right) . N_I \qquad \text{[A5.3]}$$

where

m_b is the mass in bulk of the compound

N_I is the amount of sample injections per mL

The percentage mass of compound is given by:

$$pmc = \left(\frac{m_b}{m} \right).100 \qquad \text{[A5.4]}$$

where

pmc is the percentage mass of compound

m is the mass of the block sample used in the experiment

Appendix 6 Effects of Sample Conditioning for Gas Chromatography

A6.1 Introduction

GC is susceptible to variations in sample preparation due to the high resolution of the flame ionisation detector. Small changes in set-up conditions can affect the accuracy and repeatability of results. This section looks at optimising the GC process for elution of styrene and benzaldehyde compounds from a composite material.

A6.2 Effects of Sample Preconditioning on GC Response

Sample preconditioning refers to the process used for extraction of compounds from the sample mass, i.e. styrene, benzaldehyde. This process affects the level of separation of strongly interfacing components in the capillary column. The differences between the volatility of the analytes and the varying chemical nature of the substances are important for the choice of a suitable sample preparation procedure. A low profiling unsaturated polyester system was used as a representative matrix (Table A6.1).

Table A6.1: Mould conditions

	RT2557 +30 wt% PVAc		
Resin	+30 wt% CaCO3	Mould Temp (ºC)	95
Initiator (%)	TBPB (2)	Demould (min)	30
Accelerator (%)	G (0.5)		

British standard BS 2782-4:Method 432A:1991 recommended a suspension time in Dichloromethane between 15 to 20 hours to successfully extract sufficient analytes from the sample. Using this as a basis, a test matrix was developed with suspension time varying between 1 and 20 hours.

Figure A6.1 shows the percentage mass of styrene and benzaldehyde for varying suspension times in dichloromethane at 21 ºC. It can be seen that the percentage mass of styrene and benzaldehyde increase rapidly from 1 to 15 hours, at which point both curves stabilise. This suggests that the majority of the available compound has been eluted from the sample within 15 hours.

It was seen from preconditioning trials that a stabilisation of analytes eluted from the sample occurred at 15 hours in dichloromethane solution. Because the objective of the GC test was to make it as simple and efficient as possible, it was decided to accept the 0.01 % discrepancy between the 15 to 20 hr interval. Thus, suspension time in dichloromethane solution was set to 15 hr ± 10 min.

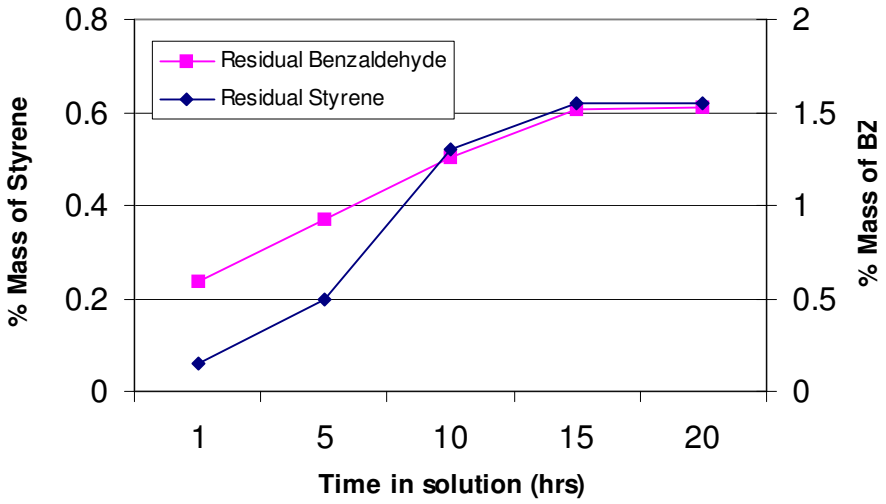

Figure A6.1: Percentage mass of styrene and benzaldehyde for preconditioning of sample by varying time in suspension of dichloromethane. A linear increase of eluted compound is seen up to a suspension time of 15 hrs. At this point, the rate of eluted compound decreases and stabilises.

A6.3 Influence of Sample Mass on GC Response

The sample mass influences the level of elute received by the capillary column which could potentially skew the results in a positive or negative fashion. Since the volume of dichloromethane solution had been fixed at 4 mL, the variation in

ratio of sample mass to solution volume could only be altered by varying sample mass.

A study was conducted on a low profiling unsaturated polyester system (Table A6.1) with the sample mass varying between 0.45g and 3.2g. The samples were suspended in dichloromethane for 15 hours before injection into the column. The results obtained for residual styrene and benzaldehyde (Figure 6.2) show that the percentage mass of compound continues to increase until stabilisation at approximately 1.5 g. After this point, a doubling of sample size has negligible increase in both situations.

It is preferable to have a small sample size to ensure that there is sufficient material for repeat trials and to reduce the need for reiterating the solution volume to ensure the sample is completely submerged. It was decided that a 1.5 ± 0.1 g sample mass provided sufficient compound extraction for 4 mL of dichloromethane solution. Any small variations in sample size are compensated for by the calculation of percentage mass compound described in Appendix 5.

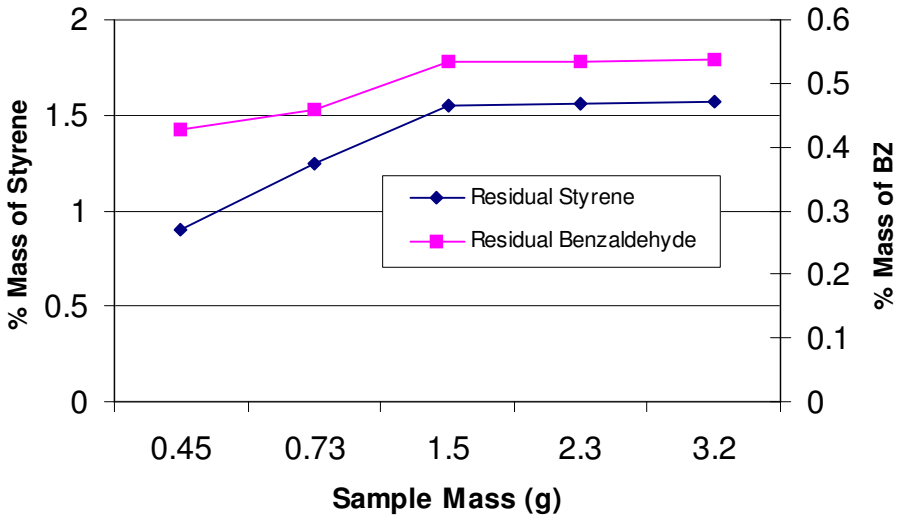

Figure A6.2: Influence of sample mass on residual styrene and benzaldehyde.

Appendix 7 Dispersion of Silicate Clays using the In-situ Intercalative Polymerisation Method

A7.1 Effects of Shear Rate

The effects of shear mixing speed on the level of exfoliation were investigated as shear mixing assists exfoliation due to mechanical separation of the gallery layers. 4 wt% Cloisite 10A in unsaturated polyester resin was mixed between 120 rpm (hand mixing) and 3000rpm (mechanical mixing) and subsequently polymerised then analysed using XRD. Figure A7.1 shows that hand mixing results in a diffraction peak with basal spacing of 1.85 nm, indicating poor intercalation/ exfoliation. All other samples developed an amorphous state, indicating that the formation of a nanocomposite is not heavily influenced by mixing speeds above 500 rpm.

The volumetric shrinkage was monitored for all samples to see if mixing speed influenced the reduction of chemical resin shrinkage. Figure A7.2 shows that the sample prepared via hand mixing showed less than 0.5 % decrease in volumetric shrinkage. All other samples showed approximately 2 % fall in chemical resin shrinkage. Minimal reduction in resin shrinkage was predicted for the sample produced at 120 rpm (hand mixing) due to the low exfoliation seen in the XRD plot (Figure A7.1). The rise in resin shrinkage at 3000 rpm is not fully understood but maybe caused by the silicate particles clumping together again. It could be argued that the values seen between the 500 rpm and 3000 rpm fall within the standard deviation range, but for the purposes of this study it was taken that 1500 rpm provided the optimal reduction in resin shrinkage.

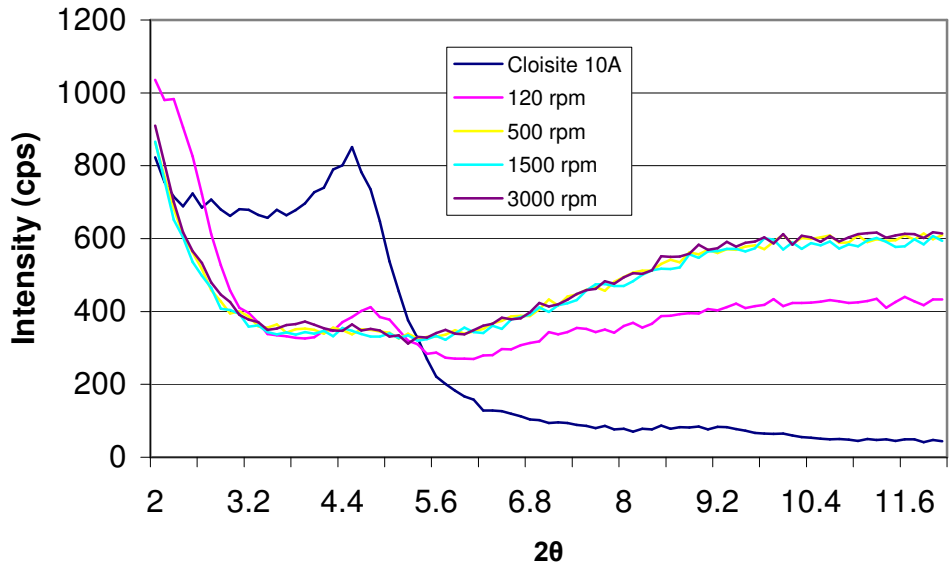

Figure A7.1: XRD of 4 wt% Cloisite 10A dispersed in unsaturated polyester at varying shear mixing speeds.

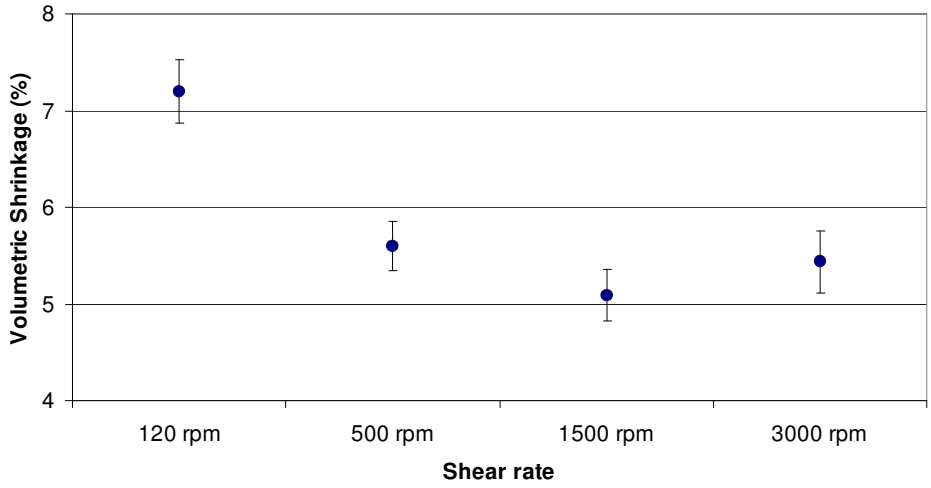

Figure A7.2: Volumetric shrinkage of 4 wt% Cloisite 10A dispersed in unsaturated polyester at varying shear mixing speeds.

A7.2 Gradient Effects of Nanocomposite Through-Thickness

X-ray diffraction only penetrates the first few microns of the surface, which raised concerns about whether the surface results were representative of the entire

sample. A study into the through-thickness effect was undertaken to determine whether an exfoliation gradient existed in the resin cast samples. Surface layers were progressively ground on a Struers® DAP-7 laboratory polisher using P1200 grit paper, with XRD analysis between each successive layer removal.

Figure A7.3 shows the XRD results for 4 wt% Cloisite 10A in unsaturated polyester for successive layer removals of a 3 mm thick sample. No diffraction peak was observed in each case, indicating that a nanocomposite structure was formed through the entire thickness of the sample.

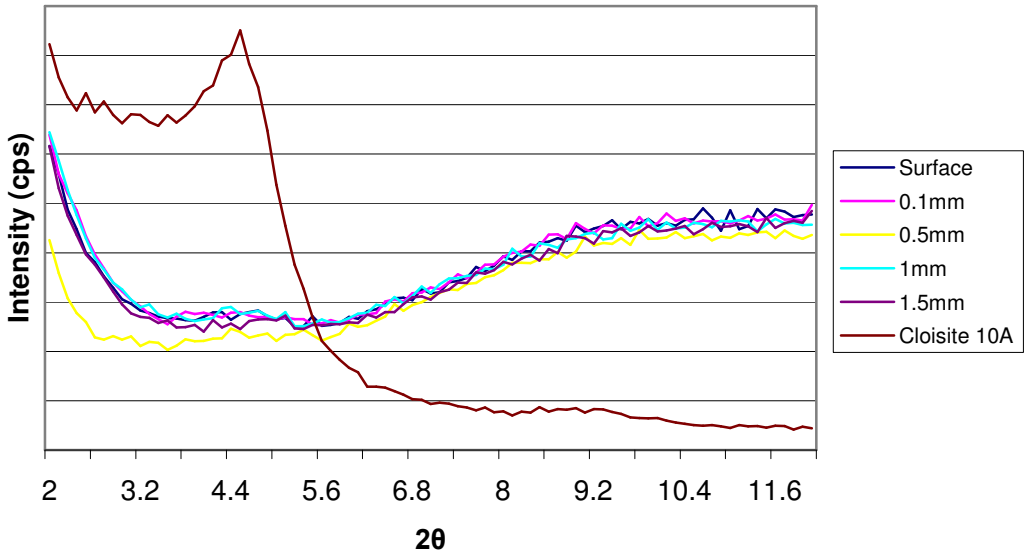

Figure A7.3: XRD on the cross-sectional gradient of 4 wt% Cloisite® 10A in unsaturated polyester.

Appendix 8 Surface Roughness Modelling of Fabric Reinforced Polymer Composites

Experimental work indicated that critical functions of the surface roughness were the textile architecture and the level of matrix shrinkage. It was decided to develop the model around an existing software package (TexGen) developed for geometric modelling of textiles by Robitaille and co-workers [1, 2]. TexGen allows a geometric model of the fabric to be created based on idealised yarn vectors with yarn cross-sections verified via optical microscopy (Figure A8.1). The measured parameters for a 3k, 6k and 12k moulded fabric were obtained (Table A8.1) and used to create the input file for the geometric generator.

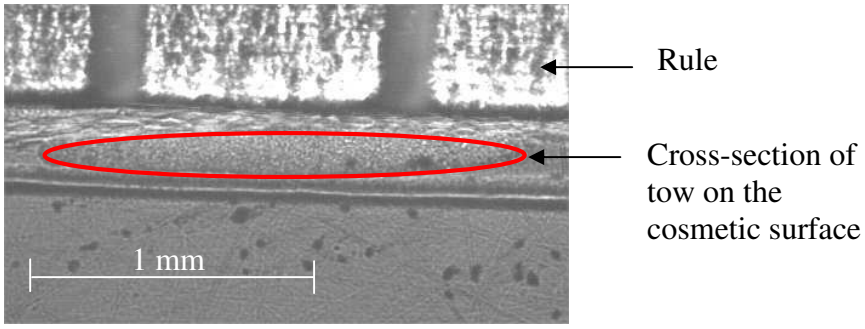

Figure A8.1: Optical microscopy of a tow (highlighted in red) on the cosmetic surface of a 6k, 2x2 twill weave fabric moulded by RTM.

Table A8.1: Tow dimensions measured using optical microscopy.

Tow Size	Width (mm)	Thickness (mm)
3k	1.8	0.15
6k	2.0	0.18
12k	2.5	0.25

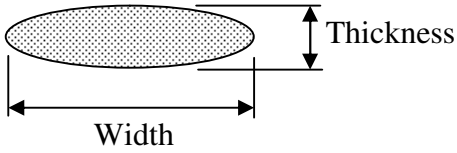

Three separate TexGen files was created for a 3k, 6k and 12k 2x2 twill weave fabric. Five nodes per vector were assigned and Bezier curves were formed (Figure A8.2).

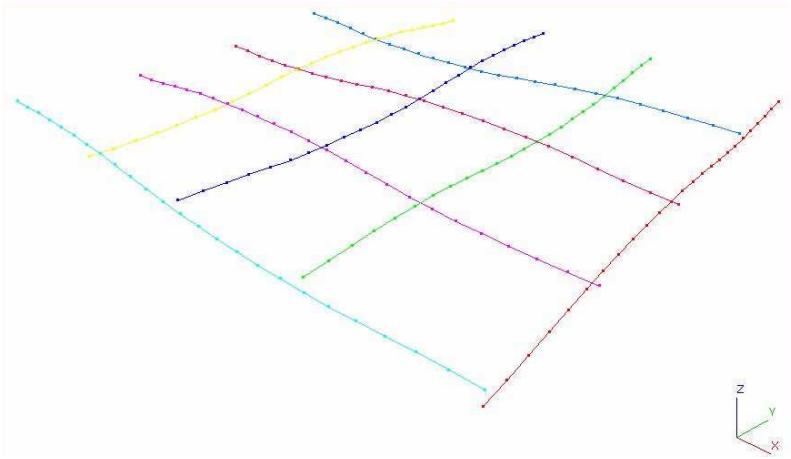

Figure A8.2: TexGen input file for a 12k, 2x2 twill weave fabric. Five nodes were assigned to each vector and Bezier curves were formed.

A powered elliptical envelope (Figure A8.3) was created around the Bezier curves with tow radial dimensions used from Table A8.1. For a geometric model, a flexible function was required to describe the tow cross-section. Equation A8.1 describes a generalised ellipse [3]:

$$\pm y = \pm\left(\frac{h_t}{2}\right)\left(1-\frac{x^2}{\left(\frac{h_t a_t}{2}\right)^2}\right)^n \qquad \text{[A8.1]}$$

where x and y are the geometric coordinates, h_t is the tow height, a_t is the tow aspect ratio and n is the shape parameter.

This equation is used to determine the shape of a general ellipse. The tow shape parameter, n, defines the shape of the curve, with n=0.5 producing a natural ellipse and n=0 producing a rectangle. For the values in the range 1>n>0.5 a lenticular shape is generated, although for the cases presented in this thesis, values in the range of 0.5>n>0 were used exclusively (Figure A8.4).

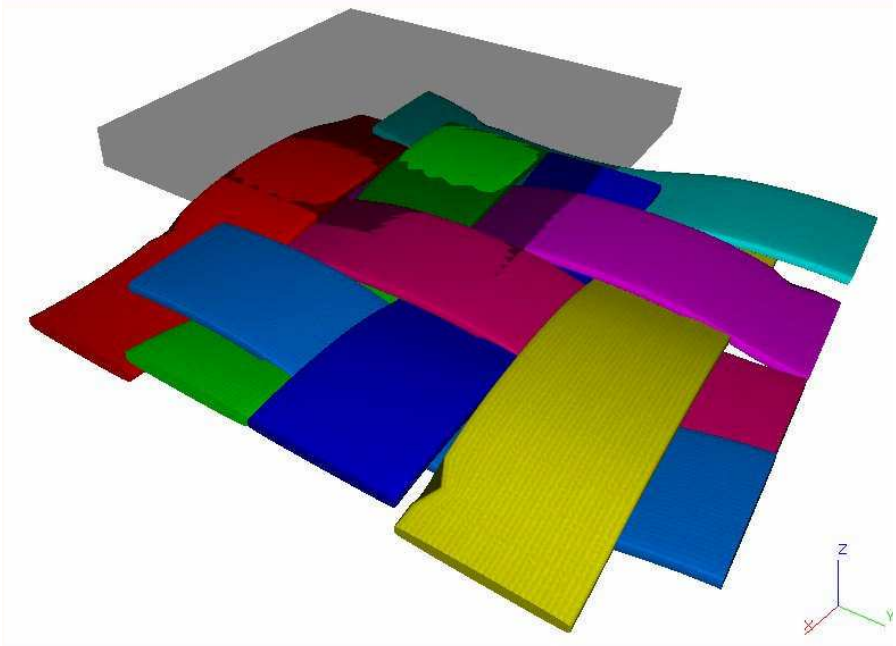

Figure A8.3: Powered elliptical envelope for a 12k, 2x2 twill weave fabric using appropriate tow dimensions from Table A8.1 and 0.35 shape parameter.

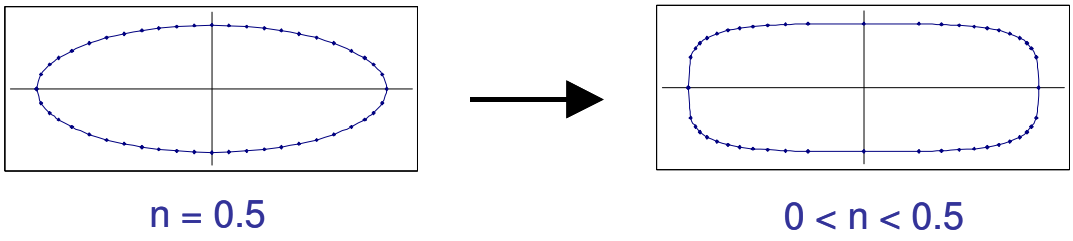

Figure A8.4: Tow shapes produced using Equation A8.1.

The domain was used to simulate the matrix and was set to a single repeat unit cell of the 2x2 twill weave, with the maximum z co-ordinate (cosmetic surface) reduced to the face of the tow envelope (Figure A8.5). This simulated the resin layer thickness on a laminate for the cosmetic surface, which was measured by optical microscopy in Figure A8.1.

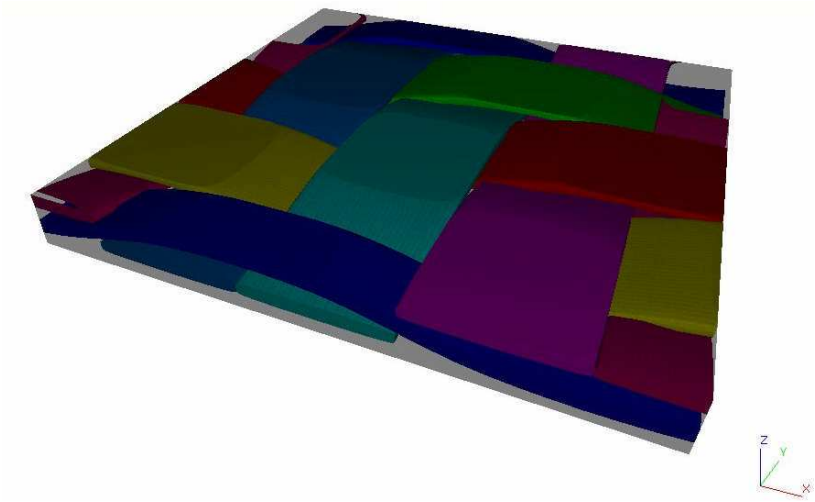

Figure A8.5: Repeat unit cell of a 12k, 2x2 twill weave fabric with the domain touching the cosmetic face of the model to represent the matrix thickness of a true laminate.

A sequence was written in C^{++} and incorporated into TexGen to output a text file of the relative portions of matrix and reinforcement for any given two-dimensional slice taken through the unit cell. This was made possible by utilising the existing grid function within TexGen (Figure A8.6) that separates the domain into a series of one-dimensional lines. These lines distinguish the relative portions of matrix and reinforcement at each interval.

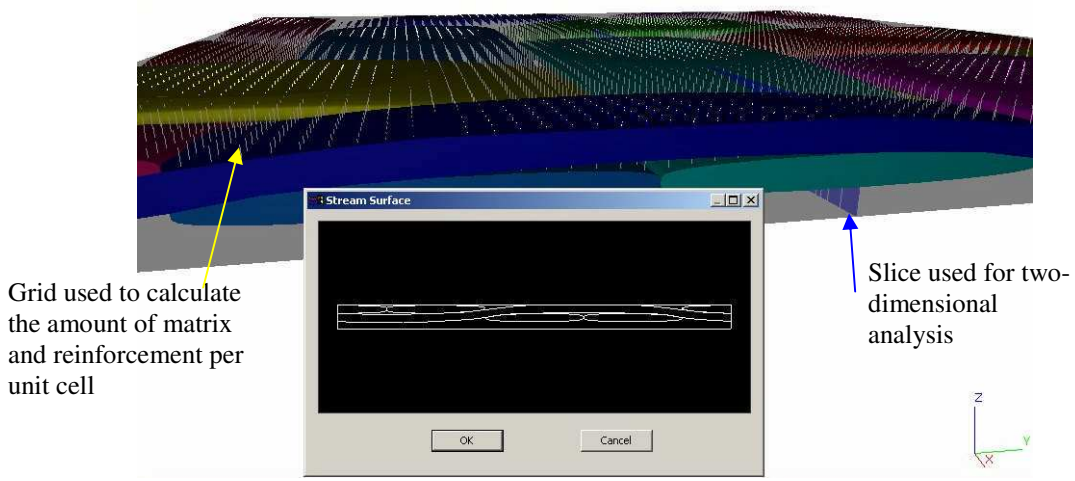

Figure A8.6: TexGen grid function used to output a two-dimensional slice through the domain. An integrated C^{++} code calculates the proportion of matrix to reinforcement for text output. Insert picture represents the matrix and reinforcement at the particular cross-section of the domain.

The relative matrix and reinforcement thickness, D_M and D_R respectively, for 0.01 mm intervals along the cross-section were output to a Microsoft Excel spreadsheet. The following assumptions were made for the numerical analysis to simplify the calculations:

- The tool surface roughness does not influence the surface of the laminate.
- The outer reinforcement layer stays in contact with the mould surface throughout the cure process.
- Matrix shrinkage only occurred in the thickness (z) direction [4].
- There was no strain induced by neighbouring cells.
- The peak exotherm temperature was considered the critical temperature for thermal expansion.
- The reinforcement phase does not experience any thermal or polymerisation shrinkage.

The analysis was based on the Fourier's heat conduction equation for a one-dimensional cure simulation, which was introduced in Section 1.3.1 (Equation 1.3). Equation 1.3 assumes that the thermal properties (k_z, ρ, *and* c_p) remain constant throughout the curing process [5].

A formulation allowing for either convective, insulated or prescribed temperature boundary conditions was employed on the laminate surface [4]:

$$k_{eff}\frac{\partial T_s}{\partial z} + h_{eff}\left[T_s - T(t)\right] = 0 \qquad \text{at } z = 0 \text{ and } z = L \qquad \text{[A8.2]}$$

The temperature and normal derivative of temperature on the laminate surface are denoted T_s and $\frac{\partial T_s}{\partial z}$ respectively. The coefficients k_{eff} and h_{eff} represent the effective thermal conductivity and convective heat transfer coefficient on the laminate surface, respectively. The cure cycle temperature is represented by *T(t)*. The temperature boundary conditions ($k_{eff} = 0$ and $h_{eff} = 1$) were employed in all

simulations presented in this work to eliminate the complexity of interpreting the influence of convection on the results [4]. Which reduces the boundary condition term to:

$$T_s = T(t) \qquad \text{[A8.3]}$$

Region II (Figure 1.5) denotes the beginning and end of the cure cycle and the peak exotherm temperature in this region was taken as the maximum cure temperature. For the analysis, the peak exotherm temperature was crudely measured by a simple gel test conducted in an oil bath at the specified mould temperature of 95 ºC. A thermocouple placed in the middle of a test tube holding 80 g of sample was used to determine the peak exotherm temperatures (Table A8.2).

Table A8.2: Values used for calculation of the total matrix shrinkage.

Resin Type	Sample ID	Peak Exotherm Temperature (ºC)	Thermal Expansivity, α_1 (10^{-6} K^{-1})	Thermal Shrinkage, ΔV (%)	Polymerisation Shrinkage, ΔV_{Chem} (%)
Epoxy	Low shrink (LS)	212 ± 15	60	1.14	0.24 ± 0.10
Unsat' polyester	High shrink (HS)	110 ± 6	150	1.32	8.34 ± 0.61

The process induced thermal shrinkage (ΔV) for each system was calculated using Equation 1.10. The change in temperature was calculated as the difference between the peak exotherm temperature and room temperature (22 ºC) whilst the coefficient of thermal expansion (α_1) was obtained from Hull et al [6] for the respective matrices (Table A8.2).

The volumetric polymerisation shrinkage (ΔV_{Chem}) given by Equation 1.6 was determined by a multipycnometer (Section 4.4.2). The total volumetric polymerisation shrinkage for the low and high shrink resin systems are listed in Table A8.2. Volumetric shrinkage needed to be converted into linear shrinkage since the analysis is only considering the matrix shrinkage in the plane normal to the laminate surface. It is assumed that every portion of the part solidifies at the same pressure and at the same time, hence the volumetric shrinkage will be

equally distributed in all directions. Therefore the linear shrinkage will approximately equal 1/3 of the volumetric shrinkage [7].

The corrected z-coordinate height (D_{Tot}), which considers the thermal and polymerisation shrinkage of the matrix, is therefore calculated at each interval by:

$$D_{Tot} = \left[D_M \left(\frac{100 - \Delta S_{Tot}}{100} \right) + D_R \right].1000 \qquad \text{[A8.4]}$$

where $\Delta S_{Tot} = \Delta V + \frac{\Delta V_{Chem}}{3}$

A representative surface profile (Figure A8.7) for the slice taken in Figure A8.6 of a 12k, 2x2 twill weave fabric with a low shrink matrix clearly shows the contraction of the matrix rich areas between adjacent tows and between the warp and weft tows.

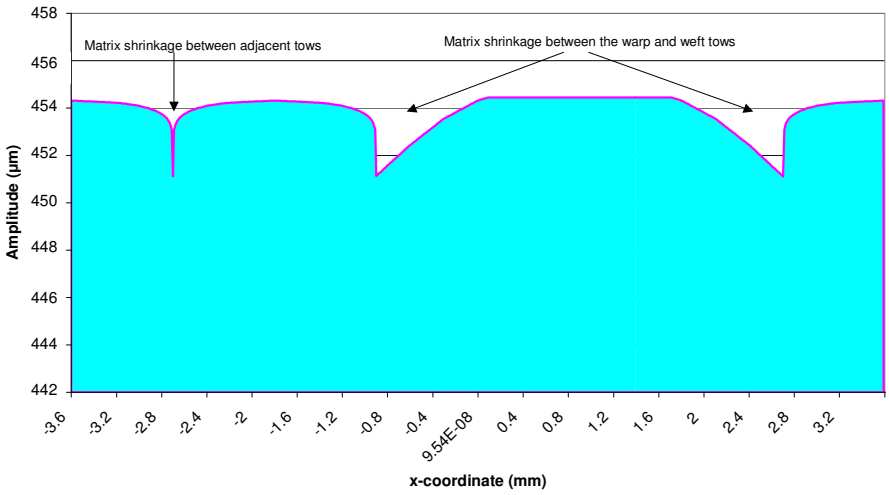

Figure A8.7: Surface profile created from Equation A8.4, which accounts for thermal and polymerisation shrinkage of the matrix.

A series of slices were taken with the matrix being subject to percentage reduction according to parameters associated with the matrix. The resultant allows for topological representation of the surface roughness (Figure A8.8 to A8.10). A comparison of the simulated result against experimental result in Figure A8.8

shows good correlation for a repeat unit cell area. The surface characteristics appear similar with both plots exhibiting amplitudes in the region of 6 to 10 μm. Similarly, Figure A8.9 shows related trends with amplitudes ranging from 25 to 30 μm for both simulated and experimental plots. The modelling techniques are not restricted to just a 2x2 twill weave fabric and can be used to simulate the surface roughness of any style of fabric (Figure A8.10).

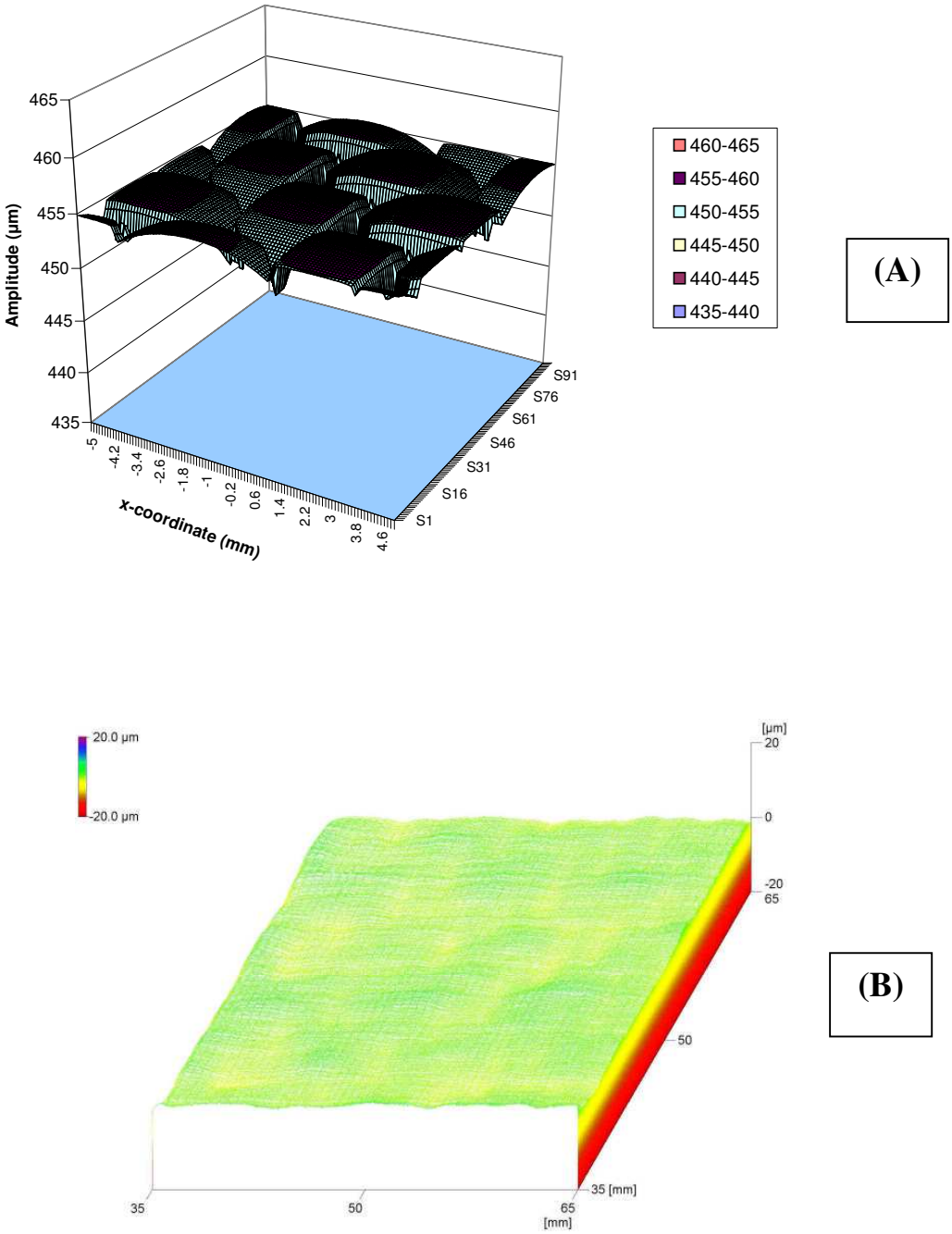

Figure A8.8: Topological plots of a 12k, 2x2 twill weave fabric moulded with a low shrink (~1%) epoxy matrix. (A) Simulated model, (B) Experimental result. Both topological plots show related trends with similar amplitude (6 to 10 µm)

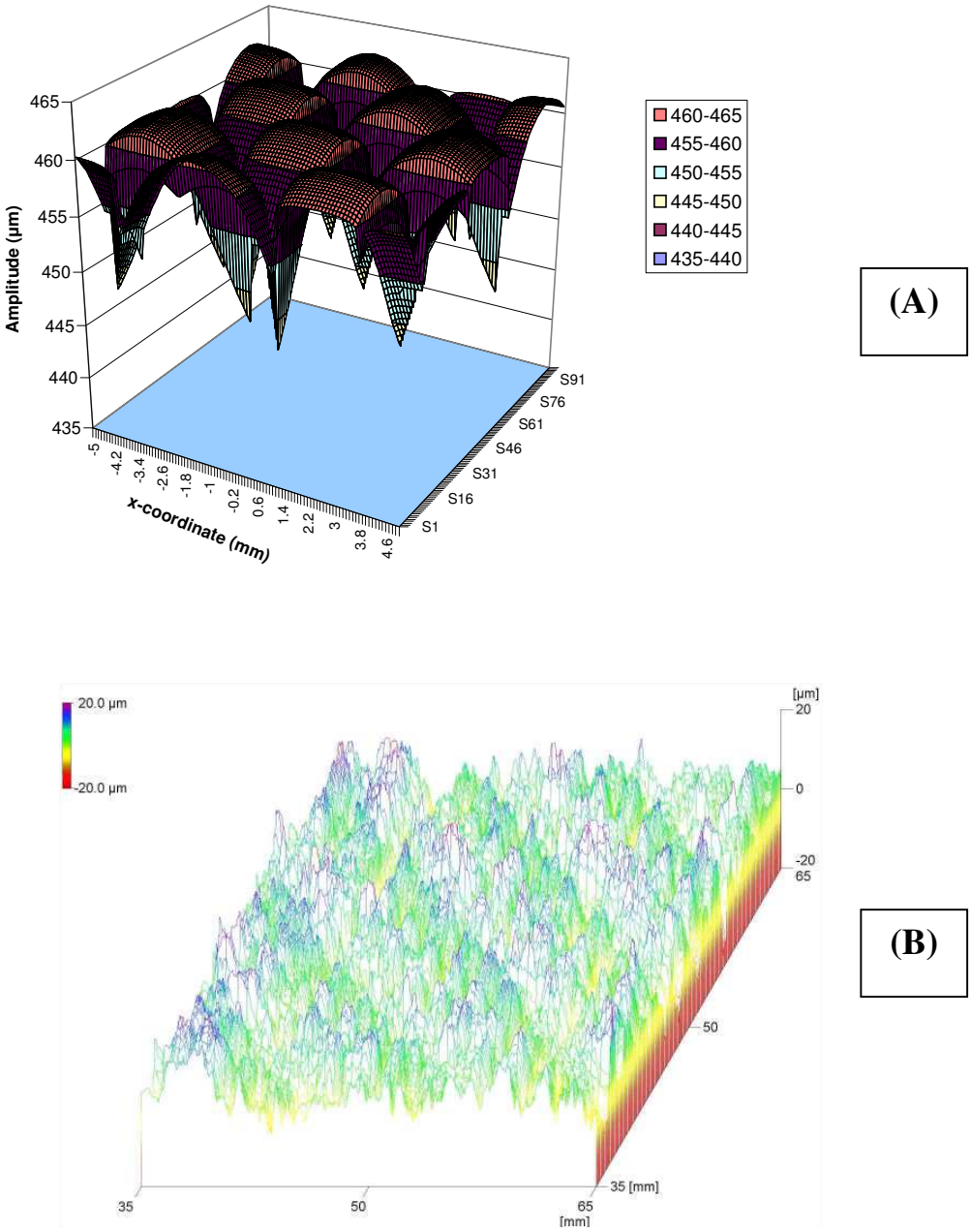

Figure A8.9: Topological plots of a 12k, 2x2 twill weave fabric moulded with a high shrink (~8%) unsaturated polyester matrix. (A) Simulated model, (B) Experimental result. Both topological plots show related trends with similar amplitude (25 to 30 µm)

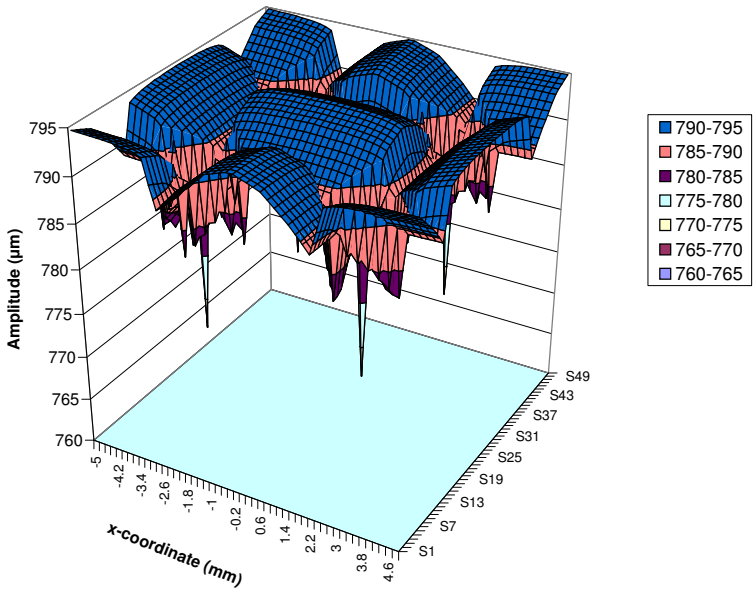

Figure A8.10: Simulated topological plot of a 12k, plain weave fabric moulded with a high shrink (~8%) unsaturated polyester matrix.

Three geometric models were developed to represent a carbon 2x2 twill weave fabric with 3, 6 and 12k tow size. These models were analysed with low and high shrink resin properties to estimate the surface profile. In each case, the arithmetic mean was calculated using Equation 2.1 from the profile values obtained through Equation 8.4. The theoretical values were plotted against experimental data obtained from the same materials moulded by RTM (Figure A8.11). A comparison of like systems in Figure A8.11 shows that the theoretical values give similar trends to the experimental data with theoretical values falling no further than 0.06 µm *Ra* outside experimental standard deviation.

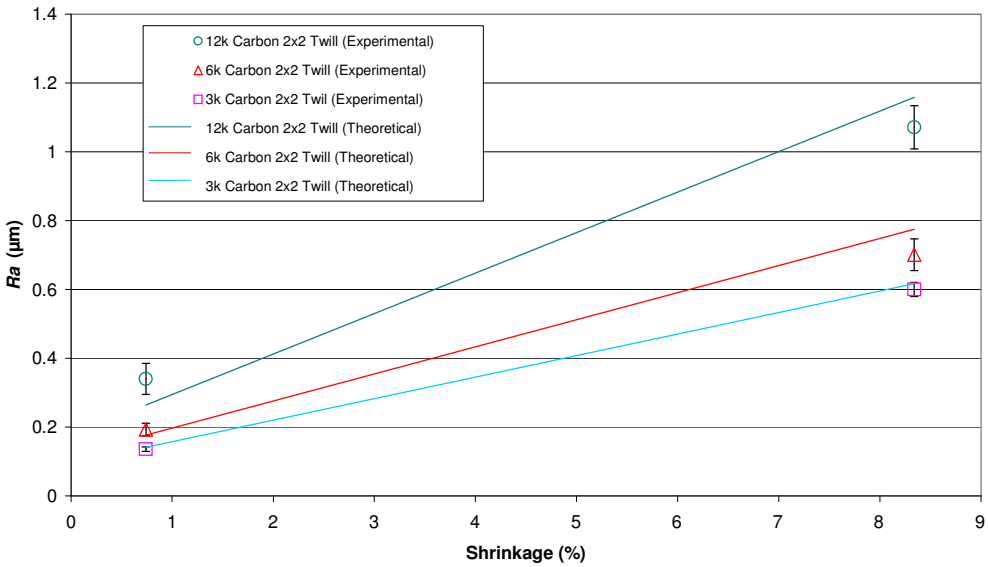

Figure A8.11: Comparison of theoretical and experimental surface roughness measurements for 3, 6 and 12k 2x2 twill weave carbon fabrics moulded using a low and high shrink matrix. Theoretical predictions show similar trends to experimental data.

References

1. Robitaille, F., Long, A.C., Jones, I., A., and Rudd, C.D., *Automatically generated geometric descriptions of textile and composite unit cells.* Composites: Part A, 2003. **34**: p. 303-312.
2. Robitaille, F., Clayton, B.R., Long, A.C., Souter, B.J., and Rudd, C.D. *Geometric modelling of industrial preforms: woven and braided textiles*. in *proceedings of the Institute of Mechanical Engineers*. 1999.
3. Crookston, J.J., *Prediction of elastic behaviour and initial failure of textile composites*, in *Mech. Eng., PhD Thesis*. 2004, University of Nottingham: Nottingham. p. 217.
4. Bogetti, T.A. and Gillespie, J.W., *Process-induced stress and deformation in thick-section thermoset composite laminates.* Journal of Composite Materials, 1992. **26**(5): p. 626-659.
5. Pusatcioglu, S.Y. and Hassler, J.C., *Effect of temperature gradients on cure and stress gradients in thick thermoset castings.* Journal of Applied Polymer Science, 1980. **25**: p. 381-393.
6. Hull, D. and Clyne, T.W., *An introduction to composite materials. 2nd Edition*. 1996, Cambridge University Press: Cambridge.
7. Bushko, W.C. and Stokes, V.W., *Estimates for material shrinkage in molded parts caused by time-varying cavity pressure.* Technical papers of the annual technical conference- Society of Plastics Engineers Incorporated Conf. 55, 1997. **1**: p. 682-686.